Przemysław Janik

Photovoltaic power generation assessment based on advanced signal processing and optimisation techniques

Oficyna Wydawnicza Politechniki Wrocławskiej
Wrocław 2014

Reviewers
Zbigniew LEONOWICZ
Harald SCHWARZ

Cover design
Marcin ZAWADZKI

OFICYNA WYDAWNICZA POLITECHNIKI WROCŁAWSKIEJ
Wybrzeże Wyspiańskiego 27, 50-370 Wrocław
http://www.oficyna.pwr.wroc.pl
e-mail: oficwyd@pwr.wroc.pl
zamawianie.książek@pwr.wroc.pl

ISBN 978-83-7493-860-0

Drukarnia Oficyny Wydawniczej Politechniki Wrocławskiej. Zam. nr 817/2014.

Contents

Notation

S_R	active apparent power
P	active power
$\mathbf{R}_x$	autocorrelation matrix
C_S	compensating capacitance
$\underline{S}$	complex apparent power
$\underline{I}$	complex value of current
$\underline{U}$	complex value of voltage
x[n]	discrete signal as function of sample number n
φ	displacement between voltage and current
S_D	distortion power
D	distortion power by Budeanu
$h_i(\mathbf{x})$	equality constrain function
f	frequency
$g_i(\mathbf{x})$	inequality constrain function
$P(0)$	initial population
$\mathbf{s}_j$	input signal vector for DWT of the length 2^j
$i(t)$	instantaneous current as function of time
p	instantaneous power
$u(t)$	instantaneous voltage as function of time
$\mathbf{W}_a^j$	j – scale discrete wavelet transform matrix for analysis
$\mathbf{W}_s^j$	j – scale discrete wavelet transform matrix for synthesis
λ	Lagrange multiplier for inequality constrains
L	length of a chromosome, length of a signal
$M(n)$	matting pool
μ	multiplier for equality constrains
$F(\mathbf{x})$	objective function
a,b	pair of numbers
PF	power factor
$\mathbf{d}_{j-1}$	prediction vector with differences
p_c	probability of parents selection form the mating pool
P_{music}	pseudospectrum obtained with MUSIC method

Q	reactive power
S_t	total apparent power
S_x	true reactive apparent power
h_0	unity step
$\mathbf{s}_{j-1}$	updated signal vector of the length 2^{j-1}

1 Introduction

1.1 Developments and motivations

Traditional model of an electrical energy distributions system [1] comprising unidirectional power flow from centralised generation units with considerably big power to geographically distributed, relatively small consumers is not more valid. Distributed generation or dispersed generation is an inevitable trend in the development of electrical energy distribution systems [2], [3]. Small and medium sized photovoltaic installations are most popular among *prosumers*. Further on, the proliferation of decentralised generation, along with other factors, triggered the development of *smart electrical grids*. The sophisticated term *smart grid* covers a wide range of concepts and innovations applied to a power grid.

One of concepts is called *smart city local grids*. They consist of local generation and consumption and realise a predefined profile (island with zero consumption, constant consumption, constant generation, etc.) toward the overlaid distribution grid in urban area. The local grid consist of traditional loads, solar generation, emergency energy source, and storage. Electrical vehicles characterised by a charging profile and able for immediate discharge to support the gird are an emerging new type of devices. Especially from the power profile point of view.

There are several driving forces substantially influencing the transition from centralised generation to renewable energy sources, from unidirectional power flow to generation at the consumer site.

Reduction of greenhouse gasses emission and other pollutions is one of the most important issues regulated by international treaties. The Large Combustion Plant Directive LCPD [4] applies to combustion plants with a thermal output of 50 MW or more. The LCPD aims to reduce acidification, ground level ozone and particles throughout Europe by controlling emissions of sulphur dioxide (SO_2) and nitrogen oxides (NO_x) and dust (particulate matter (PM)) from large combustion plants (LCPs) in power stations. A Europe-wide approach to reducing these pollutants and their impact is therefore required. Combustion plants must meet at least the emission limit values (ELVs) given in the LCPD what makes them not the most desired source of electricity.

Carbon dioxide capture and geological storage (CCS) is a bridging technology that will contribute to mitigating climate change [5]. It consists of the capture of carbon dioxide (CO2) from industrial installations, its transport to a storage site and its injection into a suitable underground geological formation for the purposes of permanent storage. It was assumed in [5] to achieve 20 % reduction in greenhouse gas emissions by 2020 and provided that CCS obtains private, national and Community support and proves to be an environmentally safe technology. Anyway, this make the production from fossil fuels more complicated and cost intensive.

The control of European energy consumption and the increased use of energy from renewable sources, together with energy savings and increased energy efficiency, constitute important parts of the package of measures needed to reduce greenhouse gas emissions and comply with the Kyoto Protocol to the United Nations Framework Convention on Climate Change, and with further Community and international greenhouse gas emission reduction commitments [6].

The climate and energy package is a set of binding legislation which aims to ensure the European Union meets its ambitious climate and energy targets for 2020 [6]. These targets, known as the "20-20-20" targets, set three key objectives for 2020:

- a 20% reduction in EU greenhouse gas emissions from 1990 levels;
- raising the share of EU energy consumption produced from renewable resources to 20%;
- a 20% improvement in the EU's energy efficiency.

As the deadline approaches, efforts were undertaken to propose an outlook and goals beyond the year 2020.

There is a new settlement proposal for the reduction of 40% of greenhouse gasses by 2030 included in the European 2030 framework for climate and energy policies. The EU Commission proposes an objective of increasing the share of renewable energy to at least 27% of the EU's energy consumption by 2030 [7]. An EU-level target is necessary to drive continued investment in the sector, thus helping to create growth and jobs. Increasing the share of renewables can also improve the EU's energy trade balance and security of supply. A roadmap for moving to a low-carbon economy in 2050 [8] ensures that a steady development of renewable energy generation will be in the focus of European policy.

Improved energy efficiency makes an essential contribution to all EU climate and energy policies. Progress towards the 2020 target of improving energy efficiency by 20% is being delivered by policy measures at the EU and national levels [7].

Increase in the share of renewables is not only motivated by air pollution reduction policies as indicated by the above passage. Protection of fossil resources, independence of energy sources in third countries, sustainable development, are the most important topics. In other words, renewable generation is inevitable for reasons of security and diversification of energy supply, of environmental protection and of so-

cial and economic cohesion. The promotion of electricity production from renewables was distinctly formulated in [9] and since then became a constant trend in the European energy policy. The need to promote renewable energy sources as a priority measure given that their exploitation contributes to environmental protection and sustainable development. In addition this can also create local employment, have a positive impact on social cohesion, contribute to security of supply and make it possible to meet Kyoto targets more quickly. It is therefore necessary to ensure that this potential is better exploited within the framework of the internal electricity market. The increased use of electricity produced from renewable energy sources constitutes an important part of the package of measures needed to comply with the Kyoto Protocol to the United Nations Framework Convention on Climate Change, and of any policy package to meet further commitments.

To ensure increased market penetration of electricity produced from renewable energy sources in the medium term, all EU Member States should be required to set national indicative targets for the consumption of electricity produced from renewable sources.

Setting rules of the internal European market for electricity. A well-functioning internal market in electricity should provide producers with the appropriate incentives for investing in new power generation, including in electricity from renewable energy sources, paying special attention to the most isolated countries and regions in the Community's energy market. A well-functioning market should also provide consumers with adequate measures to promote the more efficient use of energy for which a secure supply of energy is a precondition [10]. Cross-border interconnections should be further developed in order to secure the supply of all energy sources at the most competitive prices to consumers and industry within the European Community.

Consumer and producer, i.e. a prosumer, of electricity may be the same natural person [10]. Small prosumers' installations are the most natural way how to increase the share of renewables, and reduce energy transportation.

Smart Grids **Concepts.** The developments in electrical power distribution systems leading to a *smart gird* include many technical solutions and operational aspects of the grid [11], [12], [13].

The most important include the proliferation of *smart meters* enabling energy readings several time a day, e.g. every 10 minutes or 1 minute. It paves the way for the introduction of flexible energy tariffs and exact control over power flow [14].

Power electronic devices, i.e. *flexible alternated current transmission systems* FACTS, are a tool for managing and controlling energy transfer between energy sources and consumers.

A significant area of development is substation automation communication protocol IEC 61850 implementation [15] and rethinking of SCADA systems [16].

Virtual power plants are a concept for bundling small generation units so that they can be managed as an entity by the system operator.

Bidirectional charging of electrical vehicles gives the system operator a chance to use storage energy in order to manage a problem in the distribution network.

The introduction of all this concepts requires a robust and unified system control and data acquisition software enabling access to system data, operation of expert systems and decision centres and finally access to physical devices conducting switching operations in the distribution system.

Developments in small PV installation technologies

A small PV installation mounted on the roof of a single family house is one of the most favourite solutions among prosumers. It is relatively simple to install and maintain. Some installation rules [17] and standards, i.e. [18]. give a clear guidance for the setting of PV installations. Also legal regulations simplify the connection to the public grid and the trade with electrical energy from small PV installations in Poland [19] . The local utility is obliged to connect a PV installation build by prosumer to the public grid. There is no space for refusal if the basic technical prerequisites are fulfilled. There is no need for any further certificates or concessions to sell electrical energy. A natural person can do it.

There are many technical solutions available on the market, ranging from PV panels, DC cables, through inverters, to monitoring and supporting systems. The investor can easily choose a solution suitable for the anticipated power output and financial engagement.

A new trend in architecture is the use of *building integrated photovoltaic*. The panels are not more a spate object optimised for energy gain, but their design and layout is focused on aesthetic aspects.

Energy efficiency/demand-side management means a global or integrated approach aimed at influencing the amount and timing of electricity consumption in order to reduce primary energy consumption and peak loads by giving precedence to investments in energy efficiency measures, or other measures, such as interruptible supply contracts, over investments to increase generation capacity, if the former are the most effective and economical option, taking into account the positive environmental impact of reduced energy consumption and the security of supply and distribution cost aspects related to it [10].

In urban environment efficiency/demand-side management can be realised by means of a microgrid with traditional and solar generation, battery storage, and electrical car bidirectional charging stations, called *smart city local grids*. Electrical cars can serve as controllable loads and as energy sources as well. The microgrid is seen by the overlaid grid as an entity with a predefined production/consumption profile.

Energy marked requirements for tariff policy instruments and refinement of power quality indices.

Power quality indicia and all types of control measures for energy flow in the distribution networks are seen as instruments enabling dynamic settlement of energy prices and establishing of flexible tariffs policies by utilities. Originally, power quality indices, e.g. defined in [20], were established to enhance power delivery and not primarily to make tariffs more flexible [21], [22]. Modern developments in *smart grid* solutions [3], especially power flow control and smart metering deliver the basic instruments for enforcement of flexible energy tariffs.

1.2 Research objectives and goals

General trends and developments presented in previous section are helpful in the formulation and the right placement of the research objectives concerning this work.

The research was focused on two major areas. First one, is a small photovoltaic generation system. Immense proliferation of such systems into distribution grid becomes reality. Moreover, PV is seen as a part of fare more complicated systems comprising storage units, and wind or conventional energy converters, and loads with sophisticated patters, i.e. charging stations for electrical vehicles. PV generation is characterised by short and long term variations (seasonal, daily, instantaneous) which are immanent and contradictory to an desired ability to follow a predefined generation profile. New methods for the characterisation of power generation profiles, description of variations and distortion are needed. These characterisation and corresponding indices are not only significant form the engineering point of view, but give a tool for flexible energy price calculation accordingly to new power quality features.

Irradiation values are often compared with PV installation power output. This match indicates failures in the system and lost sun energy when solar generator was turned off due to maintenance or a persisting fault in the grid. Establishing this match becomes a problem when irradiance can be measured at one point and the geographical orientation of panels is sophisticated, i.e. panels are covering a complicated façade in urban environment. Often architectural aspects and esthetical values are more important than energy production. This is valid especially for building integrated photovoltaic. A new method is needed to provide a robust match between irradiation and PV system power output.

The second area of research is application of signal processing and optimisation methods. Mathematical tools which have to be appropriately selected, trimmed and applied to be useful for the assessment of PV power generation systems. Property

analysis of various signal processing methods was the prerequisite to their application to signals specific and typical for PV generation. Innovative approach and tools for the assessment of a PV system in terms of tariff instruments and power quality are needed.

Finally, an inevitable question regards the power components computation for nonsinusoidal waveforms of current and voltage. Those power components are used for the characterisation of PV system performance, feature power quality indicia computation. Small PV installations installed working with homely loads – in a typical prosumer installation – can't be equipped with sophisticated active filters for power factor improvement and bettering of power quality due to high cost. A simpler and cheaper approach is required, even not performing so well as active filter.

Proposed research objectives, prospective ideas, and anticipated solutions presented throughout the book are an aftermath of the following thesis:

Assessment and monitoring of photovoltaic power generation system performance is substantially enhanced by the application of innovative methods based on optimisation techniques and advanced signal processing.

The justification of thesis follows from the subsequent chapters presenting the theoretical fundamentals of proposed assessment methods, and results of numerical analysis, and computations based on real signals measured in existing installations.

Chapter 1 presents an overview of developments and trends in the operation of electrical distribution systems triggered by political and technical forces. The overview is a basis for the right placement of presented research objective and reached results.

Chapter 2 brings a detailed presentation of most important concepts for wavelet transform. Wavelets are approached not form the frequency domain and filters perspective, what is typical for the majority of publications but from the time domain perspective and the *lifting operation.*

Chapter 3. The basic concepts of MUSIC method are presented and considered an effective complementary tool in estimation of frequency components in a signal. No information about fundamental frequency is required. High noise content or overlaid exponential component in the signal are still acceptable and don't corrupt results.

Chapter 4 covers the most important aspects of optimisation techniques, including the definition of basic terms and classification of problem groups. Each group of problems is characterised by a specific mathematical approach. Trust region reflective algorithm and Evolutionary approach are presented in more details as regarded most suitable for issues concerning the monitoring of PV installation.

Chapter 5 describes the power theory of sinusoidal signals. Energy delivered by an PV system in a period of time is one of the most important characteristics and a prerequisite for financial actions. Averaged power values were used in the proposed monitoring procedure of PV systems. Presented theory is also the basis for further considerations dedicated to nonsinusoidal voltages and currents.

Chapter 6 is a continuation of the previous one and presents active and reactive power concepts for nonsinusoidal voltages and currents. There is a group of advanced method defining power components for any periodical waveform, but the compensation of reactive power requires active compensators. Therefore approaches proposing only capacitors were included. There is no full compensation, but the approach is very simple and cheap, therefore useful for small micro-generation in private households, add that's why it was included into this work.

Chapter 7. Previous theoretical chapters are followed by the description of the real PV installations used in the research. The installation were equipped with measurement systems allowing capturing and storage of data over long period of time in a database. Electrical and meteorological quantities from this database were the basis for further analysis and studies. Installations at two locations and with significantly different power outputs were used. Both of them were equipped with fixed panels and power electronic convers from the same manufacturer.

Chapter 8 starts with the notification of high variations of power levels in a PV system. This variations are considered as an deterioration of power quality and therefore should be quantified, further minimised. The *ripple* content in the power curve was assessed with wavelets. A bell shaped function was correlated to a power curve using optimisation techniques. It resulted in a very compact characterisation of the power curve and enabled conceptual correlation between real power curve and power output line given by the utility.

Chapter 9 comprises a novel approach to the monitoring of PV system performance. The novelty includes spherical measurement of irradiation components by a set of PV sells distributed on the surface of a half-pane. The measured irradiation components are then weighted and merged together during an optimisation procedure in order to follow a daily power production curve of the PV system.

Chapter 10 is the closing contribution followed only by an outlook and a literature list. It summarises research results, includes comments and conclusions.

Chapter 11 brings an outline for prospective research activities resulting directly from previously presented concepts and from reached results.

1.3 Contributions

The main contributions of the presented work are summarised in a consistent manner:

- selection and adjustment of an appropriate techniques for the characterisation of daily power curves in PV installations
- proposal of a new power quality indexes dedicated to PV generation based on the separation of approximations from details in daily power curves
- selection and adjustment of optimisation techniques for the characterisation of daily power curves in reference to a predefined reverence curve
- proposal of the utilisation of unique spherical irradiance measurements to monitoring of a photovoltaic system
- selection and adjustment of optimisation techniques for treatment of spherical irradiance components
- application of weighted spherical irradiations for the estimation of lost energy during turn off period of the PV installation
- extensive numerical simulation focused on the selection of suitable wavelet based algorithm's parameters
- proposal of reduced and simplified reactive power compensation for microsystems with photovoltaic generation

2 Wavelets transform

2.1 Means and differences

The assumption that a digital signal contains some structure and is not a set of random numbers is prior to any signal processing routine. Usually, signal processing is focused on information extraction from a sequence of sampled values.

A very basic assumption is that there is some correlation between two successive samples. The samples pairs can be processed one after another, so that a mean value and a difference between the first element of the pair and the mean are computed [23]. Obviously, this procedure can be iteratively repeated. An example taken from [24] illustrates this procedure (Table 2.1).

Table 2.1 Pairwise computation of means and differences [2]

56	40	8	24	48	48	40	16	original signal
48	16	48	28	***8***	***-8***	***0***	***12***	s,d 1st iteration
32	38	***16***	***10***	***8***	***-8***	***0***	***12***	s,d 2nd iteration
35	***-3***	***16***	***10***	***8***	***-8***	***0***	***12***	s,d 3rd iteration

The second row in Table 2.1 contains the four means followed by four differences (***italic bold***). They were obtained from raw data in first row. In the next iterative steps the differences are unchanged and the mean and difference computation is applied only to the first entries representing mean values from previous step. The procedure can be repeated until the first entry in the last row represents the mean value of all original samples. The other entries represent successively computed differences.

This type of transformation preserves all information about the signal. The calculation can be reversed. Moreover, this is an "in place" transform, e.g. there is no need for extra memory to do this transformation.

For a pair of numbers a,b the mean value and the difference are obtained in two steps: the first step

$$a,b \to a,\frac{1}{2}(a+b)=s \tag{2.1}$$

and the second step

$$a, s \to a - s = d, s \tag{2.2}$$

The initial sample values a, b are replaced by the computed means and differences s, d. The inverse transform enables a return to the initial sample values in two steps: the first step

$$d, s \to s + d, s \tag{2.3}$$

and the second

$$a, s \to 2s - a \tag{2.4}$$

There are various possible modifications to the described procedure. It is possible to store mean vales and differences of two samples. Another modification is the storage of a mean value and a difference between the mean and the second element. Both variants can be regarded as slight modifications of the details (***bold italic*** entries) in Table 2.1. The changes are multiplication by "-2" and "-1", respectively. The two steps for the computations of means and differences of two subsequent samples are given as

$$a, b \to a, (b - a) = \delta \tag{2.5}$$

$$a, \delta \to a + \frac{\delta}{2} = s, \delta \tag{2.6}$$

And the corresponding inversion

$$s, \delta \to \frac{s - \delta}{2} = a, \delta \tag{2.7}$$

$$a, \delta \to a, a + \delta = b \tag{2.8}$$

If some loss of information can be accepted, a certain level of data compression is possible. The details with absolute value below a certain *threshold* are made equal to zero. Consequently, the inverse transformation is featured by error.

2.2 Lifting procedure

The core ideas of mean and difference presented briefly in the previous section are fundamental for the lifting technique. Two basic operations have a fundamental meaning in lifting: ***prediction*** and ***update***, which are a generalized case of mean and difference. The time domain representation of a discrete wavelet transform is constructed upon the lifting technique and is complementary to the filter bank notation.

Again, some correlation between samples in a given signal is assumed. A simple correlation detection is done using the difference between two successive samples. The difference is small if the samples are almost identical, and therefore the prediction is good. That means, the first sample may be interpreted as a good ***prediction*** of a successive one. Usually, the prediction procedure is more sophisticated than just computing the difference between samples. Examples will be given later on.

As an opposite to the difference calculation, the mean value of two successive samples may be seen. Repetitive mean value building of two samples holds some information about the original signal while reducing the signal length (even, up to one sample).In the example above that is the mean value. Mean value building is also a method for extracting some useful features of a signal, as a pair-wise mean value computation preserves the global structure of the original vector. The term ***update*** is usually in use for description. Similarly as for prediction, more complicated methods exist as the pure mean value computation of two samples.

The elementary operations of a lifting block scheme element along with the separation procedure are presented in Fig. 2.1. The input signal $\mathbf{s}_j$ has the length 2^j and it is transformed into two vectors of the length 2^{j-1}. The intermittent blocks are characterised as follows:

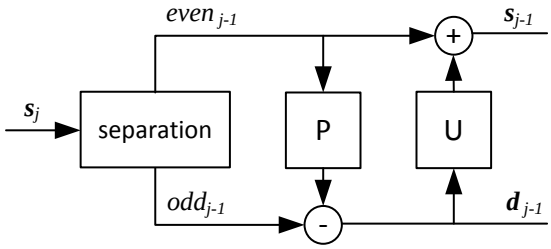

Fig. 2.1 Building block in lifting scheme

separation:

The input vector is split into odd and even elements, both of the length 2^{j-1}. This is only a functional operation, necessary for understanding but not performed in real applications.

prediction:

The correlation between successive samples is assumed, e.g. the signal yields some structure. Knowing the value of the input signal at sample $2n$ the value at sample $2n+1$ is assumed to be identical. Then, the value at $2n+1$ is replaced with the difference, quantifying the discrepancy between the prediction and actual sample value

$$d_{j-1}[n] = s_j[2n+1] - s_j[2n] \tag{2.9}$$

The prediction algorithm is in a general case more complicated and can be given as

$$\mathbf{d}_{j-1} = odd_{j-1} - P\left(even_{j-1}\right) \tag{2.10}$$

The difference is constructed using one odd sample and a prediction based upon a number of even samples.

update:
After prediction the even entry is updated. In the most simple case it is replaced by the average value, representing the knowledge about signal features

$$s_{j-1}[n] = s_j[2n] + d_{j-1}[n]/2 \tag{2.11}$$

Generally, the updating operation may be more sophisticated and is expressed as

$$s_{j-1} = even_{j-1} + U\left(\mathbf{d}_{j-1}\right) \tag{2.12}$$

The described procedure is a one-step lifting.

The discrete wavelet transform is a result of a combination of some basic lifting steps. The differences $\mathbf{d}_{j-1}$ are kept unchanged and the mean values $\mathbf{s}_{j-1}$ are used as an input for the next lifting step .

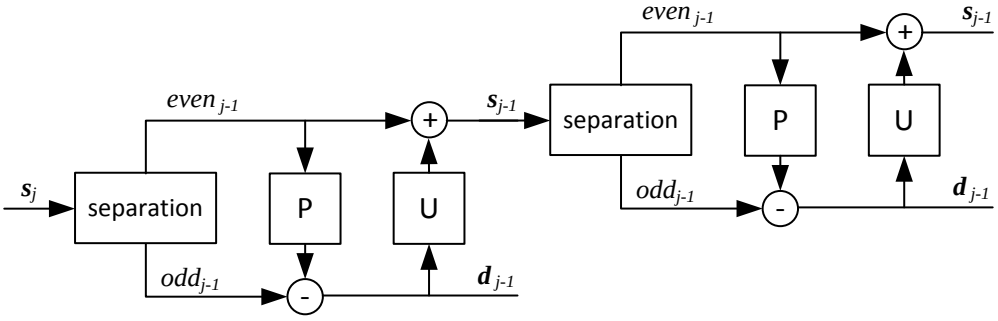

Fig. 2.2 Lifting scheme with two basic blocks

The prediction procedure presented previously was correct for a constant signal. It was assumed that the next sample is the same as the previous one. Further on a prediction of a linear signal is desired. A linear signal is given by the *n*-dependence of the form

$$s_j[n] = \alpha n + \beta \tag{2.13}$$

the samples of the signal constitute a straight line. For a given odd entry $s_j[2n+1]$ the prediction is based on two nearest samples, so that the prediction equation is $\frac{1}{2}\left(s_j[2n]+s_j[2n+2]\right)$. Consequently, the difference is now the discrepancy between the actual value of the middle sample and the prediction Fig. 2.3.

$$d_{j-1}[n] = s_j[2n+1] - \frac{1}{2}\left(s_j[2n]+s_j[2n+2]\right) \tag{2.14}$$

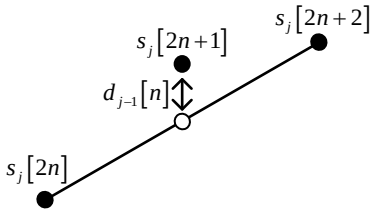

Fig. 2.3 Prediction of a linear signal

According to (2.12) and Fig. 2.1 the prediction is now based on two previous differences

$$s_{j-1}[n] = s_j[2n] + A\left(d_{j-1}[n-1]+d_{j-1}[n]\right) \tag{2.15}$$

The value of A must be settled in a way, that the mean value

$$\sum_n s_{j-1}[n] = \frac{1}{2}\sum_n s_j[n] \tag{2.16}$$

will be preserved in the in the prediction. Substituting (2.14) into (2.15) and finding A with accordance to (2.16) results in $A=\frac{1}{4}$. Finally, the transformation par has the form

$$d_{j-1}[n] = s_j[2n+1] - \frac{1}{2}\left(s_j[2n] + s_j[2n+2]\right) \tag{2.17}$$

$$s_{j-1}[n] = s_j[2n] + \frac{1}{4}\left(d_{j-1}[n-1] + d_{j-1}[n]\right) \tag{2.18}$$

Additionally, the transformation preserves also the *first moment* [25] of the signal.

$$\sum_n n s_{j-1}[n] = \frac{1}{2}\sum_n n s_j[n] \tag{2.19}$$

The mean values is regarded as the *zeroth moment* of the signal.

2.3 General notation of lifting for DWT

Using analogue steps as in section 2.2 the lifting procedure may be reversed. The direct transform given in (2.10) and (2.12) is reversed through simple sign change

$$even_{j-1} = s_{j-1} - U\left(\mathbf{d}_{j-1}\right) \tag{2.20}$$

$$odd_{j-1} = \mathbf{d}_{j-1} + P\left(even_{j-1}\right) \tag{2.21}$$

Accordingly, the example given in (2.17) and (2.18)

$$s_j[2n] = s_{j-1}[n] - \frac{1}{4}\left(d_{j-1}[n-1] + d_{j-1}[n]\right) \tag{2.22}$$

$$s_j[2n+1] = d_{j-1}[n] + \frac{1}{2}\left(s_j[2n] + s_j[2n+2]\right) \tag{2.23}$$

Graphical representation of the inverse lifting step is similar to the direct transform in Fig. 2.1. The general difference (Fig. 2.4) is the reversal of arrows and change of signs.

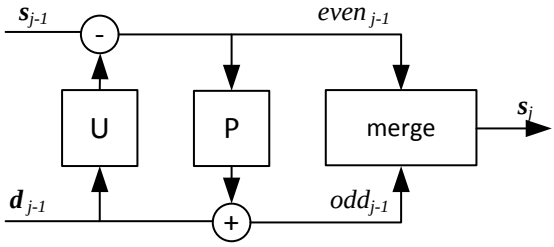

Fig. 2.4 Inverse lifting step

The direct and inverse transform can have several U and P steps included. It is possible as the direct and reverse operations are done by the same U or P blocks, independently. To keep the pairwise notation a "blind" block may be introduced, so that no operation will be done in U or P block if a different number of either operation is required for presentation clarity (Fig. 2.7).

The lifting blocks for the direct (Fig. 2.1) and inverse (Fig. 2.4) transform can be more sophisticated, as shown in the examples in section 2.4. Nonetheless, as a general rule the input sequence $\mathbf{s}_j$ is transformed into two sequences $\mathbf{s}_{j-1}$ and $\mathbf{d}_{j-1}$ of half the length of the original one. This is the direct transform or *analysis*. The reverse operation is called *synthesis*. The graphical representation uses the blocs $\mathbf{T}_a$ for analysis (Fig. 2.5) and $\mathbf{T}_s$ for synthesis .The blocs can be joined in sequence to represent a transform of *j* scales.

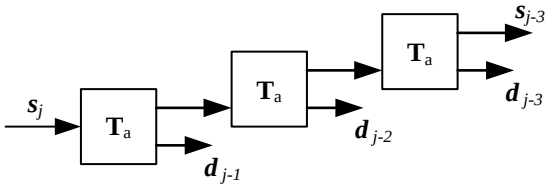

Fig. 2.5 Three scales Discrete Wavelet Transform - analysis

The symbol W_a^j is used to denote the *j*-scale DWT, i.e. the three scale transform from Fig. 2.5 is

$$W_a^3 : \mathbf{s}_j \rightarrow \mathbf{s}_{j-3}, \mathbf{d}_{j-2}, \mathbf{d}_{j-1} \tag{2.24}$$

The corresponding inverse transform (synthesis) is

$$W_s^3 : \mathbf{s}_{j-3}, \mathbf{d}_{j-3}, \mathbf{d}_{j-2}, \mathbf{d}_{j-1} \rightarrow \mathbf{s}_j \tag{2.25}$$

If the transform is applied to a signal of the length 2^j, vectors in (2.24) and (2.25) have the lengths $2^{j-3}, 2^{j-3}, 2^{j-2}, 2^{j-1}$. Fig. 2.6 shows the three blocks of the synthesis.

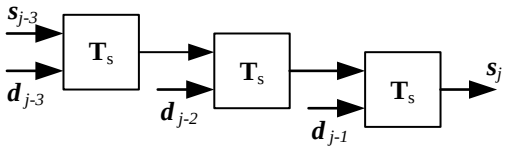

Fig. 2.6 Three scales Discrete Wavelet Transform – synthesis

The matrices describing the direct (2.24) and inverse (2.25) transform can be constructed by transforming a vector with only one entry equal to one and the rest equal to zero. Taking the transformed signal given in Table 2.1 and substituting the vector

$$s_{trans,base1} = [1\ 0\ 0\ 0\ 0\ 0\ 0\ 0] \tag{2.26}$$

into the bottom row a reconstruction can be executed (Table 2.2). The basic transform, deploying means and differences, was taken as a simple example.

Table 2.2 Reconstruction over three scales

1	1	1	1	1	1	1	1	reconstructed signal
1	1	1	1	***0***	***0***	***0***	***0***	2nd iteration
1	1	***0***	***0***	***0***	***0***	***0***	***0***	1st iteration
1	***0***	***0***	***0***	***0***	***0***	***0***	***0***	transformed signal (start)

Repeating the procedure with a one placed at the position 1 to 8 in (2.26) the reconstruction matrix over three scales (2.25) can be obtained.

$$\mathbf{W}_s^{(3)} = \begin{bmatrix} 1 & 1 & 1 & 0 & 1 & 0 & 0 & 0 \\ 1 & 1 & 1 & 0 & -1 & 0 & 0 & 0 \\ 1 & 1 & -1 & 0 & 0 & 1 & 0 & 0 \\ 1 & 1 & -1 & 0 & 0 & -1 & 0 & 0 \\ 1 & -1 & 0 & 1 & 0 & 0 & 1 & 0 \\ 1 & -1 & 0 & 1 & 0 & 0 & -1 & 0 \\ 1 & -1 & 0 & -1 & 0 & 0 & 0 & 1 \\ 1 & -1 & 0 & -1 & 0 & 0 & 0 & -1 \end{bmatrix} \tag{2.27}$$

Similarly, the direct transform applied iteratively to a vector in the form (2.26) with sliding position of the "one" entry results in the corresponding direct transform matrix. For simplicity, only three scales and a vector length 2^3=8 were selected.

$$\mathbf{W}_a^{(3)} = \begin{bmatrix} \frac{1}{8} & \frac{1}{8} & \frac{1}{8} & \frac{1}{8} & \frac{1}{8} & \frac{1}{8} & \frac{1}{8} & \frac{1}{8} \\ \frac{1}{8} & \frac{1}{8} & \frac{1}{8} & \frac{1}{8} & -\frac{1}{8} & -\frac{1}{8} & -\frac{1}{8} & -\frac{1}{8} \\ \frac{1}{4} & \frac{1}{4} & -\frac{1}{4} & -\frac{1}{4} & 0 & 0 & 0 & 0 \\ 0 & 0 & 0 & 0 & -\frac{1}{4} & -\frac{1}{4} & \frac{1}{4} & \frac{1}{4} \\ \frac{1}{2} & -\frac{1}{2} & 0 & 0 & 0 & 0 & 0 & 0 \\ 0 & 0 & \frac{1}{2} & -\frac{1}{2} & 0 & 0 & 0 & 0 \\ 0 & 0 & 0 & 0 & \frac{1}{2} & -\frac{1}{2} & 0 & 0 \\ 0 & 0 & 0 & 0 & 0 & 0 & \frac{1}{2} & -\frac{1}{2} \end{bmatrix} \tag{2.28}$$

Multiplication of the matrices results in

$$\mathbf{W}_s^{(3)} \cdot \mathbf{W}_a^{(3)} = \mathbf{W}_a^{(3)} \cdot \mathbf{W}_s^{(3)} = \mathbf{I} \tag{2.29}$$

2.4 Examples of wavelets in lifting notation

Using the generalized lifting notation some useful wavelets transform can be described as they are implemented. The procedure for the direct and inverse transform is given.

An example follows with a three operations U, P and U. The transform is shown graphically in Fig. 2.7, where a pairwise scheme is used. In the first P-U pair the P operation is omitted.

$$s_{j-1}[n] = s_j[2n] + \sqrt{3}s_j[n] \tag{2.30}$$

$$d_{j-1}^{(1)}[n] = s_j[2n+1] - \frac{1}{4}\sqrt{3}s_{j-1}^{(1)}[n] - \frac{1}{4}\left(\sqrt{3}-2\right)s_{j-1}^{(1)}[n-1] \tag{2.31}$$

$$s_{j-1}^{(2)}[n] = s_{j-1}^{(1)}[n] - d_{j-1}^{(1)}[n+1] \tag{2.32}$$

Finally, the normalisation (rescaling) is performed

$$s_{j-1}[n] = \frac{\sqrt{3}-1}{\sqrt{2}} s_{j-1}^{(2)}[n] \tag{2.33}$$

$$d_{j-1}[n] = \frac{\sqrt{3}+1}{\sqrt{2}} d_{j-1}^{1}[n] \tag{2.34}$$

where the scaling factors satisfy

$$\frac{\sqrt{3}-1}{\sqrt{2}} \cdot \frac{\sqrt{3}+1}{\sqrt{2}} = 1 \tag{2.35}$$

The transformation given in (2.30) to (2.34) describes one iterative step of an important wavelet *Daubechies 4*.

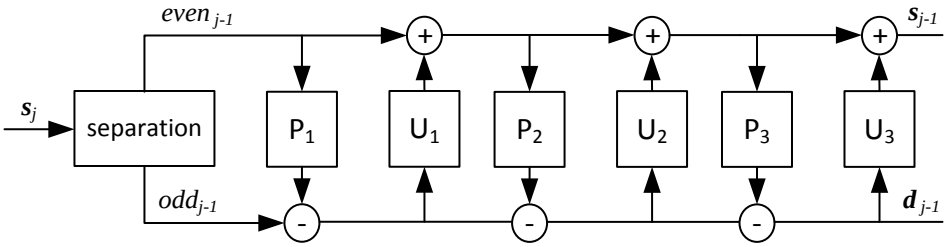

Fig. 2.7 Three lifting steps in pairwise notation

In an analogue manner the inverse *Daubechies 4* transform can be given

$$d_{j-1}^{(1)}[n] = \frac{\sqrt{3}-1}{\sqrt{2}} d_{j-1}[n] \tag{2.36}$$

$$s_{j-1}^{(2)}[n] = \frac{\sqrt{3}+1}{\sqrt{2}} s_{j-1}[n] \tag{2.37}$$

$$s_{j-1}^{(1)}[n] = s_{j-1}^{(2)}[n] + d_{j-1}^{(1)}[n+1] \tag{2.38}$$

$$s_j[2n+1] = d_{j-1}^{(1)}[n] + \frac{1}{4}\sqrt{3} s_{j-1}^{(1)}[n] + \frac{1}{4}\left(\sqrt{3}-2\right) s_{j-1}^{(1)}[n-1] \tag{2.39}$$

$$s_j[2n] = s_{j-1}^{(1)}[n] - \sqrt{3}s_j[2n+1] \tag{2.40}$$

Starting the computation, e.g. $n=0$, the information at $[n-1]$ is not known. *Zero padding* is a possible solution to the problem. More sophisticated methods also exist [24].

In section 2.2 an basic transform was given in (2.9) and (2.11). Adding the normalization step the implementation of the *Haar wavelet* is obtained. That is the only transformation performed on a signal with the length 2^j where no zero padding is needed.

The direct transform is given as

$$d_{j-1}^{(1)}[n] = s_j[2n+1] - s_j[2n] \tag{2.41}$$

$$s_{j-1}^{(1)}[n] = s_j[2n] + \frac{1}{2}d_{j-1}^{(1)}[n] \tag{2.42}$$

$$s_{j-1}[n] = \sqrt{2}s_{j-1}^{(1)}[n] \tag{2.43}$$

$$d_{j-1}[n] = \frac{1}{\sqrt{2}}d_{j-1}^{(1)}[n] \tag{2.44}$$

Corresponding inverse transform is

$$d_{j-1}^{(1)}[n] = \sqrt{2}d_{j-1}[n] \tag{2.45}$$

$$s_{j-1}^{(1)}[n] = \frac{1}{\sqrt{2}}s_{j-1}[n] \tag{2.46}$$

$$s_j[2n] = s_{j-1}^{(1)} - \frac{1}{2}d_{j-1}^{(1)}[n] \tag{2.47}$$

$$s_j[2n+1] = s_j[2n] + d_{j-1}^{(1)}[n] \tag{2.48}$$

The third example is a member of a large family of biorthogonal wavelet transforms. The underlying core idea is given (2.14) and (2.15) which represent the CDF(2,2) transform. The acronym CDF is derived from the inventors of the transform: A. Cohen, I. Daubechies, J.-C. Feauveau [26]. The first parameter indicates the number of P-U operations in one step of the operation, the second one the number of sub-

sequent differences used in the prediction computation. The formulas were published in [24] and [27].

Firstly, the two steps subfamily is shown. In this group the first step and the final normalization is the same.

$$d_{j-1}^{(1)}[n] = s_j[2n+1] - \frac{1}{2}\left(s_j[2n] + s_j[2n+2]\right) \tag{2.49}$$

CDF(2,2) $$s_{j-1}^{(1)}[n] = s_j[2n] + \frac{1}{4}\left(d_{j-1}[n-1] + d_{j-1}[n-1]\right) \tag{2.50}$$

CDF(2,4) $$s_{j-1}^{(1)}[n] = s_j[2n] - \frac{1}{64}\begin{pmatrix} 3d_{j-1}[n-2] - 19d_{j-1}[n-1] + \\ -19d_{j-1}[n] + 3d_{j-1}[n+1] \end{pmatrix} \tag{2.51}$$

CDF(2,6) $$s_{j-1}^{(1)}[n] = s_j[2n] - \frac{1}{512}\begin{pmatrix} -5d_{j-1}[n-3] - 39d_{j-1}[n-2] - 162d_{j-1}[n-1] \\ -162d_{j-1}[n] + 39d_{j-1}[n+1] + 5d_{j-1}[n+2] \end{pmatrix} \tag{2.52}$$

normalization $$d_{j-1}[n] = \frac{1}{\sqrt{2}} d_{j-1}^{(1)}[n] \tag{2.53}$$

$$s_{j-1}[n] = \sqrt{2} s_{j-1}^{(1)}[n] \tag{2.54}$$

The next subfamily utilizes three P-U groups and it starts with the update, so

$$s_{j-1}^{(n)}[n] = s_j[2n] - \frac{1}{3} s_j[2n-1] \tag{2.55}$$

$$d_{j-1}^{(1)}[n] = s_j[2n+1] - \frac{1}{8}\left(9s_{j-1}^{(1)}[n] + 3s_{j-1}^{(1)}[n+1]\right) \tag{2.56}$$

CDF(3,1) $$s_{j-1}^{(2)}[n] = s_{j-1}^{(1)}[n] + \frac{4}{9} d_{j-1}^{(1)}[n] \tag{2.57}$$

CDF(3,3) $$s_{j-1}^{2}[n] = s_{j-1}^{(1)} + \frac{1}{36}\left(3d_{j-1}^{(1)}[n-1] + 16d_{j-1}^{(1)}[n] - 3d_{j-1}^{(1)}[n+1]\right) \tag{2.58}$$

CDF(3,5) $$s_{j-1}^{(2)}[n]=s_{j-1}^{(1)}[n]-\frac{1}{288}\begin{pmatrix}5d_{j-1}^{(1)}[n-2]-34d_{j-1}^{(1)}[n-1]+\\-128d_{j-1}^{(1)}[n]-34d_{j-1}^{(1)}[n+1]-5d_{j-1}^{(1)}[n-2]\end{pmatrix} \tag{2.59}$$

normalisation $$d_{j-1}[n]=\frac{\sqrt{2}}{3}d_{j-1}^{(1)}[n] \tag{2.60}$$

$$s_{j-1}[n]\frac{3}{\sqrt{2}}s_{j-1}^{(2)}[n] \tag{2.61}$$

In all the above examples a normalization step was introduced and an explanation for the apparently superfluous computational burden is justified.

It was assumed that the processed signal belongs to $\ell^2(\mathbb{Z})$. The signals energy is

$$\|\mathbf{s}\|^2=\sum_{n\in\mathbb{Z}}|s[n]|^2 \tag{2.62}$$

and is the squared value of the L_2 norm of the signal vector $\mathbf{s}$. The norms of the signals in the upper and lowest row in Table 2.2

$$\|[1,1,1,1,1,1,1,1]\|=\sqrt{8} \tag{2.63}$$

$$\|[1,0,0,0,0,0,0,0]\|=1 \tag{2.64}$$

If signal length in Table 2.2 is increased to 2^N, e.g. it consist of a single one and 2^N-1 zeros than the inverse Haar transform is a vector of the length 2^N. It consist only of ones and the norm is $2^{N/2}$. The norm grows exponentially with N. When longer signals are transformed the exponential norm increase can result in numerical instability. Normalization of the transform blocks helps to avoid the instability. The consequence of normalization is that for any scale k

$$\left\|W_s^{(k),Haar,norm}\mathbf{x}\right\|=\|\mathbf{x}\| \tag{2.65}$$

$$\left\|\mathbf{W}_a^{(3),Harr,norm}\mathbf{x}\right\|=\|\mathbf{x}\| \tag{2.66}$$

For more complicated transforms than Haar it is not always possible to fulfil (2.65) and (2.66). At least, it can be required that the norm of the signal and the norms of is

direct and inverse transform indicate similar order of magnitudes. This requirement is expressed by the constants $A, B, \tilde{A}, \tilde{B}$ satisfying

$$A\|\mathbf{x}\| \le \|T_a\mathbf{x}\| < B\|\mathbf{x}\| \tag{2.67}$$

$$\tilde{A}\|\mathbf{x}\| \le \|T_s\mathbf{x}\| < \tilde{B}\|\mathbf{x}\| \tag{2.68}$$

The requirements (2.67) and (2.68) with all constants equal one are fulfilled by the *Haar* and *Daubechies 4* transforms.

Hence the transform matrices $\mathbf{W}_a^{(N)}$ and $\mathbf{W}_s^{(N)}$ are generated by iterating the basic building blocks, similar estimates hold for these transforms, with constants that may on the signal length N.

2.5 Wavelet function and scaling function

The transform based on means and differences, which is in fact the Harr transform, can be given with a *scaling* function and a *wavelet* function. Such a notation is generally suitable for various wavelet transforms. Usually, both functions are derived from the filter bank approach to wavelet transform. Keeping the lifting notation here, the scaling function and a wavelet functions for the basic Haar transform are given. Some prerequisites and preliminary steps are required.

The entries in columns in (2.27) represent a certain pattern. It was obtained by the reconstruction over three scales of vectors related to (2.26) with a one at iteratively moved position. To represent the pattern with scaling and wavelet functions it is assumed that all he columns come from sampled continuous functions in the time interval [0,1]. For a signal with the length 2^N the sampled points are

$$\left[1\cdot 2^{-N}, 2\cdot 2^{-N}, 3\cdot 2^{-N}, ..., 2^N\cdot 2^{-N}\right] \tag{2.69}$$

The first column in (2.27) is obtained from the sampled function

$$h_0(t) = 1 \qquad t \in [0,1] \tag{2.70}$$

The second column is a result of sampling

$$h_1(t) = h(t) = \begin{cases} 1 & t \in \left[0, \frac{1}{2}\right] \\ -1 & t \in \left(\frac{1}{2}, 1\right] \end{cases} \tag{2.71}$$

and successively the remaining columns can be defined. To formalise the notation a specific way of notating integers is used. For $n = 1, 2, 3, ...$

$$n = k + 2j \tag{2.72}$$

where $j \geq 0$ and $0 \leq k \leq 2^j$, so every integer can be given by specific values of k, j. Using this notation the *wavelet* function is given generally as

$$h_n(t) = h\left(2^j t - k\right) \tag{2.73}$$

where $t \in [0,1]$ and $n = 1, 2, 3, 4, ...$ Both functions are defined as independent from N. For a specific value of N the signal length is 2^N and also 2^N vectors defining the square transform matrix (2.27) are obtained by sampling $h_0, h_1, ..., h_{2^N-1}$ at the points defined in (2.69). It must be stressed that all matrix columns (2.27) are derived from just two functions. The function $h_0(t)$ (2.70) which is called the *scaling* function and the function $h(t)$ (2.73) which is called the *wavelet* function. The functions $h_n(t)$ are obtained from the basic $h(t)$ by *scaling* according to j and *translation* given by k.

Scaling and wavelet functions given above are called the *Haar basis functions*. The first eight functions (n=0,1,…,7) are given in Fig. 2.8. The sampled values of those functions are the columns in (2.27).

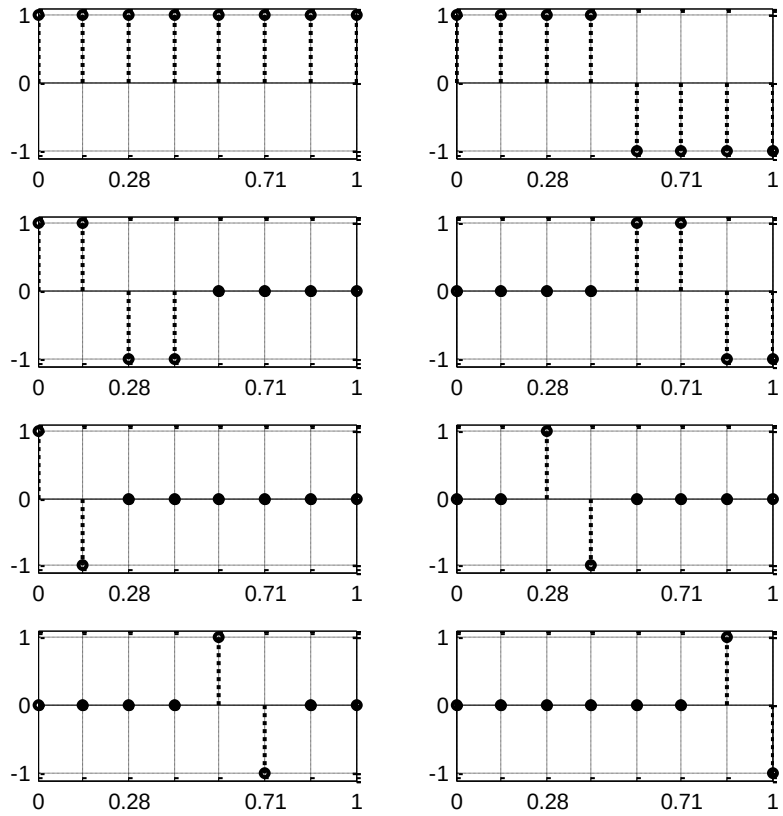

Fig. 2.8 Haar functions discretised for *N*=8, not normalized

Other wavelet transforms are also given by the scaling and wavelet transforms. The expression (2.73) is usually normalized and has the form

$$h_n^{norm} = 2^{\frac{j}{2}} h\left(2^j t - k\right) \tag{2.74}$$

The direct Haar transform can be interpreted in terms of the basic functions. For simplicity and consistence with previous considerations $N = 3$, so that there are eight functions $h_0,...,h_7$ sampled at $\frac{1}{8},\frac{2}{8},...,\frac{8}{8}$, resulting in $\mathbf{h}_0,...,\mathbf{h}_7$. The direct transforms of this functions over three scales are the basis vectors

$$\begin{aligned}
\mathbf{e}_0 &= [1,0,0,0,0,0,0,0] \\
\mathbf{e}_1 &= [0,1,0,0,0,0,0,0] \\
&\vdots \\
\mathbf{e}_7 &= [0,0,0,0,0,0,0,1]
\end{aligned} \tag{2.75}$$

The direct and inverse transform is given as

$$\mathbf{W}_a^{(3)}(\mathbf{h}_n') = \mathbf{e}_n' \tag{2.76}$$

$$\mathbf{W}_s^{(3)}(\mathbf{e}_n') = \mathbf{h}_n' \tag{2.77}$$

A general signal $\mathbf{x}$ of length 8 transformed directly gives

$$\mathbf{y} = \mathbf{W}_a^{(3)}(\mathbf{x}) \tag{2.78}$$

Direct and inverse transforms are linear so they can be expressed with the superposition

$$\mathbf{y} = \sum_{n=0}^{7} y[n]\mathbf{e}_n \tag{2.79}$$

$$\mathbf{x} = \mathbf{W}_s^{(3)}(\mathbf{y}) = \sum_{n=0}^{7} y[n]\mathbf{h}_n \tag{2.80}$$

The direct transform $\mathbf{W}_a^{(3)}$ is used to transform the signal $\mathbf{x}$ into coefficients $\mathbf{y}$. The original signal is represented as a weighted summation of elementary functions $\mathbf{h}_0,...,\mathbf{h}_7$. The corresponding weights are the transform coefficients $y[n]$.

Similar representations can be written to more general transforms. The way to find the pattern is unfortunately more complicated than in the case of Haar transform.

The further example is based on the Daubechies 4 inverse transform. It is assumed that the transformed signal of length $N = 2^k$ has a single one at sixth position. The *k* values are 3, 5, 9, 12. Comparison of the approximations to the wavelet function similar to (2.74) is given in Fig. 2.9. Different signals lengths have been compressed to the unity range to make the comparison possible. The plots approach a limiting curve, where $k = 12$ is a satisfactory approximation (Fig. 2.9). Varying the locations of the single one would have a scaling and translating effect on the graph with accordance to

(2.73). An exception is the one located at the beginning, which defines the corresponding scaling function.

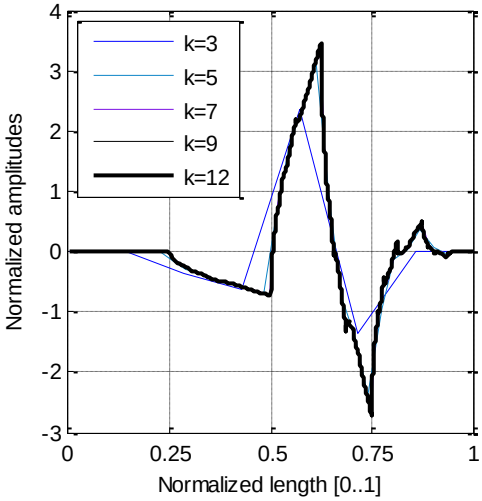

Fig. 2.9 Inverse Daubechies 4 discretized for $N=2^k$

The conclusion is, that there are two functions for the direct transform and corresponding two functions for the inverse transform. Inverse transforms of unit vectors with ones placed at the positions 1 to 2^{N-k} return the translated versions of the scaling function. Inverse transform of unit vectors with a one placed at positions form $2^{N-k}+1$ to 2^{N-k+1} gives the translated versions of the wavelet function. The statement is true in a limited sense, whereas the boundary corrections were not considered.

An important interpretation of those considerations is that the direct transform resolves the signal into components given by the waveform of the wavelet and scaling functions. In fact it is a superposition of the these components with the weight according to the entry in the transform. As the basic waveforms were established with a single once as entry value. More rigorous treatment can be found in [28] and [29].

2.6 Two Dimensional Transform

The discrete wavelet transform can be applied to two dimensional signals. The two versions of 2D DWT are called separable and non-separable transforms. In both cases considerations are restricted to real valued two dimensional functions, e.g. grey scale images.

The two dimensional transform is a natural extension of the 1D case as it is applied to a matrix instead of a vector. The simplest approach means concatenating the rows of a matrix in order to get a single vector and apply already presented methods. This

approach is not favourable. Likely correlations between neighbouring entries in columns are not recognized. Concatenating the rows makes only use of the correlations in one dimension, in rows.

A different approach may be applied to the two dimensional problem. The wavelet transform can be represented as a matrix operation in a form similar to the Haar transform presented in (2.28). The matrix $\mathbf{W}_a$ computes the one scale wavelet transform from the columns of the signal matrix $\mathbf{X}$

$$\mathbf{Y}^c = \mathbf{W}_a \mathbf{X} \tag{2.81}$$

This operation is just a matrix multiplication. The index "c" underlines that columns wise operation was performed. Columns can be seen as separate signals.

Then, the multiplication (2.81) is performed on the rows of $\mathbf{Y}^c$. Firstly $\mathbf{Y}^c$ is transposed, then multiplied by $\mathbf{W}_a$ then the result transposed again. The result is

$$\mathbf{Y}^{c,r} = \left(\mathbf{W}_a \left(\mathbf{Y}^c \right)^T \right)^T = \mathbf{Y}^c \mathbf{W}_a^T \tag{2.82}$$

which can be rewritten in the form

$$\mathbf{Y}^{c,r} = \mathbf{W}_a \mathbf{X} \mathbf{W}_a^T \tag{2.83}$$

where the superscripts on the left hand side indicate that firstly the columns have been transformed and then the rows. However, the same results will be obtained for interchanged order of those operations, as

$$\left(\mathbf{W}_a \mathbf{X} \right) \mathbf{W}_a^T = \mathbf{W}_a \left(\mathbf{X} \mathbf{W}_a^T \right) \tag{2.84}$$

The inverse transform can also be given in the matrix notation

$$\mathbf{X} = \mathbf{W}_a^{-1} \mathbf{Y}^{c,r} \left(\mathbf{W}_a^{-1} \right)^T = \mathbf{W}_s \mathbf{Y}^{c,r} \mathbf{W}_s^T \tag{2.85}$$

where $\mathbf{W}_s = \mathbf{W}_a^{-1}$ is the synthesis matrix.

Matrix multiplication is numerically not the most efficient method for practical computation. Usually, one dimensional transforms implemented as lifting steps are used. The result however, is the same. The coding of the transform is different.

The separable 2D transform defined in (2.83) holds the properties of the one dimensional transform. One step of the transform applied to a square matrix $\mathbf{S}_j$ results in four matrices of half the size (Fig. 2.10). The sub-matrix $\mathbf{SS}_{j-1}$ with the dimensions $2^{j-1} \times 2^{j-1}$ represents the update step applied to columns and rows. The box $\mathbf{SD}_{j-1}$ includes the results of the update operation applied to columns and prediction applied to rows. Finally, there is the box with prediction operation performed upon columns and rows.

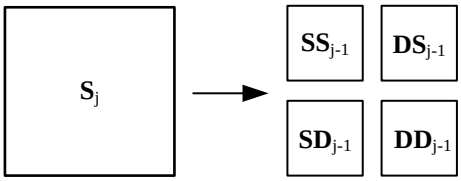

Fig. 2.10 Graphical representation of 2D transform

In order to obtain the results of the second step of transformation, similar to Fig. 2.2, the whole procedure should be applied to the updated block $\mathbf{SS}_{j-1}$.

The drawback of separable transform is that the horizontal, vertical and diagonal structures are processed variously. A negligible rotation of the 2D pattern changes significantly the results.

Therefore, the non-separable transform is more favourable The underlying idea of the non-separable transform includes the consideration of the nearest neighbours. The signal is given as a matrix

$$\mathbf{X} = \left\{ x[m,n] \right\}_{m,n \in \mathbb{Z}^2} \tag{2.86}$$

where infinite dimensions are assumed to avoid the boundary problems. A selected element $x[m,n]$ has four nearest neighbours

$$\begin{aligned} &x[m+1,n] \\ &x[m-1,n] \\ &x[m,n+1] \\ &x[m,n-1] \end{aligned} \tag{2.87}$$

Such assignment results, with accordance to the integer superscripts *m, n* into a division of the matrix elements into two classes. Selecting a starting $x[m,n]$ point and

denoting it with “x” the nearest neighbours must be marked differently, i.e. with “o”. Then, the “o” point must be selected and all the nearest neighbours of it are again marked “x”. Whereas one entry has already been marked. This procedures is repeated until the whole input space is divided into two classes as symbolically depicted in Fig. 2.11.

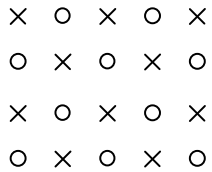

Fig. 2.11 Separation of the lattice into two groups

The simplest proposal of the non-separable algorithm, similar to 1D case in (2.10), replaces the original entry of the initial point with the computed difference. In a 2D case every “x” point is replaced with the difference between the original value and the predicted one. In the second stage all the “o” points are considered and their values updated using the fresh values of the “x” points. Complimentary to the 1D case given in (2.12). This is the brief description of a one scale transformation unit.

Establishing a two dimensional transform requires keeping the values at “x” points and the use of the lattice of “o” points as a new lattice for which the two computational procedures – prediction and update – are performed. The “o” points in Fig. 2.11 build a square lattice rotated by 45 degrees to the integer lattice constituting a distance of $\sqrt{2}$ between nearest neighbours.

The 2D case is an in place operations, because new values are inserted into old ones. The reverse transform can be made similarly to the inversion procedure in 1D, changing the order of operations with reverted signs.

A proposal of a basic procedure illustrating the concept is given for an “x” point located at (m,n). The predicted value at this point equals to the average of four nearest neighbours

$$x_{\times}(m,n) = x(m,n) - \frac{1}{4}\left(x[m-1,n] + x[m+1,n] + x[m,n+1]x[m,n-1]\right) \qquad (2.88)$$

The update procedure in this basic approach should preserve the average value. The average computed at “o” points should be half of the average of the initial values. The coefficient 0.5 is placed because there are half as many “o” values as in the original matrix. This feature can by guaranteed by the update procedure.

$$x_o[m,n] = x[m,n] + \frac{1}{8} x_\times \begin{pmatrix} [m-1,n] + x_\times[m+1,n] + \\ + x_\times[m,n+1] + x_\times[m,n-1] \end{pmatrix} \tag{2.89}$$

The proposed basic DWT, as simple as it is, has no directional effects as the separable transform described previously.

There exist more sophisticated lattices (e.g. hexagonal lattice) and prediction/update procedures.

3 Multiple Signal Classification MUSIC

The wavelet transform and the ***S*** transform are examples of non-parametric methods of signal analysis. The non-parametric methods are a wide group of methods including SFTF, Wigner-Wille transform and many more. Applying them requires no explicate knowledge of the signal model itself.

An opposite group are parametric methods. An parametric approach is substantially different as the a priori knowledge of the signal model is required. The Prony algorithm and SVD based methods are useful and commonly applied for PQ problems.

Waveforms of common distortions have spectral components in narrow bands or at discrete frequencies. That are harmonic or interharmonic frequencies.

A sinusoidal model is most suitable for the characterisation of harmonics and interharmonics with a parametric method like MUSIC.

3.1 Sinusoidal model of a signal

A discrete time signal of length L has a model with K sinusoidal components buried in noise

$$x[n] = \sum_{k=1}^{K} a_k \cos(n\omega_k + \phi_k) + w[n] \tag{3.1}$$

where $a_k \geq 0$ is the amplitude, ϕ_k is the initial phase angle, $\omega_k = 2\pi f_k$ is the harmonic or interharmonic frequency and K the total number of sinusoids. In this model the amplitude and frequency are assumed to be deterministic and unknown. The initial phase angle ϕ_k is random and uniformly distributed in $[-\pi, \pi]$. An equivalent expression for the signal given in (3.1) is based on complex exponentials buried in noise, so called *harmonic model*

$$x[n] = \sum_{k=1}^{K} \underline{A}_k e^{jn\omega_k} + w[n] \tag{3.2}$$

where $A_k = |\underline{A}_k| e^{jn\omega_k}$ is the complex amplitude of the k[th] harmonic signal component.

If the voltage or current in a power system contains only odd harmonics beside the fundamental, then a signal model of the order K contains only $K-1$ odd harmonicas beside the fundamental. On the contrary, the same model has $K-1$ even harmonics and the fundamental if there are only even harmonics present in the power system.

In the signal model (3.2) the range of frequencies $\omega_k = 2\pi f_k$ is $[-\pi, \pi]$ therefore can be located at any nonharmonic frequency. There is no assumption about the frequency being an multiply of the fundamental component.
The frequency resolution of a method used for model's parameter estimation is quite high. The biggest advantage is the possibility to identify interharmonics. Anyway, the number of harmonics determined by the model order K must be known to avoid erroneous results.

3.2 MUSIC Algorithm

The MUSIC is a noise subspace method. For a given parametric model (3.1) the MUSIC method computes corresponding frequencies and amplitudes of spectral components in the signal. Whereas the frequencies are not necessarily harmonics, i.e. the integer multiplies of the fundamental.

The autocorrelation matrix $\mathbf{R}_x$ of the signal $x[n]$ is a result of an operation on the signal samples

$$\hat{\mathbf{R}}_x = \frac{1}{N}\mathbf{X}^H\mathbf{X} \tag{3.3}$$

It is assumed that the signal $x[n]$ given in has the length $L = N + M - 1$. The autocorrelation matrix $\mathbf{R}_x$ has the size $M \times M$. The matrix $\mathbf{X}$ with the dimensions $N \times M$ is given as

$$\mathbf{X} = \begin{bmatrix} \mathbf{x}^T(0) \\ \mathbf{x}^T(1) \\ \vdots \\ \mathbf{x}^T(N-1) \end{bmatrix} = \begin{bmatrix} x(0) & x(1) & \cdots & x(M-1) \\ x(1) & x(2) & \cdots & x(M) \\ \vdots & \vdots & \ddots & \vdots \\ x(N-1) & x(N) & \cdots & x(N+M-2) \end{bmatrix} \tag{3.4}$$

The superscript $(\ )^H$ denotes the Hermitian operator.

Putting (3.2) into (3.4) results in

$$\hat{\mathbf{R}}_x = \mathbf{R}_s + \mathbf{R}_w = \mathbf{E}\mathbf{P}\mathbf{E}^H + \sigma_w^2\mathbf{I} \tag{3.5}$$

where

$$\mathbf{E} = \begin{bmatrix} \mathbf{e}_1 & \mathbf{e}_2 & \cdots & \mathbf{e}_k \end{bmatrix} \tag{3.6}$$

$$\mathbf{P} = diag\left\{ \begin{matrix} |\underline{A}_1|^2 & |\underline{A}_2|^2 & \cdots & |\underline{A}_K|^2 \end{matrix} \right\} \tag{3.7}$$

The eigenvectors of $\mathbf{R}_s$ are

$$\mathbf{e}_l = \begin{bmatrix} 1 & e^{j\omega_l} & \cdots & e^{j(M-1)\omega_l} \end{bmatrix}^T \tag{3.8}$$

and $l = 1,2,...,K$.

The signal and noise subspace can be introduced. Given is $\hat{\mathbf{R}}_x$ of full rank M. The eigenvalues of $\hat{\mathbf{R}}_x$ are ordered decreasingly and the corresponding eigenvectors are $s_1, s_2, ..., s_M$, therefore

$$\hat{\mathbf{R}}_x \mathbf{s}_i = \lambda_i \mathbf{s}_i \tag{3.9}$$

The eigenvectors represent two groups. K eigenvectors matching the K biggest eigenvalues belong to the signal subspace. The rest of eigenvectors $(M-K)$ belongs to the noise subspace. In the MUSIC method the noise subspace is used to determine the unknown harmonic frequencies ω_k. For that the pseudospectrum is computed

$$P_{music}\left(e^{j\omega}\right) = \frac{1}{\sum_{i=K+1}^{M} \left|\mathbf{e}^H \mathbf{s}_i\right|^2} \tag{3.10}$$

where $\mathbf{s}_i$ ($i = K+1,...,M$) are eigenvectors associated with the noise subspace and orthogonal to the signal eigenvector $\mathbf{e}_l = \begin{bmatrix} 1 & e^{j\omega_l} & \cdots & e^{j(M-1)\omega_l} \end{bmatrix}^T$ and $\mathbf{e}^H$ denotes

the complex-conjugate transpose. As a result the denominator has zeros at the frequencies related to the signal eigenvectors. The plot of (3.10) shows no real spectrum. The peaks of the pseudospectrum coincide with frequencies of the outraging frequency components. Equation (3.10) can also be given in the Z-domain

$$P_{music}(z)=\left[\sum_{i=K+1}^{M} S_i(z)S_i^*\left(\frac{1}{z^*}\right)\right]^{-1} \tag{3.11}$$

where $S_i(z)=\sum_{m=0}^{M-1} s_i(m)z^{-m}$ and $s_i(m)$ is the m-th element in the i-th eigenvector.

Signal and noise subspace are orthogonal to each other, so the denominator in (3.11) is zero at the harmonic frequencies.

The frequencies ω_k of the components in the signal model (3.2) are detectable using the frequency locations corresponding to the K highest peaks in the pseudospectrum $P_{music}\left(e^{j\omega}\right)$. An alternative way is the use of the angles of K roots nearest the unit circle in Z-domain in (3.11).

Additionally to harmonic components the magnitudes and powers of components can be obtained. When ω_k is given, then $P_k=\left|\underline{A}_k\right|^2$ can be estimated by jointly solving the K equations

$$\sum_{k=1}^{K} P_k\left|\mathbf{e}_k^H\mathbf{s}_i\right|^2=\lambda_i-\hat{\boldsymbol{\sigma}}_w^2 \tag{3.12}$$

where $i=1,2,...,K$ and the noise is estimated by

$$\hat{\boldsymbol{\sigma}}_w^2=\frac{1}{M-K}\sum_{i=K+1}^{M}\lambda_i \tag{3.13}$$

Due to the fact

$$\mathbf{e}_k^H\mathbf{s}_i=S_i\left(e^{j\omega_k}\right)=\sum_{m=0}^{M-1} s_i(m)e^{-jm\omega_k} \tag{3.14}$$

the equation (3.12) can be rewritten in the matrix notation

$$\begin{bmatrix} \left|S_1\left(e^{j\omega_1}\right)\right|^2 & \left|S_1\left(e^{j\omega_2}\right)\right|^2 & \cdots & \left|S_1\left(e^{j\omega_K}\right)\right|^2 \\ \left|S_2\left(e^{j\omega_1}\right)\right| & \left|S_2\left(e^{j\omega_2}\right)\right|^2 & \cdots & \left|S_2\left(e^{j\omega_K}\right)\right|^2 \\ \vdots & \vdots & \ddots & \vdots \\ \left|S_K\left(e^{j\omega_1}\right)\right| & \left|S_K\left(e^{j\omega_2}\right)\right|^2 & \cdots & \left|S_K\left(e^{j\omega_K}\right)\right|^2 \end{bmatrix} \begin{bmatrix} P_1 \\ P_2 \\ \vdots \\ P_K \end{bmatrix} = \begin{bmatrix} \lambda_1 - \hat{\sigma}_w^2 \\ \lambda_2 - \hat{\sigma}_w^2 \\ \vdots \\ \lambda_K - \hat{\sigma}_w^2 \end{bmatrix} \tag{3.15}$$

Solving (3.15) returns the harmonic power P_K for $K = 1, 2, ..., K$ and the amplitudes in (3.2) are given as $\sqrt{2P_K}$.

3.3 Block based application of MUSIC

The signal model (3.2) assumes that the signal is stationary or at least statistically time invariant. In power systems signals often change over time. For nonstationary signals the proposed MUSIC method must be modified using the block-based signal modelling. In this approach the data is divided into blocs, within which the signal is approximately stationary. The blocs can be overlapped or non-overlapped. The parameters can be estimated for each data block separately. Therefore, the parameters will vary with time, as the estimations vary with sliding window.

The samples of a recorded signal $x[n]$ are divided into blocks of fixed length L. The size of blocks is determined empirically in order to regard the data within the blocks as stationary. The overlap of two adjacent blocks is denoted with K and $K < L$. The *m*-th sample in the *j*-th block is $x^{(j)}[m]$ where $m = 0, 1, 2, ..., L-1$, $j = 1, 2, ...$ Then the data sample $x^{(j)}[m]$ in the *j*-th block is related to the original sample ordering n in the original signal

$$x^{(j)}[m] = x[m + (j-1)(L-K)] \tag{3.16}$$

The time index m is related to the time index n by

$$n = m + (j-1)(L-K) \tag{3.17}$$

The modified signal model given in (3.1) and used un the blocked approach is

$$x^{(j)}[m] = \sum_{k=1}^{K} a_k^{(j)} \cos\left(m\omega_k^{(j)} + \phi_k^{(j)} + w^{(j)}[m]\right) \tag{3.18}$$

For different windows the number of spectral components $K^{(j)}$ may be different.

3.4 Analysis of signals with MUSIC

Firstly, a signal containing odd and even harmonics has been analysed. The fundamental component has been deliberately omitted. The amplitudes of all components were equalized to better visualise the performance of the method. Harmonics from 2 to 8 were included. Each value settled to 10 per cent of the fundamental. Additional noise with mean zero and standard deviation 2 was added and then multiplied by 30 The signal is shown in Fig. 3.1 and Fig. 3.2. Parameters of the original clean signal and estimated from the signal with noise are given in Table 3.1.

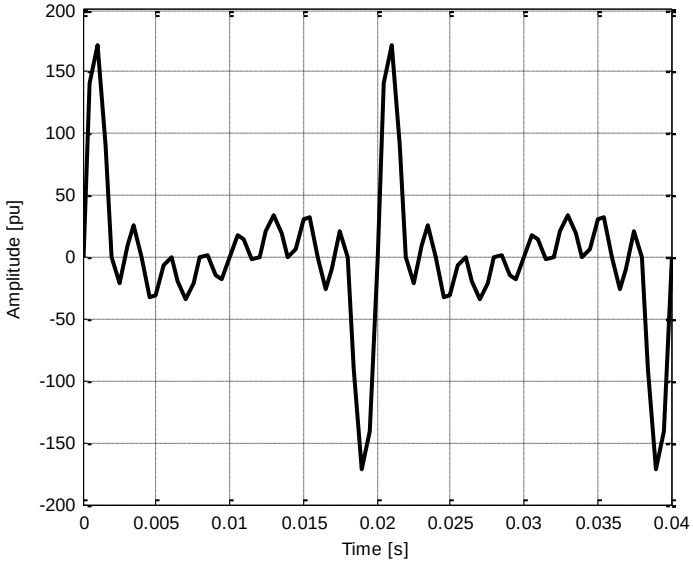

Fig. 3.1 Artificial signal with harmonics 2 to 8: phase angle of harmonics made zero, no noise

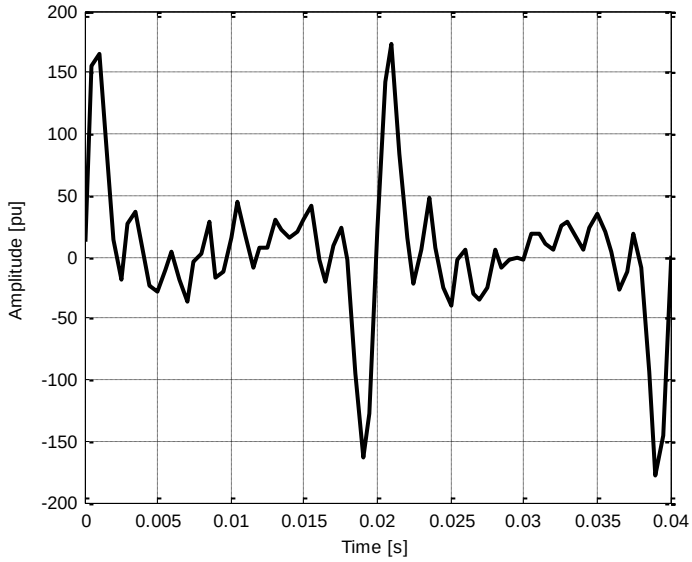

Fig. 3.2 Artificial signal with harmonics 2 to 8: phase angle of harmonics made zero, noise

Table 3.1 Computation results of spectral components for artificial signal with harmonics 2 to 8.

Frequencies of spectral components		
theoretical value [Hz]	computed, no noise [Hz]	computed, noise [Hz]
100	100	100.27
150	150	151.76
200	200	198.22
250	250	249.81
300	300	300.26
350	350	354.22
400	400	402.80

The method performed satisfactory even for noisy signals Table 3.1. Similar tests were conducted for a signal with linearly changing initial phase of spectral components. There was no significant influence of the initial phase of harmonics on the accuracy of components' frequency estimation.

Compensation of reactive power with a capacitor bank is a common practice [30] and requires frequent switching operations for vast varying loads. A typical waveform following switching operation in a small wind generator (160 kW) equipped with an induction machine is shown in Fig. 3.3.

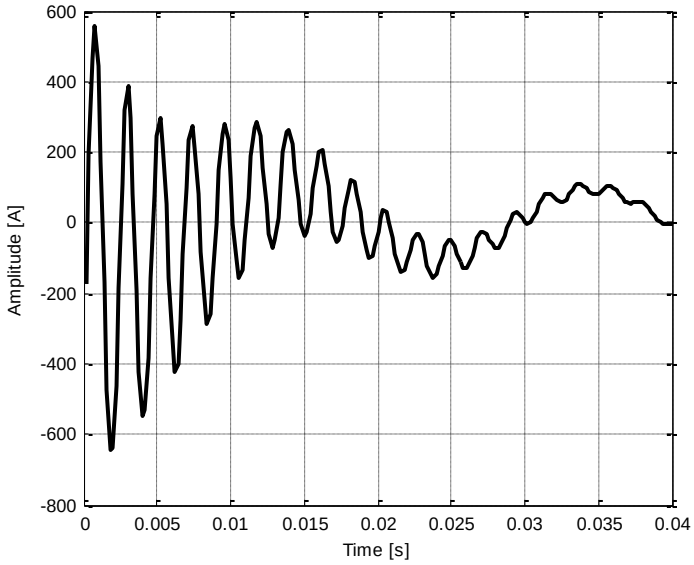

Fig. 3.3 Capacitor switching in a small wind generator with induction machine, no noise.

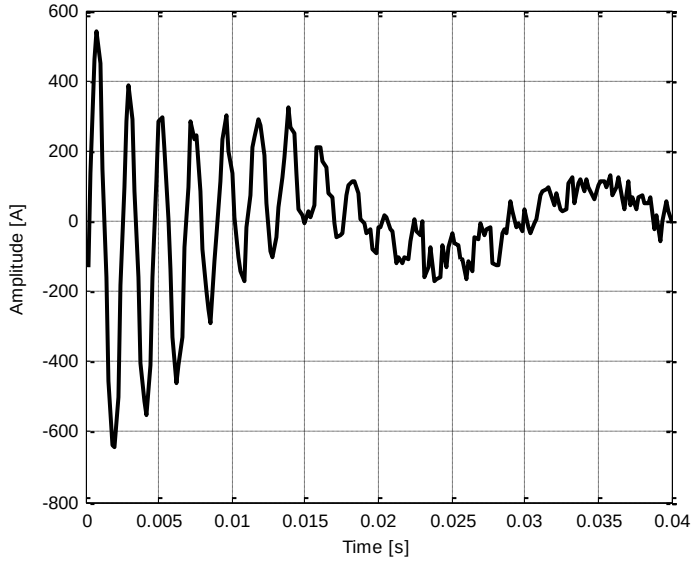

Fig. 3.4 Capacitor switching in a small wind generator, with induction machine, noise added

The results of spectral component estimation are given in Table 3.2. There are no theoretical values hence a real measured signal was analysed. The additional noise

with mean zero and standard deviation 2 was added artificially and then multiplied by 30 to increase the amplitude of distortions. Fig. 3.4 presents the distorted signal.

As in the case of signal with high harmonic content, the frequency of a decaying component was detected adequately, even in the presence of noise.

Table 3.2 Computation results of spectral components for capacitor switching operation

Frequencies of spectral components		
theoretical value [Hz]	computed, no noise [Hz]	computed, with noise [Hz]
--	48.21	49.11
--	456.31	457.67

Another common phenomenon in the public distribution gird is switching of heavy loads . Especially in weak networks or in islanded networks it results in rapid increase of current amplitude overlaid with and decaying exponential component (Fig. 3.5).

The additional noise with mean zero and standard deviation 2 was added artificially and then multiplied by 30 to increase the amplitude of distortions. Fig. 3.5 presents the distorted signal.

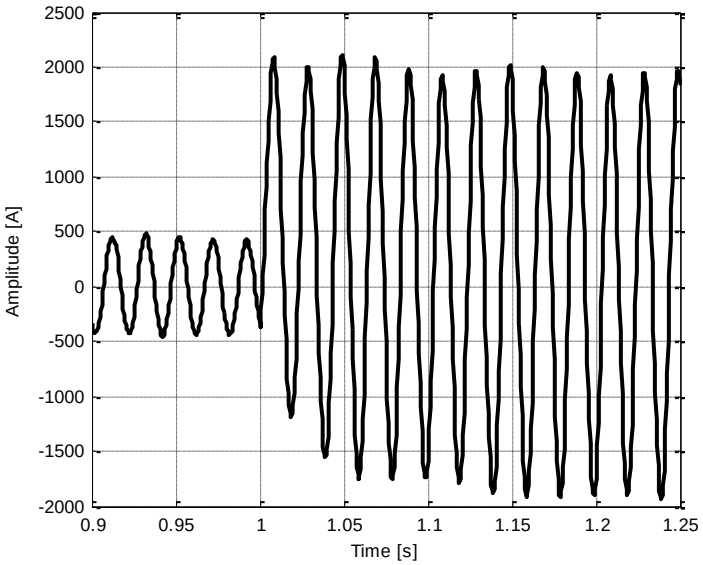

Fig. 3.5 Switching on a heavy load

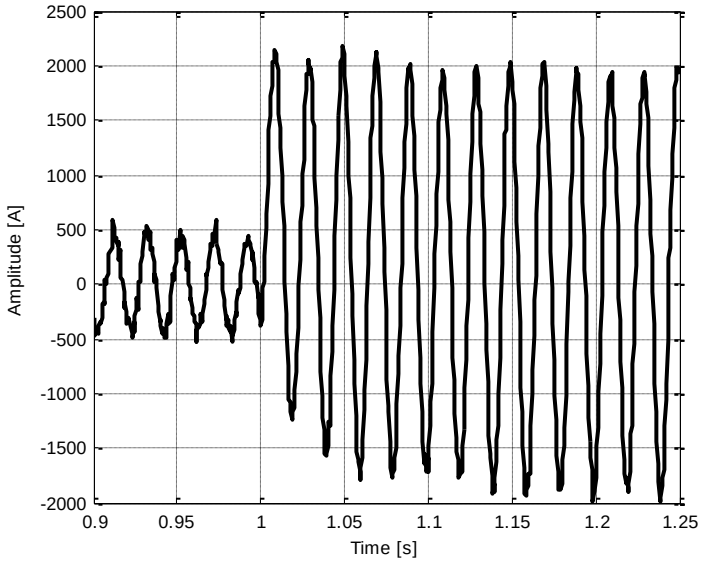

Fig. 3.6 Switching on a heavy load, with noise

Frequency estimation results are given in

Table 3.3 Computation results of spectral components for switching of a heavy load

Frequencies of spectral components		
theoretical value [Hz]	computed, no noise [Hz]	computed, with noise [Hz]
--	50.15	50.22
--	49.03	48.53

Presented method is an appropriate tool for the estimation of frequencies of spectral components in signals. The method is relatively immune against distortion by noise. Decaying exponential component or varying amplitude were also not deteriorating the computation of frequencies. Spectral components are an important factor for the estimation of power quality, i.e. *Total Harmonic Distortion* THD value, and are crucial for the proper computation of active and reactive powers for nonsinusoidal voltage and current waveforms. Therefore, the MUSIC method is regarded as an important verifying tool in the identification of spectral components' frequencies in distorted signals.

4 Optimisation

A brief characterisation of optimisation problem types and corresponding algorithms is given and followed by more rigorous formulation of an optimisation problem. Genetic algorithms and trust region reflective algorithm are presented in more extend as regarded most suitable for practical problems presented later on.

4.1 Approaches to optimisation problems

Optimisation is directly associated with decision making [31]. Obviously, best possible decision is always desired. Three aspects must be considered and translated into mathematical formulation to allow any optimisation algorithm or procedure to be applied [32], [33], [34].

Firstly, decision making is understood as selecting between various possibilities [35]. The existing possibilities are referred to as *optimisation variables*. If there is no choice then nothing can be optimised.

Secondly, an *objective function* taking one or multiple optimisation variables as its input returns an real valued output indicating the correctness or goodness of a particular choice, i.e. selected optimisation variables. Optimisation is understood as a maximisation or minimisation process regarding the value of an given objective function.

Optimisation variables are real numbers, integers or binary values corresponding to the particular choices. An integer must be used, e.g. for the number of e-cars served at a time by a micro-grid and not a real number.

Finally, there are restrictions or constrains imposed upon optimisation variables. The set of constrains includes generally equality constrains, inequality constrains and bound type constrains [36]. A relatively small number of problems allows any value of input variable. So that, there are *constrained optimisation problems* and *unconstrained optimisation problems* [37]. Decisions not violating constrains are called *feasible decision*s and the allowed inputs to the objective function are referred to as *feasible points* [38], [39].

Optimisation methods are tailored to seek the best solution in the sense of predefined objective function [40]. Algorithms and methods are grouped around problem types they are good for. There is no one universal method suitable for all types of problems.

From the mathematical point of view real unconstrained problems are the simplest to be analysed [41], [42]. A subgroup constitute one dimensional problems for which one-directional search methods exist. Most typical are *Golden Section Search*, *Fibonacci Search*, *Secant Method* [40], [31].

All unconstrained problems are mostly approached by iterative methods where the optimum is sought by maximising the decrease of objective function in every individual step. The direction of search is determined by the value of the gradient of the objective function in the *Gradient Method* [40]. The *Newton Method* uses gradient and inverse hessian of the objective function to find the descent direction [43]. Usually it performs better than Gradient Method but requires the computation of the inverse hessian matrix what is somehow troublesome. Therefore quasi Newton's methods has been proposed such as DFP or BFGS algorithms where no inverse hessian is used. A method performing better then Gradient Method but being less computationally intensive then Newton is the *Conjugated Gradient Algorithm* utilising the information of the search direction from previous iterative steps [31].

Artificial neural networks [44], [45], [46], [47] represent another useful tool for solving unconstrained problems. A neural network consist of neurons connected one with another. The input to an neuron consist of weighted outputs of neurons in previous layer. The optimisation is performed in an iterative learning algorithm, so that the output of the network and desired output value are convergent.

Constrained problems are more common. The term *linear programming* [48] refers to linear objective function which is subject to linear constrains. *Simplex Method* is an established method to handle linear programming problems. Other non-simplex methods are *Khachiyan's Method, Affine Scaling Method, Karmarkar's Method* [31].

The most general group of problems is described by an nonlinear objective function and a set of nonlinear constraints [41], [40], [49]. Equality and inequality constraints are possible. Mathematically, those problems are more difficult to define and handle. The treatment of equality and inequality constraints is often presented separately. Utilising *Lagrange function* [31], [32] it becomes possible to formulate a coherent problem which may be solved in two ways, which are known as *primal problem approach* and *dual problem approach.* It is possible due to the fact, that a solution constitutes a *saddle point* of the *Lagrange function* which is a minimum of the *primal problem* and a maximum of the *dual problem* at the same time. Sometimes it is even easier to solve the dual problem. Also the formulation of necessary and sufficient conditions for a point being a minimiser is more elaborated and is known as *Karush-Kuhn-Tucker conditions* [32].

A group of methods dedicated to nonlinear constrained problems exists. *Penalty methods* [50], [51] are a group of methods using techniques from unconstrained optimisation to solve a constrained problem. The core idea is to approximate an constrained problem with a series of unconstrained problems, consisting of the original objective function plus a parameter multiplied by a specific *penalty function* [52]. The

penalty function grows after violating or approaching the borders of the trusted region. Its value is zero within the set of feasible points. Then, the unconstrained problem is solved and its solution is used as an approximation of the minimizer of the original problem. The change of the mentioned parameter enables high convergence between the modified and original problem in a limit sense. It is true, that the solution of the original problem may not be equal to the solution of the approximated problem. It depends mostly on the penalty function and the associated parameter. Usually, the greater the value of the multiplying parameter the better the overall approximation.

Three main groups of penalty functions can be named [50], [52]. Using *inner penalty function* or *border function* there is no possibility of violating the region of feasible points throughout the whole procedure. The optimisation algorithm must start within the domain of objective function, which may be a difficulty if constrains are quite sophisticated. *Outer penalty function* enables a free selection of the starting point, even outside the trusted region. A drawback of this approach is a possibility of fulfilling a stopping criterion if the computed minimiser is located outside the domain of the goal function. *Mixed penalty function* combines the *inner* and *outer* penalty functions usually at different ends of the trusted region.

Theoretical considerations and preliminary results indicate the usefulness of *trust region reflective algorithm* and *genetic algorithm* for nonlinear constrained problems.

4.2 Mathematical Formulation

In a general way the optimisation problem can be formulated as [31], [36]

$$\begin{aligned} &\text{minimize:} && F(\mathbf{x}) \\ &\text{subject to:} && h_i(\mathbf{x}) = 0 \quad i = 1,...,m \\ & && g_j(\mathbf{x}) \le 0 \quad j = 1,...,p \end{aligned}$$

where $\mathbf{x} \in \mathbb{R}^n$, $F : \mathbb{R}^n \to \mathbb{R}$, $h_i : \mathbb{R}^n \to \mathbb{R}$, $\mathrm{g}_j : \mathbb{R}^n \to \mathbb{R}$, and $m < n$.

The above problem can also be given in a matrix notation in so called *standard form*

$$\begin{aligned} &\text{minimize:} && F(\mathbf{x}) \\ &\text{subject to:} && h(\mathbf{x}) = 0 \\ & && g(\mathbf{x}) \le 0 \end{aligned}$$

where $\mathbf{x} \in \mathbb{R}^n$, $F : \mathbb{R}^n \to \mathbb{R}$, $h : \mathbb{R}^n \to \mathbb{R}^m$, $\mathrm{g} : \mathbb{R}^n \to \mathbb{R}^p$

The multidimensional objective function F can be linear or nonlinear or even have only one dimension. The constrains are usually grouped into quality type constrains, denoted by h and inequality type constrains g.

Any point satisfying the constrains is a *feasible point* and belongs to the *feasible set* being the domain Ω of the objective function F.

$$\left\{\mathbf{x} \in \mathbb{R}^n : h(\mathbf{x}) = 0, g(\mathbf{x}) \leq 0\right\} \tag{4.1}$$

As described in previous section for various types of problem (linear, nonlinear, unconstrained, constrained) different approaches exist.

Necessary conditions for $\mathbf{x}$ being a minimiser are *Karush-Kuhn-Tucker conditions* [32]. Let $\hat{\mathbf{x}}$ be a regular point and a local minimiser for the problem of minimising $F(\mathbf{x})$ subject to constrains. Then, there exist $\boldsymbol{\lambda} \in \mathbb{R}^m$ and $\boldsymbol{\mu} \in \mathbb{R}^p$ such that following conditions are fulfilled

$$\nabla F(\hat{\mathbf{x}}) + \sum_{i=1}^{m} \lambda_i \nabla g_i(\hat{\mathbf{x}}) + \sum_{j=1}^{p} \mu_j h_j(\hat{\mathbf{x}}) = 0 \tag{4.2}$$

$$g_i(\hat{\mathbf{x}}) \leq 0 \quad \text{for} \quad i \in \{1,...,m\} \tag{4.3}$$

$$h_j(\hat{\mathbf{x}}) = 0 \quad \text{for} \quad j \in \{1,...,p\} \tag{4.4}$$

$$\lambda_i \geq 0 \quad \text{for} \quad i \in \{1,...,m\} \tag{4.5}$$

$$\lambda_i g_i(\mathbf{x}) = 0 \quad \text{for} \quad i \in \{1,...,m\} \tag{4.6}$$

Point $\hat{\mathbf{x}}$ is regarded regular if at that point exist gradients of all constrains and are linearly independent. Every point from Ω is considered regular if all constrains functions are linear (proposed by Karlin) [31].

4.3 Genetic Algorithms

Genetic algorithms can be characterised as fundamentally different from methods described in the previous section. Beginnings can be traced back to J. Holland who proposed first ideas in the begin of 1970s [53]. Genetic algorithms are deeply correlated with genetics therefore there is a similarity in the vocabulary. There is no use of any derivative of the objective function – gradient or Hessian – as it is in many other

methods. As a consequence, genetic algorithms can be successfully applied to a wide range of problems in the fields of artificial intelligence, optimization, computer programming, neural network training, etc [54], [55], [56].

A probabilistic search technique constitutes the underlying idea of this approach with many references to principles of genetic [57]. Most generally, the problem to be solved is given as an objective function $F(\mathbf{x})$ to be maximized, which is subject to constrains $\mathbf{x} \in \Omega$. Firstly, an initial set of points from Ω have to be selected and it is called the *initial population* $P(0)$ [58]. Then, the objective function has to be evaluated at points in $P(0)$ which is the prerequisite for the creation of new set of starting points denoted $P(1)$. The new set is obtained through two fundamental operations *crossover* and *mutation*. The procedure has an repetitive character, so that next populations $P(2), P(3)...$ are created. As any iterative method this algorithm is terminated after the stopping criterion was satisfied.

The crossover and mutation operations should help in the creation of new generations for which the objective function value is statistically smaller than for the previous populations [59], [60], [61].

A kind of *encoding* of the points in the domain of objective function is an prerequisite for genetic algorithm. The set of feasible points Ω must be mapped on equally long specific strings, named *chromosomes*. Chromosomes are built-up of string of symbols form a set named *alphabet*. The most simple alphabet is the set $\{0,1\}$ allowing the construction of chromosomes in the form of binary strings. Usually, the length of a chromosome is denoted with L and gives the number of elements used. The *fitness* of a chromosome is given by the value of the objective function. Often the notation $F(\mathbf{x})$ is used to describe the original objective function and to measure fitness of chromosomes in a set.

The term *representation scheme* refers to a particular problem for which the encoding mechanism, alphabet and chromosome length were chosen. In order to solve a given problem an adequate representation scheme must be identified and selected. This is the first step of the algorithm. The next one is dedicated to the initialisation of the population $P(0)$ and based on a random selection of a set of chromosomes. After the initial population was constructed than the crossover and mutation operations are applied on it. In every iterative step k the fitness measure $F(\mathbf{x}^k)$ for all elements $\mathbf{x}^k$ in the population $P(k)$ has to be computed. Based on this information, a new population $P(k+1)$ can be formed in a process including two steps.

Selection operation is applied in the first step and a set $M(k)$ with exactly the same number of elements, called *population size* N, as in $P(k)$ is constructed. The set $M(k)$ named *matting pool*, being a reshuffle of $P(k)$ is formed using a random procedure. The set $M(k)$ consist of points $\mathbf{m}^k$ equal to points $\mathbf{x}^k$ in $P(k)$ with the probability

$$\frac{F(\mathbf{x}^k)}{F_{sum}(k)} \tag{4.7}$$

where

$$F_{sum}(k) = \sum F(\mathbf{x}_i^k) \tag{4.8}$$

and the summation is done over the entire population $P(k)$. Chromosomes with probabilities proportional to their fitness are taken into the mating pool. For that reason this selection scheme is called *roulette wheel scheme*. In the imaginative roulette wheel each slot is assigned to a chromosome in $P(k)$. The number of slots associated with a particular chromosome depends on its fitness. Multiple assignments are common. For the inclusion in $M(k)$ the roulette will is span and the slot on which the ball stopped indicates the chromosome to be selected. This scheme has to be repeated N times to guarantee the same number of chromosomes in the mating pool as in the population $P(k)$.

An alternative selection scheme is called *tournament scheme*. In this scheme a pair of chromosomes has to be selected randomly from the set $P(k)$. Then, the fitness values of both chromosomes has to be compared and the chromosome with the higher value has to be selected into the mating pool $M(k)$. The procedure has to be stopped after N chromosomes are in the mating pool.

Evolution is the second stage of the algorithm in which the mutation and crossover operations take place. A pair of chromosomes named *parents* produces a new par called *offspring* chromosomes in the *crossover* operation. Exchange of substrings in the parents' chromosomes is the underlying idea for crossover operation. Pairs of parents are taken randomly from the mating pool with the probability p_c. It is assumed that the selection probability of a particular chromosome is independent from the selection of other chromosomes for the crossover procedure.

There are several ways how to randomly choose parents' chromosomes . If exactly two chromosomes were selected randomly, then $p_c = 2/N$ where N is the total number of chromosomes. If $2k$ chromosomes were taken into the mating pool forming $2k$ pairs of parents, then $p_c = 2k/N$. The number of parents' pairs and the total number of chromosomes are fixed, so that p_c depends on that number and $k < N/2$. On the contrary, for a preselected value of p_c a random number of parents' pairs to reach an average number of pairs equal to $k = p_c N/2$.

After the determination of the parents the crossover operation must be applied on them. There are several ways how to realize the crossover operation. The most simple one is called *one-point crossover* (Fig. 4.1).

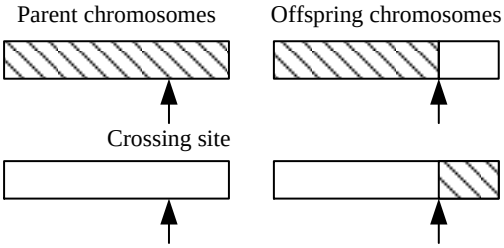

Fig. 4.1 Crossover operation at one point

In this approach a random number between 1 and $L-1$have to be chosen with accordance to an uniform distribution. L is the chromosome's length. This random number is called *crossing site* where substrings of the parents are exchanged to the right of the crossing site.

Crossover operation can be performed at multiple crossing sites at one time (Fig. 4.2).

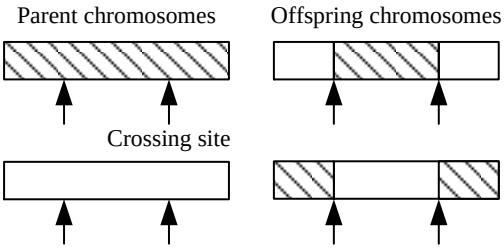

Fig. 4.2 Crossover operation at two points

Two chromosomes 00000000 and 11111111 with the length $L=8$ can be considered an example. Two crossing sides are given at 2 and 5. Two offspring chromosomes are derived from the parents after the application of crossover operation: 11000111 and 00111000.

The parent's chromosomes are replaced by the offspring in the mating pool after the crossover operation. It can be noticed, that the mating pool, however changed, still has the same number of chromosomes.

In the further step the *mutation* operation has to be applied (Fig. 4.3).

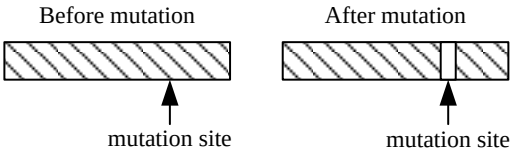

Fig. 4.3 Illustration of mutation operation

In the mutation operation each chromosome from the mating pool undergoes an random change of each symbol with a given probability p_m. When binary alphabet is used this operation means the change of the bit value from 0 to 1 and from 1 to 0 with the probability p_m. If there are more than two symbols used in the alphabet, then a symbol is randomly substituted by another element of the alphabet. Usually, the probability value p_m is very small, e.g. smaller than 0.001. Accordingly, only a few of the chromosomes are changed due to mutation and in those affected only a few of the symbols are modified. Relatively, the mutation operation has a minor priory in the genetic algorithm as the crossover operation.

The result of crossover and mutation operations on the mating pool $M(k)$ is a new population $P(k+1)$. Once again, the procedures of evaluation, selection and evolution has to be repeated. A rudimentary flowchart of the algorithm is given in Fig. 4.4.

Throughout the whole iterative genetic procedure the *best-so-fare* chromosome, i.e. the chromosome with the best fitness, is regarded as a possible solution to the original problem [62]. This chromosome is copied without changes into each new population according to a procedure called *elitism*. This strategy results in the domination of the population by the best chromosomes and usually improves the performance of the algorithm.

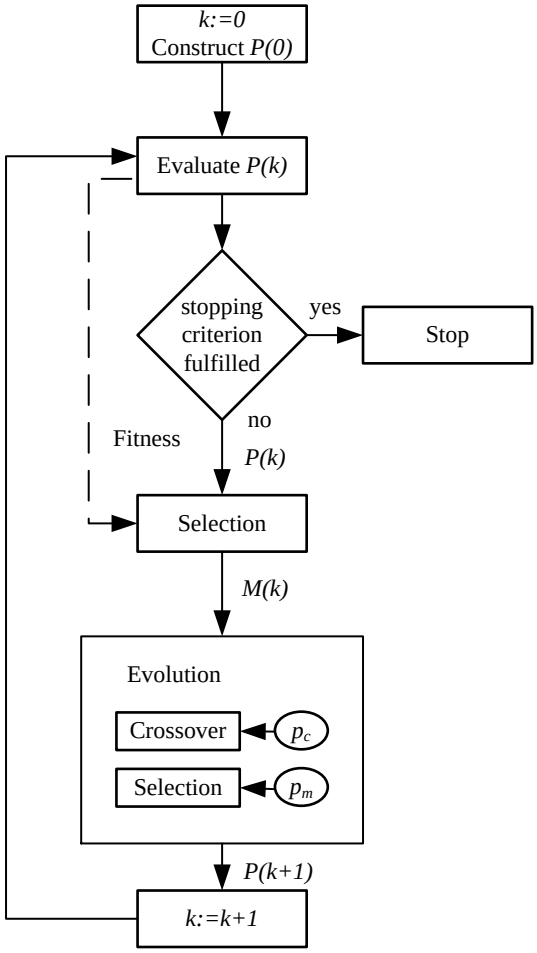

Fig. 4.4 Genetic algorithm flow chart

There exist various possibilities for the implementation of a stopping criterion. A predefined number of iteration is a very simple solution. Another criterion is to stop when the fitness for the best-so-fare chromosome changes very little during subsequent iterations or to stop when the fitness has trespassed a pre-specified value.

Genetic algorithm presented above worked with binary strings which represented elements of the domain of the objective function.

For simplification reasons the above description is restricted to binary strings which are encoded elements from the original domain Ω. Binary representation enables simple analysis of algorithms. Similarly, the objective function $F(\mathbf{x})$ is not the original goal function, but a composition of F and the decoding function g, so that the problem can be formulated as

$$\text{maximise: } F\left(g\left(\mathbf{x}\right)\right)$$
$$\text{subject to: } \mathbf{x} \in \{\mathbf{y} \in \{0,1\}^L : g\left(\mathbf{y}\right) \in \Omega\}$$

where $g : \{0,1\}^L \to \Omega$ is a decoding function. The modified problem may be more complex and may have additional local minimisers making the search for the global minimum even more troublesome.

Therefore, algorithm operating directly on the domain Ω, in other words on a subset of $\mathbb{R}^n$, seems more suitable for the applications dedicated to practical problems. The procedure is identical with the previous one (Fig. 4.4) with the only difference, that the members of the population are taken directly from Ω. Accordingly, the crossover and mutation operations have to be redefined. Various possibilities exist.

Averaging is an option for crossover [63]. The offspring

$$\mathbf{d} = \left(\mathbf{a} + \mathbf{b}\right)/2 \tag{4.9}$$

is an average of the parents' vectors $\mathbf{a}$ and $\mathbf{b}$. In a modified approach, randomly generated vectors $\mathbf{w}_i$ with a zero mean can be added to the average (4.9). If necessary, a procedure called projection can be used [64] to guarantee that the offspring will not violate the set of feasible points Ω. Next possibility for crossover is to take random convex combinations of the parents. For a pair of parents' vectors $\mathbf{a}$ and $\mathbf{b}$ a random number $\alpha \in \left(0,1\right)$ has to be generated to enable the computation of two offspring chromosomes

$$\mathbf{d}_1 = \alpha\mathbf{a} + \left(1-\alpha\right)\mathbf{b} + \mathbf{w}_1 \tag{4.10}$$

$$\mathbf{d}_2 = \left(1-\alpha\right)\mathbf{a} + \alpha\mathbf{b} + \mathbf{w}_2 \tag{4.11}$$

This procedure does not allow the offspring to violate the set of feasible points, therefore no checking is needed in subsequent iterative steps. Only assumption for that is that Ω is a convex set.

Addition of a random vector $\mathbf{w}$ to the chromosome is the simplest implementation of mutation. For a given chromosome $\mathbf{a}$ the mutation is given as

$$\mathbf{a}' = \mathbf{a} + \mathbf{w} \tag{4.12}$$

and called *reel number creep*. As ever, mutated chromosome must be located in the feasible region.

Another method for mutation is a replacement of the given chromosome with a randomly generated vector in the domain Ω. Random number $\alpha \in (0,1)$ and a random vector $\mathbf{w} \in \Omega$ are used to express the mutated chromosome

$$\mathbf{a}' = \alpha\mathbf{a} + (1-\alpha)\mathbf{w} \tag{4.13}$$

If the domain Ω is convex, the mutated chromosome will also belong to the feasible set.

The most important features of a genetic algorithm can be summarised as follows :

- it works with an encoding of the feasible set, rather than the set itself
- it searches from a set of points rather than a single point at each iteration
- it does not use derivatives of the objective function
- it uses operations that are random within each iteration.

4.4 Trust Region Reflective Algorithm

Trust region reflective algorithm is dedicated to minimisation of a smooth nonlinear function which is subject to bound type of constrains. It is considered suitable for the solution of least squared problems [65], [66].

An over-determined system of linear equations

$$\mathbf{A}\mathbf{x} = \mathbf{b} \tag{4.14}$$

has no solution. The objective of this least-square linear problem can be altered to find a vector $\mathbf{x}$ minimizing

$$\min_{\mathbf{x}} \|\mathbf{A}\mathbf{x} - \mathbf{b}\|^2 \tag{4.15}$$

the vector $\hat{\mathbf{x}}$ is considered the least squares solution of (4.15) and is given as

$$\hat{\mathbf{x}} = \left(\mathbf{A}^T\mathbf{A}\right)^{-1}\mathbf{A}^T\mathbf{b} \tag{4.16}$$

In a case of a general nonlinear least squares problem

$$\min\left(r(\mathbf{x})^2\right) \tag{4.17}$$

the solution can be found by an iterative method. An adopted Newton's method procedure is given as

$$\mathbf{x}^{k+1} = \mathbf{x}^k - \left(\mathbf{J}\left(\mathbf{x}\right)^T \mathbf{J}\left(\mathbf{x}\right) + \mathbf{S}\left(\mathbf{x}\right) \right)^{-1} \mathbf{J}\left(\mathbf{x}\right) r\left(\mathbf{x}\right) \tag{4.18}$$

Often modifications of (4.18) called *Gauss Newton Method* or *Levenberg-Marquard Algorithm* are in use [31].

For quadratic programming problems with bound type constrains further modifications are necessary in the iterative process. The Trust Region Method seems to be well suited. According to Tylor's theorem [67], within a sufficient small neighborhood (trust region) of the point $\hat{\mathbf{x}}$ the function $r\left(\mathbf{x}^k + \mathbf{s}\right)$ can be approximated by

$$r\left(\mathbf{x}^k\right) + \psi_k\left(\mathbf{s}\right) \tag{4.19}$$

where

$$\psi_k\left(\mathbf{s}\right) = \mathbf{g}_k^T \mathbf{s} + \frac{1}{2} \mathbf{s}^T \mathbf{H}_k \mathbf{s} \tag{4.20}$$

and the original problem (4.17) is replaced by

$$\min\left(\psi_k\left(\mathbf{s}\right) = \mathbf{g}_k^T \mathbf{s} + \frac{1}{2} \mathbf{s}^T \mathbf{H}_k \mathbf{s} \ : \ \left\| \mathbf{D}_k \mathbf{s} \right\| < \Delta_k \right) \tag{4.21}$$

with $\left\| \mathbf{D}_k s \right\| < \Delta_k$ defining the trust region. Algorithm idea given in [68] needs further modifications to incorporate the bound type constrains

$$\psi_k\left(\mathbf{s}\right) = \mathbf{g}_k^T \mathbf{s} + \frac{1}{2} \mathbf{s}^T \left(\mathbf{H}_k + \mathbf{C}_k \right) \mathbf{s} \tag{4.22}$$

where

$$\mathbf{C}_k = \mathbf{D}_k diag\left(\mathbf{g}_k\right) \mathbf{J}_k^v \mathbf{D}_k \tag{4.23}$$

is a positive definite matrix with the information of constrains. The minimizer is sought in an iterative method solving (4.21).

5 Power for sinusoidal waveforms

5.1 Preliminary considerations

Generally, the presence of a voltage u results in replacement of an elementary charge dq in a conducting element over the elementary time dt. The voltage is understood as electric potential difference between points A and B in the presence of electric field with an intensity $\mathbf{E}$

$$u = V_A - V_B = \int_{AB} \mathbf{E} dl \tag{5.1}$$

If the conducting element is located in magnetic field, then the induced voltage u is proportional to the change of magnetic flux Φ

$$u = \frac{d\Phi}{dt} \tag{5.2}$$

The elementary work dW, i.e. elementary energy delivered to the load equals

$$dW = udq = uidt \tag{5.3}$$

The derivative of electrical energy dW with regard to time is the measure of energy delivery fastness

$$p = \frac{dW}{dt} = ui \tag{5.4}$$

In electrical circuits the product of voltage and current is an expression for *instantaneous power* p. Consequently, the energy delivered over a closed time interval is an integral of p

$$W = \int_{t_1}^{t_2} p\,dt \tag{5.5}$$

5.2 Circuits with sinusoidal voltages and currents

These considerations are restricted to linear time invariant systems (LTI) whereas the voltages and currents at various circuit elements are purely sinusoidal, i.e. the instantaneous values are defined as

$$\begin{aligned} u(t) &= \sqrt{2}U \sin(\omega t + \psi_U) \\ i(t) &= \sqrt{2}I \sin(\omega t + \psi_I) \end{aligned} \tag{5.6}$$

In linear circuits with sinusoidal current and voltage waveforms of the same frequency the phase shift between voltage and current is denoted with $\varphi = \psi_U - \psi_I$. Assuming, that initial phase in the voltage is equal to zero, i.e. $u = \sqrt{2}U \sin(\omega t)$, the instantaneous power is expressed as

$$\begin{aligned} p = ui = \sqrt{2}U\sqrt{2}I \sin(\omega t)\sin(\omega t - \varphi) = \frac{\sqrt{2}U\sqrt{2}I}{2}\left(\cos(\varphi) - \cos(2\omega t - \varphi)\right) = \\ = UI\left(\cos(\varphi) - \cos(2\omega t - \varphi)\right) = UI\cos(\varphi) - UI\cos(2\omega t - \varphi) \end{aligned} \tag{5.7}$$

Instantaneous power (5.7) has two components:

- the constant term $UI\cos\varphi$
- the variable term $UI\cos(2\omega t - \varphi)$ with two times higher frequency.

The instantaneous power p oscillates sinusoidal around the constant term $UI\cos\varphi$ with doubled frequency $2f$. The amplitude of oscillations is UI .The maximum value of p in (5.7) is reached when the argument of the variable term is $k\pi$

$$p_{\max} = UI\cos\varphi + UI \tag{5.8}$$

The minimum value of p is reached for the value of variable term equal to zero

$$p_{\min} = UI\cos\varphi - UI \tag{5.9}$$

The value of the constant term changes with accordance to the phase shift φ defining the character of the load (inductive, capacitive). The maximum of the constant term equal to UI is reached for $\varphi = 0$ (purely resistive load) and the minimum 0 for $\varphi = \pm\pi / 2$.

In three phase system the instantaneous power is the sum of powers in all three phases.

5.3 Active, reactive and apparent power

Generally, the energy transport from a source to a load is characterised by terms of power. In one phase circuits with sinusoidal currents and voltages that are *active power* P*, reactive power* Q *and apparent power S.* Every power has a strict technical meaning.

The energy delivered to a source (5.5) in precisely one cycle is given by

$$W_T = \int_t^{t+T} p\,dt \tag{5.10}$$

The energy in (5.10) divided by time T gives the average value of instantaneous power over one period, defining active power P given in watts [W]

$$P = \frac{1}{T}\int_0^T p\,dt = \frac{1}{T}\int_0^T \left(UI\cos\varphi - UI\cos\left(2\omega t - \varphi\right)\right)dt = UI\cos\varphi \tag{5.11}$$

Active power is always non negative and reaches its maximum for a purely resistive load. The integral of active power over a clearing period gives the amount of energy delivered to a consumer, indirectly the sum to be paid to the utility.

Electrical equipment, i.e. electrical drives, transformers, apparatus, have nominal values of voltage and current. The voltage values results from isolation durability and current values are restricted by heating and electro-dynamic forces. Therefore, electrical equipment is characterized by the product of voltage and current RMS values, called *apparent power* S with the unit volt-ampere [VA]

$$S = \sqrt{\frac{1}{T}\int_0^T u^2 dt}\cdot\sqrt{\frac{1}{T}\int_0^T i^2 dt} = UI \tag{5.12}$$

Apparent power gives the maximal possible value of active power for a given voltage U and current I. The ratio of active power to apparent power defines the power factor PF for sinusoidal waveforms

$$PF = \frac{P}{S} = \frac{P}{\sqrt{P^2 + S^2}} = \frac{UI\cos\varphi}{UI} = \cos\varphi \tag{5.13}$$

The design and dimensioning process of electrical energy distribution system requires precise information about apparent power of distribution system elements.

Reactive power Q with the unit volt-ampere reactive [var] is often regarded as unwanted power component accompanying active power if a load causes a phase shift between voltage and current

$$Q = \frac{1}{T}\int_0^T u(t)\,i(t - \frac{T}{4})dt = UI\sin\varphi \tag{5.14}$$

The presence of reactive power in one phase circuit is a result of reactive elements, such as inductances and capacitors. In a serial connected RL or RC branch the voltage is expressed as $U\sin\varphi = XI$, in a parallel branch $I\sin\varphi = -BU$, therefore

$$Q = XI^2 = BU^2 \tag{5.15}$$

In an inductive circuit the phase shift φ between current and voltage is positive and in a capacitive circuit it is negative. If $\varphi > 0,\ Q > 0$ inductive reactive power is positive. If $\varphi < 0,\ Q < 0$ capacitive reactive power is negative.

Rewriting (5.7) the instantaneous power in sinusoidal circuits can be expressed as

$$\begin{aligned} &p = ui = UI\cos\varphi - UI\cos\varphi\cos 2\omega t - UI\sin\varphi\sin 2\omega t = \\ &= UI\cos\varphi(1 - \cos 2\omega t) - UI\sin\varphi\sin 2\omega t = P(1 - \cos 2\omega t) - Q\sin 2\omega t = \\ &p_a + p_r \end{aligned} \tag{5.16}$$

That is as a sum of a non-negative term $p_a = P(1 - \cos 2\omega t)$ and an oscillatory term $p_r = Q\sin 2\omega t$. The reactive power Q in (5.16) is interpreted as the amplitude of the oscillatory term of instantaneous power.

The current drown form the source has the form

$$i = \sqrt{2}I\cos\varphi\cos\omega t + \sqrt{2}I\sin\varphi\sin\omega t = \sqrt{2}\frac{P}{U}\cos\omega t + \sqrt{2}\frac{Q}{U}\sin\omega t \tag{5.17}$$

and the corresponding RMS value of the current

$$\|i\| = \sqrt{\left(\frac{P}{U}\right)^2 - \left(\frac{Q}{U}\right)^2} \tag{5.18}$$

Reactive power Q in sinusoidal circuits has an extraordinary significance due to three major properties:

- reactive power has an unambiguous physical interpretation as the amplitude of the oscillatory term in instantaneous power. Reactive power equal to zero means no energy oscillations between source and load. The energy flaw however, due to the form of p_a has an pulsative character.
- reactive power Q and active power P along with voltage U define the RMS value of the current (5.18).
- the compensation of reactive power to zero $Q = 0$, reduces current RMS value to its minimum. The energy oscillations and additional losses are reduced to zero.

Setting together the equations (5.11), (5.12) and (5.14) the apparent power equals

$$S = \sqrt{P^2 + Q^2} \tag{5.19}$$

and

$$\tan\varphi = \frac{Q}{P} \tag{5.20}$$

Equations (5.19) and (5.20) can be illustrated graphically, forming a power triangle (Fig. 5.1).

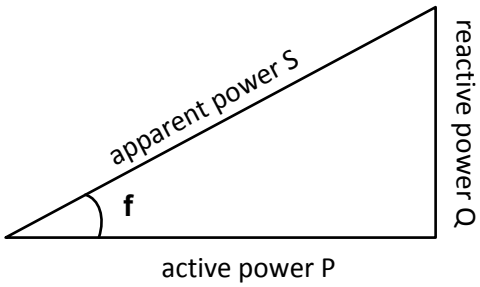

Fig. 5.1 Triangle of powers

Applying the notation manner used in (5.11) and (5.14) the apparent power may be also expressed as

$$S = \sqrt{\frac{1}{T}\int_0^T u^2(t)\,dt}\sqrt{\frac{1}{T}\int_0^T i^2(t)\,dt} = UI \tag{5.21}$$

5.3.1 Apparent power expressed with complex numbers

Sinusoidal voltage at the clamps of an inductive branch results in a timely shifted current (Fig. 5.2).

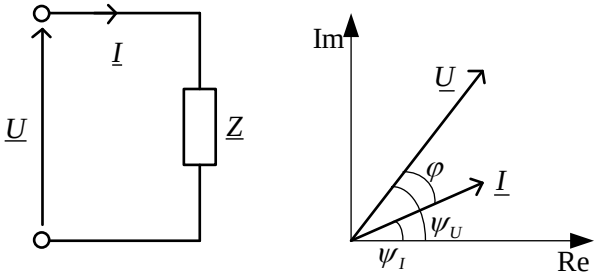

Fig. 5.2 Inductive branch with corresponding vector diagram

Voltage and current can be expressed as complex values

$$\underline{U} = Ue^{j\psi_U} \qquad \underline{I} = Ie^{j\psi_I} \tag{5.22}$$

The apparent power is given as

$$\underline{S} = P + jQ = UI\cos\varphi + jUI\sin\varphi = UIe^{j\varphi} \tag{5.23}$$

From Fig. 5.2 it is visible that $\varphi = \psi_U - \psi_I$ and (5.23) may be rewritten

$$\underline{S} = UIe^{j(\psi_U - \psi_I)} = Ue^{j\psi_U} Ie^{j\psi_I} = \underline{U}\,\underline{I}^* \tag{5.24}$$

Apparent power in complex form is also a product of the RMS value of voltage and conjugate complex value of current. The expressions for active and reactive power can be directly obtained from (5.24), '*' denotes complex conjugate

$$P = \mathrm{Re}\left(\underline{UI}^*\right) \qquad \mathrm{Q{=}Im\,Re}\left(\underline{UI}^*\right) \tag{5.25}$$

5.4 Powers in sinusoidal three phase systems

A three phase system with sinusoidal currents and voltages can be characterised in terms of power with previously presented concepts. Symmetrical and unsymmetrical circuits require different approaches, whereas symmetrical circuit allows fare reaching simplifications. Classical treatment of power measurement assumes usage of analogue watt meters. However, the same approach is also built into modern PQ analysers.

5.4.1 Load connections in delta and wye

The analysis of a sinusoidal three phase system is usually performed via symbolic method approach. The voltages and currents are given as complex numbers. A four wire, wye connected circuit is shown in Fig. 5.3.

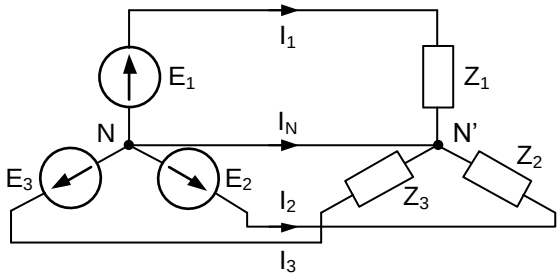

Fig. 5.3 Three phase wye connected circuit

Assuming equal RMS voltage values and symmetrical load the currents are also symmetrical

$$\underline{I}_1 = \underline{I}_2 = \underline{I}_3 \tag{5.26}$$

Obviously, the current in the neutral wire is zero $I_N = 0$.

The active power is

$$P = 3P_1 = 3U_1 I_1 \cos\varphi = 3RI_1^2 = \sqrt{3}U_{LL} I_L \cos\varphi \tag{5.27}$$

In case of an unsymmetrical load the powers in every phase must be computed separately and added. In a similar way to (5.27) the reactive and apparent power can be obtained

$$Q = 3U_1 I_1 \sin\varphi = 3XI_1^2 = \sqrt{3}U_{LL} I_L \sin\varphi \tag{5.28}$$

$$S = 3U_1 I_1 = 3ZI_1^2 = \sqrt{3}U_{LL} I_L \tag{5.29}$$

In the case of a load connected in delta (Fig. 5.4) the line to line voltages are equal to the respective source voltages.

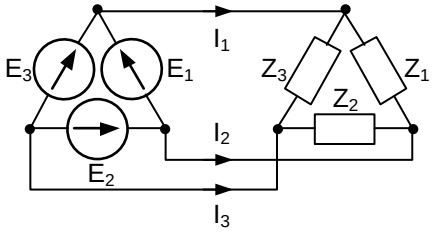

Fig. 5.4 Delta connected three phase circuit

$$\underline{E}_1 = \underline{U}_{12} \tag{5.30}$$

In symmetrical case all he voltages sum up to zero

$$\underline{U}_{12} + \underline{U}_{23} + \underline{U}_{31} = 0 \tag{5.31}$$

The line to line currents are $\sqrt{3}$ higher than line currents, therefore the active power in one phase is

$$P = 3P_1 = 3U_{12}I_{12}\cos\varphi = RI_{12}^2 = \sqrt{3}U_{12}I_1\cos\varphi \tag{5.32}$$

Analogically, the reactive power and apparent power are given as

$$Q = 3U_{12}I_{12}\sin\varphi = 3XI_{12}^2 = \sqrt{3}U_{12}I_1\sin\varphi \tag{5.33}$$

$$S = 3U_{12}I_{12} = 3ZI_{12}^2 = \sqrt{3}U_{12}I_1 \tag{5.34}$$

A practical consequence from above considerations is a unique to power computation, regardless the connection of the load. Required are only line to line voltage, line current and the sin or cos value of the load phase shift.

5.4.2 Measurement in circuits with symmetrical load

The RMS values of voltages are equal and shifted by 120° in every phase. A symmetrical three phase circuit with sinusoidal voltages and currents represents the simplest case for power computation. Active power can be measured with only one wattmeter, as the result is three times the value indicated by the meter,

$$P = 3P_1 \tag{5.35}$$

whereas the voltage claps are connected to L_1 and N. In circuit without the neutral wire N an artificial neutral point must be provided. Usually, three equal, highly resistive elements are used (Fig. 5.5).

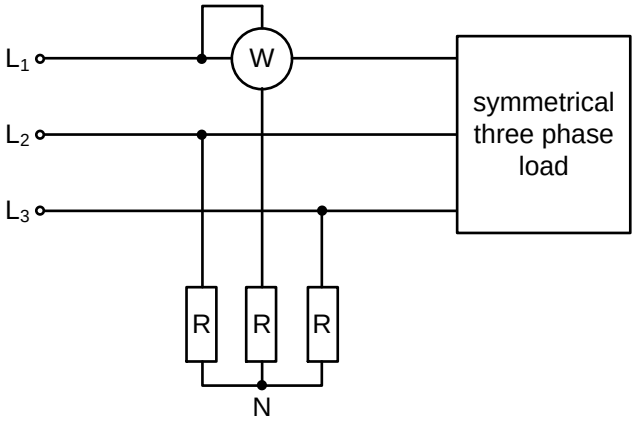

Fig. 5.5 Active power measurement with artificial neutral point

An alternative method in circuits without neutral is a measurement with two wattmeters. The apparent power is given by an complex expression

$$\underline{S} = \underline{U}_{L1}\underline{I}_{L1}^{*} + \underline{U}_{L2}\underline{I}_{L2}^{*} + \underline{U}_{L3}\underline{I}_{L3}^{*} \tag{5.36}$$

The sum of three line currents is zero

$$\underline{I}_{L1} + \underline{I}_{L2} + \underline{I}_{L3} = 0 \tag{5.37}$$

Consequently, the sum of complex conjugated currents is also equal zero, therefore

$$\underline{S} = \left(\underline{U}_{L1} - \underline{U}_{L3}\right)\underline{I}_{L1}^{*} + \left(\underline{U}_{L2} - \underline{U}_{L3}\right)\underline{I}_{L2}^{*} = \underline{U}_{L1L3}\underline{I}_{L1}^{*} + \underline{U}_{L2L3}\underline{I}_{L3}^{*} \tag{5.38}$$

The active power is the real part of apparent power in (5.38)

$$P = \mathrm{Re}\,\underline{S} = U_{L1L3}I_{L1}\cos\varphi_1 + U_{L2L3}I_{L2}\cos\varphi_2 \tag{5.39}$$

whereby the angles φ_1 and φ_2 are measured between the line to line voltage and corresponding current. The connection of wattmeters is a direct result of the (5.39) relationship and was named after Herman Aron (Fig. 5.6).

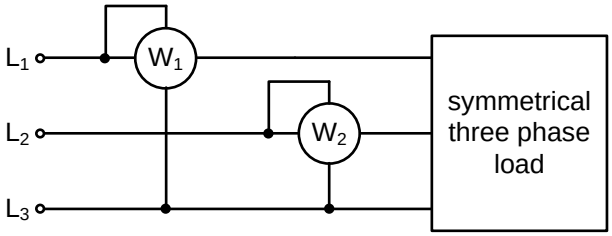

Fig. 5.6 Aron connection

Expressing $\underline{I}_{L2}$ or $\underline{I}_{L1}$ as a function of the two remaining currents (5.37) results in two additional ways how to connect the wattmeters.

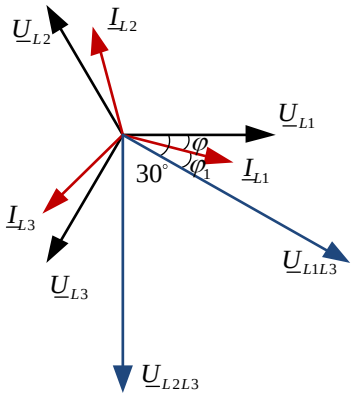

Fig. 5.7 Voltage and current vectors in symmetrical circuit with inductive load

Voltage and currents vectors in Fig. 5.7 correspond with (5.39). The load is symmetric, wye-connected and inductive. In a symmetric circuit the phase angels are

$$\varphi_1 = \varphi - 30^\circ \quad \varphi_2 = \varphi + 30^\circ \tag{5.40}$$

moreover

$$U_{L1L3} = U_{L2L3} = U_{LL} \qquad I_{L1} = I_{L2} = I_L \tag{5.41}$$

Inserting (5.40), (5.41) to (5.39) gives

$$P = U_{LL} I_L \cos\left(\varphi - 30^\circ\right) + U_{LL} I_L \cos\left(\varphi + 30^\circ\right) = P_1 + P_2 = \sqrt{3} U_{LL} I_L \cos\varphi \tag{5.42}$$

The values indicated by two watt meters are generally unequal (Fig. 5.8). Only with symmetrical resistive load the indication are equal. If the phase angle φ is in the

range $\pm\frac{\pi}{3}$ then both watt meters readings are positive. In the range $\left[\frac{\pi}{3},\frac{\pi}{2}\right]$ and $\left[-\frac{\pi}{3},-\frac{\pi}{2}\right]$ the readings have different signs.

The measuring arrangement in Fig. 5.6 can be directly applied for the determination of reactive power

$$P_1 - P_2 = U_{LL} I_L \cos\left(\varphi - 30^\circ\right) - U_{LL} I_L \cos\left(\varphi + 30^\circ\right) = U_{LL} I_L \sin\varphi \tag{5.43}$$

therefore the reactive power

$$Q = \sqrt{3} U_{LL} I_L \sin\varphi \tag{5.44}$$

Consequently, the phase shift may be determined using only the readings of two watt meters. From (5.42) and (5.43) we get the expression

$$tg\varphi = \sqrt{3}\frac{P_1 - P_2}{P_1 + P_2} \tag{5.45}$$

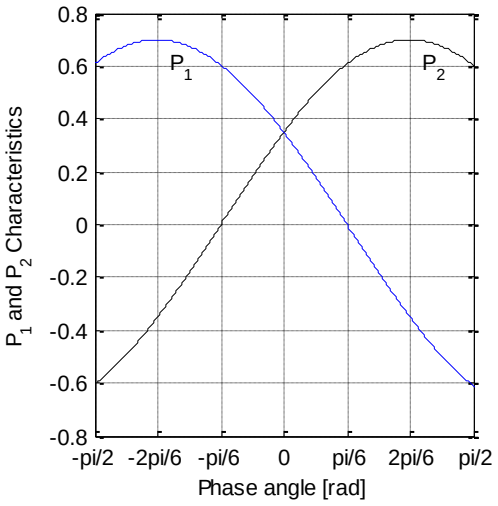

Fig. 5.8 Wattmeters readings as a function of phase shift φ

An alternative method utilises only one wattmeter to determine the reactive power in a symmetrical circuit (Fig. 5.9).

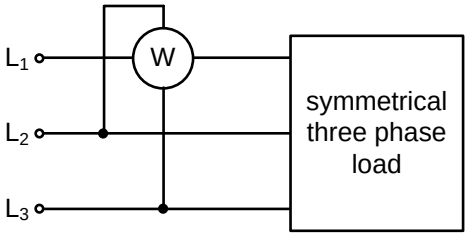

Fig. 5.9 Reactive power measurement

The reactive power is given by

$$Q = \sqrt{3} U_{L2L3} I_{L1} \cos\left(90^{\circ} - \varphi\right) = \sqrt{3} U_{LL} I_L \sin\varphi \tag{5.46}$$

5.4.3 Measurements in circuit with unsymmetrical load

In an unsymmetrical circuit, relation (5.36) is used for the computation of apparent power. Active power is the real part of (5.36). Consequently, three watt meters must be used

$$P = U_{L1} I_{L1} \cos\varphi_{L1} + U_{L2} I_{L2} \cos\varphi_{L2} + U_{L3} I_{L3} \cos\varphi_{L3} \tag{5.47}$$

This method can only be used in the presence of the neutral wire N (Fig. 5.10).

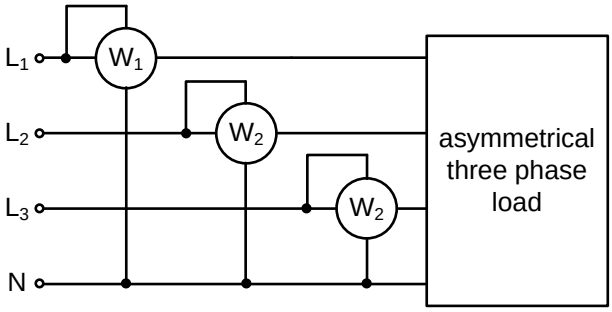

Fig. 5.10 Active power measurement with three watt meters

Two meters method – Aron connection – can be used to in unsymmetrical circuits. Circuits without neural and withholding (5.37) are suitable for Aron method. The algebraic sum of readings (5.42) is correct for symmetrical and non-symmetrical circuits.

6 Active and reactive power concepts for non-sinusoidal circuits

Experimenting with a mercury arc devices Ch. P. Steinmetz observed in 1892 a certain irregularity [69]. Despite of the lack of reactive power Q, the value of apparent power S was higher than active power P. This observation started a long discussion about power properties of non-sinusoidal circuits [70], [71], [72].

The historical approaches along with definitions for sinusoidal currents are inevitable for the contemporary understanding of power concepts. The most crucial ideas and approaches are presented in brief form.

Pioneers, Budeanu and Fryze, proposed two complementary approaches in frequency domain and in time domain respectively [73].

6.1 Reactive Power proposal by Budeanu

The active and reactive power for sinusoidal waveforms are given by (5.11) and by (5.14). Moreover, active power for non-sinusoidal but periodic waveforms can be expressed as

$$P = \sum_{n=0}^{\infty} U_n I_n \cos\varphi_n \tag{6.1}$$

In a natural way Constantin Budeanu proposed in 1927 a definition for reactive power of non-sinusoidal voltages and currents [74]

$$Q = Q_B = \sum_{n=0}^{\infty} U_n I_n \sin\varphi_n \tag{6.2}$$

This definition was then widely popularised [75], [76], accepted by CIGRE [77] and included into the IEEE standard dictionary of electrical and electronics terms. Definition (6.2) was interpreted as a measure of energy oscillation between a source and a load.

Despite similarity of Q_B to reactive power in sinusoidal circuits, relation (5.19) is not more valid, instead

$$P^2 + Q_B^2 \le S^2 \tag{6.3}$$

Budeanu reactive power Q_B is not more the gap between active and apparent power. To fill the gap an additional component has been introduced. The new *distortion power* D component is given as

$$D = \sqrt{S^2 - P^2 - Q_B} \tag{6.4}$$

This component can be interpreted as a measure of apparent power increase caused by distortions in the periodical current and voltage waveforms. The power equations is given as

$$S^2 = P^2 + Q_B^2 + D^2 \tag{6.5}$$

Graphical interpretation of (6.5) is presented in Fig. 6.1 as a cuboid of powers.

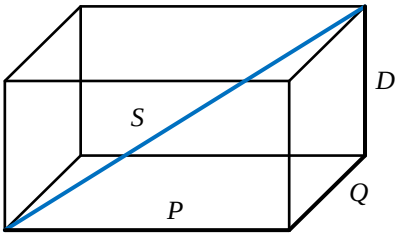

Fig. 6.1 Cuboid of powers

Practical computation and utilisation of Q_B is restricted by certain obstacles. Precise Fourier transformation [25] is a necessary prerequisite. Discrete Fourier Transform requires [78] a measurement window length exactly matching an integer multiply of the fundamental component period [79]. Variations of power system frequency cause leakage effect [80], introducing fictive spectral components and deteriorating Q_B computation accuracy. Usually windowing is used to minimise leakage [81], but it introduces unwanted phase shift in spectral components. According to (6.2) exact phase computation of voltage and current is needed to guarantee reliable values of Q_B. Despite a proposal [76] to compute Q_B in time domain

$$Q_B = \frac{1}{T}\int_0^T u(t)H\left(i(t)\right)dt \tag{6.6}$$

Fourier series expansion necessity is a considerable drawback of the original (6.2) proposal. A considerably sophisticated signal processing is needed.

An alternative method of computing reactive power by means of simple watt meters was proposed in [82]. It slightly differs from (6.2) by the term $\frac{1}{n}$ or n into the definitions

$$Q_{ICap} = \sum_{0}^{\infty} nU_n I_n \sin\varphi_n \tag{6.7}$$

$$Q_{IInd} = \sum_{0}^{\infty} \frac{1}{n} U_n I_n \sin\varphi_n \tag{6.8}$$

Those terms are a result of a capacitive or inductive character of the wattmeter's voltage circuit (Fig. 6.2).

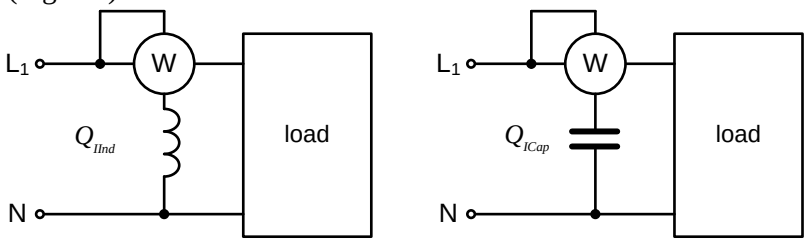

Fig. 6.2 Wattmeter based evaluation of reactive power by Illovici

The power component defined by (6.7) or (6.8) can be relatively simply measured, but the resulting value do not fulfil (6.5) and it is not suitable for the dimensioning of a compensator [70]. Also compensation of Q_B is not a straightforward way for achieving a minimal current in a circuit by the same active power of the load [83].

Budeanu proposal is considered a fundamental framework in the frequency domain [73]. An alternative framework proposed in parallel restricts power components considerations to time domain.

6.2 Reacive Power by Fryze

A purely resistive load can be regarded optimal in terms of supply efficiency. This assumption motivated S. Fryze to restrict power components considerations solely to time domain [84].

Regarding the active power P, a purely resistive load is an equivalent of a particular load fed by the same supply voltage if

$$G_{equiv} \|u\|^2 = P \tag{6.9}$$

i.e. the conductance G_{equiv} of the purely resistive load is

$$G_{equiv} = \frac{P}{\|u\|^2} \tag{6.10}$$

where G_{equiv} is an *equivalent conductance* and P stands for the active power of a particular load. The current over the resistive equivalent load is

$$i_{active}(t) = G_{equiv} u(t) \tag{6.11}$$

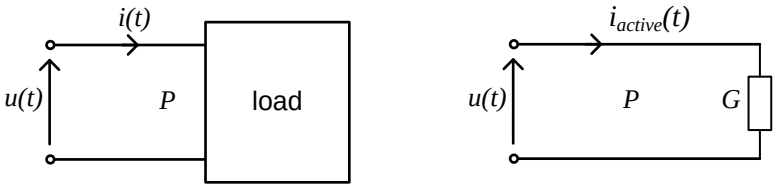

Fig. 6.3 Equivalent circuits in terms of active power by Fryze

The value of the *active current* i_{active} is minimal and exactly guaranteeing that the load consumes active power P. The rms value of the active current is

$$\|i_{active}\| = G_{equiv} \|u\| = \frac{P}{\|u\|^2} \|u\| = \frac{P}{\|u\|} \tag{6.12}$$

The remnant of the current feeding a particular load

$$i_{react}(t) = i(t) - i_{active}(t) \tag{6.13}$$

constitutes no contribution to P and increases the rms value of feeding current what is a plain disadvantage.

Both current components are orthogonal as the scalar product

$$\begin{aligned}
&\left\langle i_{active}, i_{react} \right\rangle = \frac{1}{T}\int_0^T i_{active}\left(t\right) i_{react}\left(t\right) dt = \\
&\frac{1}{T}\int_0^T i_{active}\left(t\right)\left(i\left(t\right) - i_{active}\left(t\right)\right) dt = \\
&\frac{P}{\left\|u\right\|^2}\frac{1}{T}\int_0^T u\left(t\right) i\left(t\right) dt - \frac{1}{T}\int_0^T \left(i_{active}\left(t\right)\right)^2 dt = \\
&\left\|i_{active}\right\|^2 - \left\|i_{active}\right\|^2 = 0
\end{aligned} \tag{6.14}$$

The rms values of current components are related to each other

$$\left\|i\right\|^2 = \left\|i_{active}\right\|^2 + \left\|i_{react}\right\|^2 \tag{6.15}$$

Multiplying (6.15) by the squared rms voltage value $\left\|u\right\|^2$ results in a power equations

$$S^2 = P^2 + Q_{Fryze}^2 \tag{6.16}$$

where

$$Q_{Fryze} = \left\|u\right\|\left\|i_{react}\right\| \tag{6.17}$$

However, there is no straightforward way from the power definition (6.17) to a compensation procedure [73]. The compensation problem was still open [70]. An attempt to define power components in time domain is a noticeable achievement made by Fryze.

6.3 Power definition by Shepherd and Zakikhani

The Authors observed, that applying the Budeanu concept of reactive power to the compensation strategy does not result in the maximal power factor PF [83]. Therefore, new concepts have been presented, resulting in a higher value of PF. Additionally, a linear capacitor has been proposed as a compensating device [71]. However, as the Authors stated in [85] ‘a power factor of unity cannot be reached at all in non-sinusoidal circuit by reactive power compensation of any kind, linear or non-linear’. It was intended to achieve the possibly maximal value of PF. The proposed definitions

were not intended to reveal a direct physical meaning, rather than to contribute to PF maximisation problem.

The authors propose a new expression called *total apparent power* S_t consisting of *active apparent power* S_R, *true reactive apparent power* S_X *and distortion power* S_D [83], [72].

$$S_R = \sum_1^n E_n^2 \sum_1^n I_n^2 \cos^2 \varphi_n \neq P^2 \tag{6.18}$$

$$S_X^2 = \sum_1^n E_n^2 \sum_1^n I_n^2 \sin^2 \varphi_n \tag{6.19}$$

$$S_D^2 = \sum_1^n E_n^2 \sum_1^p I_p^2 + \sum_1^m E_m^2 \left(\sum_1^n I_n^2 + \sum_1^p I_p^2 \right) \tag{6.20}$$

Summation gives

$$S_t^{\,2} = S_R^2 + S_X^2 + S_D^2 \tag{6.21}$$

The total apparent power is a figure of merit and can be sued to characterise the conveyance of energy

$$S_t^2 = \frac{1}{T}\int_0^T e^2(t)dt \frac{1}{T}\int_0^T i^2(t)dt = \left(\sum_1^n E_n^2 + \sum_1^m E_m^2 \right)\left(\sum_1^n I_n^2 + \sum_1^p I_p^2 \right) \tag{6.22}$$

Introduced definitions are based on an assumption of non-sinusoidal voltage feeding a non-sinusoidal load [83],

$$e = \sqrt{2}\sum_1^n E_n \sin\left(n\omega t + \psi_{En}\right) + \sqrt{2}\sum_1^m E_m \sin\left(m\omega t + \psi_{Em}\right) \tag{6.23}$$

Therefore the resulting current may be generally expressed as

$$i(t) = \sqrt{2}\sum_1^n I_n \sin\left(n\omega t + \psi_{In}\right) + \sqrt{2}\sum_1^p I_p \sin\left(p\omega t + \psi_{Ip}\right) \tag{6.24}$$

and the displacement

$$\varphi_n = \psi_{En} - \psi_{In} \tag{6.25}$$

Representing the non-linear load with a hypothetical, equivalent resistive and reactive braches leads to the idea of a purely resistive and purely reactive currents i_R, i_X .

$$i_R = \sqrt{2}\sum_1^n I_n \cos\varphi_n \sin\left(n\omega t + \alpha_n\right) \tag{6.26}$$

$$i_X = \sqrt{2}\sum_1^n I_n \sin\varphi_n \cos\left(n\omega t + \alpha_n\right) \tag{6.27}$$

An inductive current is lagging in relation to voltage. Those currents are directly involved in the definitions (6.18) and (6.19). The powers S_R and S_X may be understood as related to those purely resistive and reactive currents (6.26) and (6.27).

In circuits with sinusoidal voltages the terms S_R, S_X, S_D are identical with the Budeanu approach

$$P = S_R \quad Q=S_X \quad D=S_D \tag{6.28}$$

For non-sinusoidal waveforms they are no, especially

$$D^2 = S^2 - P^2 - Q^2 \neq S_D^2 \tag{6.29}$$

Power factor computation and correction is the most critical issue. The power factor indicates the value to be multiplied by apparent power to result in active power, i.e. mean value of power over one period.

A compensation in non-sinusoidal circuits should be focused on the minimisation of S_X and not Q. However, a full compensation is not achievable when applying only passive reactive elements. The minimum value of S_X, somehow greater than zero can be reached.

A summary of PF characteristics for various circuit and supply voltage parameters is compactly presented in Table 6.1.

Table 6.1 Power components and PV values vs. circuit and waveforms features [83]

	Sinusoidal voltage		Non-sinusoidal voltage	
	Linear circuit	Non-linear circuit	Linear circuit	Non-linear circuit
Apparent power components	S_R, S_X	S_R, S_X, S_D	S_R, S_X	S_R, S_X, S_D
PF if S_X fully compensated	$\frac{P}{S_R}=1$	$\frac{P}{\sqrt{S_R^2+S_D^2}}<1$	$\frac{P}{S_R}<1$	$\frac{P}{\sqrt{S_R^2+S_D^2}}<1$
S_X to be compensated by reactance	yes	yes	no	no
Maximum value of power factor	$\frac{P}{S_R}<1$	$\frac{P}{\sqrt{S_R^2+S_D^2}}<1$	$\frac{P}{\sqrt{S_R^2+S_{X\min}^2}}<1$	$\frac{P}{\sqrt{S_R^2+S_{X\min}^2+S_D^2}}<1$

In linear sinusoidal circuits the power factor is $\cos\varphi$. Generally PF is given as

$$PF=\frac{P}{S}=\frac{P}{EI}=\frac{\sum_1^n E_n I_n\cos\varphi_n}{\sqrt{\left(\sum_1^n E_n^2+\sum_1^m E_m^2\right)\left(\sum_1^n I_n^2+\sum_1^p I_p^2\right)}} \tag{6.30}$$

Power factor cannot be maximized by a reduction of Q in Budeanu sense, but by the minimization of newly introduced term S_X. Moreover, PF may be deteriorated by the compensation of Q only, as has been shown in a numerical example [86]. In the presence of non-sinusoidal voltage, the term S_X cannot be compensated to zero using linear reactive elements as compensators. A possibly minimal value $S_{X\min}$ can be obtained, so that the highest power factor is generally given as

$$PF=\frac{P}{\sqrt{S_R^2+S_{X\min}^2+S_D^2}}<1 \tag{6.31}$$

Further consideration are restricted to a linear capacitor connected in parallel to a load for compensation purposes (Fig. 6.4), [87]. The condition for maximal PF is reached when the value of S_X and therefore S is minimal with regard to capacitance [71], [86]. Therefore, the necessary condition of a minimum is satisfied when the derivative

$$\frac{dS_X}{dC}=0 \tag{6.32}$$

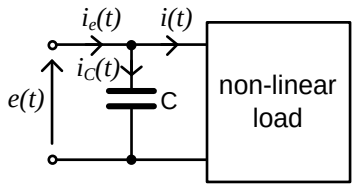

Fig. 6.4 Linear capacitor as a compensator

Condition (6.32) may be applied due to the quadratic character of the minimisation problem.

Voltage $e(t)$ and current $i(t)$ in Fig. 6.4 are given by the expressions (6.23) and (6.24), respectively. The current across capacitor is [87]

$$i_C(t) = \sqrt{2}\sum_1^n E_n n\omega C \sin\left(n\omega t + \psi_n + \frac{\pi}{2}\right) + \sqrt{2}\sum_1^m E_m m\omega C \sin\left(m\omega t + \psi_m + \frac{\pi}{2}\right) \tag{6.33}$$

The S_X component includes the $i_e(t)$ current and is given as

$$S_X^2 = E^2 I_X^2 = \left(\sum_1^n E_n^2 + \sum_1^m E_m^2\right)\left(\sum_1^n \left(E_n n\omega C - I_n \sin\varphi_n\right)^2 + \sum_1^m \left(E_m m\omega C\right)^2\right) \tag{6.34}$$

Total apparent power is

$$S^2 = E^2 I^2 = S_R^2 + S_X^2 + S_D^2 \tag{6.35}$$

where

$$S_R^2 = E^2 I_R^2 = \left(\sum_1^n E_n^2 + \sum_1^m E_m^2\right)\sum_1^n I_n^2 \cos^2\varphi_n \tag{6.36}$$

$$S_D^2 = E^2 I_D^2 = \left(\sum_1^n E_n^2 + \sum_1^m E_m^2\right)\sum_1^p I_p^2 \tag{6.37}$$

Substituting (6.34) into the condition for a minimum (6.32) and computing the derivative results in

$$C_S = \frac{\sum_1^n E_n I_n n \sin\varphi_n}{\omega\left(\sum_1^n E_n^2 n^2 + \sum_1^m E_m^2 m^2\right)} \tag{6.38}$$

In a general case, the compensating capacitance C_S imposed in (6.34) does not reduce the true reactive power to zero.

The active power P of the load in Fig. 6.4 is unchanged by the capacitor.

$$P = \sum_1^n E_n I_n \cos\varphi_n \tag{6.39}$$

The maximum value of the power factor PF for C_S is

$$PF_{\max} = \frac{P}{S_{\min}} = \frac{\sum_1^n E_n I_n \cos\varphi_n}{\sqrt{\left(\sum_1^n E_n^2 + \sum_1^m E_m^2\right) I_{\min}^2}} \tag{6.40}$$

where

$$I_{\min}^2 = \sum_1^n \left(E_n^2 n^2 \omega^2 C_S^2 + I_n^2 - 2E_n I_n n\omega C_S \sin\psi_{In}\right) + \sum_1^m E_m^2 m^2 \omega^2 C_S^2 + \sum_1^p I_p^2 \tag{6.41}$$

Despite the major drawback of this presented – no full compensation possibility – there was a further discussion in the literature . An practical converter has been proposed, indicating a DC current value proportional to the capacitor capacitance.

The lacking physical interpretation of the introduced method was regarded as one of significant drawbacks [88].

6.4 Numerical evaluation of compensation for given voltage and current

The following example was adopted from [87] and considers a periodical non-sinusoidal voltage feeding a load with a corresponding non-linear current

$$e(t) = \sqrt{2}\left(230\sin\omega t + 30\sin\left(5\omega t + 30°\right) + 20\sin\left(7\omega t + 30°\right)\right) \tag{6.42}$$

$$i(t)=\sqrt{2}\begin{pmatrix}20\sin(\omega t-45°)+10\sin(5\omega t-30°)...\\+10\sin(7\omega t-30°)+10\sin(9\omega t-30°)\end{pmatrix} \tag{6.43}$$

The optimum value of power factor with the help of a compensating capacitor should be find. Additionally, the capacitance for 50 Hz operation should be determined.

Firstly, the terms in (6.38) were computed

$$\sum_{1}^{n}E_n^2n^2=230^21^2+30^25^2+20^27^2=95\cdot10^3\ \text{V}^2 \tag{6.44}$$

$$\sum_{1}^{m}E_m^2m^2=0 \tag{6.45}$$

$$\sum_{1}^{n}E_nI_nn\sin\varphi_n=5,7642\cdot10^3\ \text{VA} \tag{6.46}$$

And accordingly the optimal capacitance is

$$C=\frac{5.7642\cdot10^3}{2\pi\cdot50\cdot95\cdot10^3}=\ 193,14\ \mu\text{F} \tag{6.47}$$

The minimal value of current with regard to (6.41) is

$$I_{\min}=18,7152\ \text{A} \tag{6.48}$$

The minimum value of apparent input power is a product of the above current and RMS value of feeding voltage

$$E=\sqrt{\left(\sum_{1}^{n}E_n^2\right)}=\sqrt{230^2+30^2+20^2}=232,8089\ \text{V} \tag{6.49}$$

Therefore

$$S_{\min}=EI_{\min}=4.3571\cdot10^3\ \text{VA} \tag{6.50}$$

The value of active power (6.39) is

$$P = 3502,7 \text{ W} \tag{6.51}$$

Further on, the highest value of power factor due to the compensation with a capacitor is

$$PF_{\max} = \frac{P}{S_{\min}} = 0.8039 \text{ inductive} \tag{6.52}$$

After compensation the RMS current value in load is

$$I_{load} = \sqrt{20^2 + 10^2 + 10^2 + 10^2} = 26.4575 \text{ A} \tag{6.53}$$

The connection of an optimally sized capacitor has improved the power factor by ca. 41% in comparison to previous, uncompensated value

$$PF = \frac{P}{EI} = \frac{4560}{6950} = 0.5687 \text{ inductive} \tag{6.54}$$

In a fictive case of a full compensation of the true reactive S_X a new formula or PF should be used, where

$$PF = \frac{P}{\sqrt{S_R^2 + S_D^2}} = 0.1828 \cdot 10^{-3} \tag{6.55}$$

Practical meaning and usefulness of (6.55) in [87] is highly disputable as there is no mean for elimination of S_X and comparison to previously computed values.

A comparison to the Budeanu approach is justified at this point. The reactive power value computed accordingly to Budeanu definition is

$$Q = \sum_{1}^{n} E_n I_n \sin\varphi_n = 3.6857 \text{ kVA} \tag{6.56}$$

Therefore, the maximum power factor with the full compensation of Q

$$PF = \frac{P}{\sqrt{S^2 - Q^2}} = 0.7097 \tag{6.57}$$

Remarkably, using a capacitor corresponding to 3.6857 kVA at 50 Hz leads to overcompensation. From this example it is visible that compensation of Q does not result in the maximal power factor [89].

In general, the discrepancy between S_X and Q is due to voltage distortion rather than load nonlinearity and this discrepancy still occurs even with linear load impedances [87].

For sinusoidal voltage $S_X = Q$ but it is not recommended to apply the Budeanu approach to calculate tariffs for reactive power when high deterioration of voltage quality is anticipated.

7 Research Installations with PV generation

Data collected from installations equipped with photovoltaic generation were used to work with proposed algorithms and methods. Presentation of existing installations used in research should be helpful in establishing a correlation between properties and dimensions of an installations and anticipated signal parameters.

7.1 Research PV installation with 15 kW

The research installation with maximal power output15 kW consists of three independent one phase systems constructed in different technologies. Schematic view is shown in Fig. 7.1. The photovoltaic research installation is located at the university campus and arranged on the roof of an existing building. The geographical orientation of the roof was accepted and do mounting structures used.

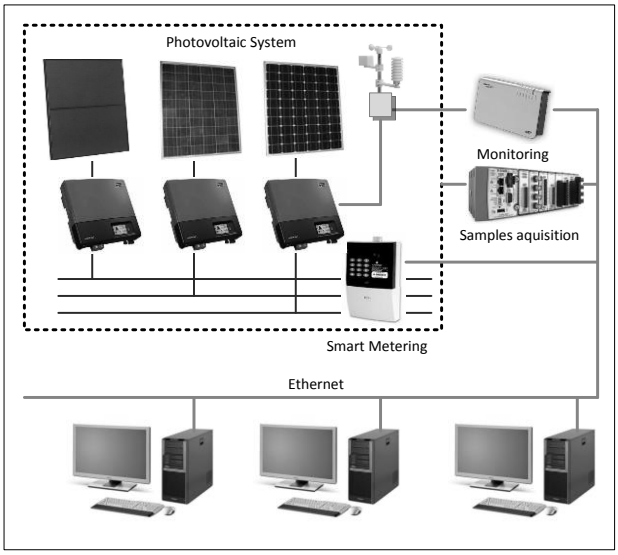

Fig. 7.1 Overview of the 15 kW PV installation with monitoring

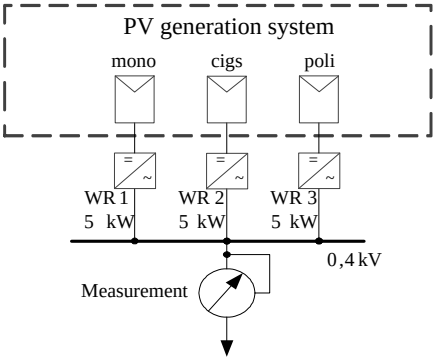

Fig. 7.2 Schematic view of the grid connection of PV panels

The details of the three systems can be given in Table 7.1. The installation is connected directly with a substation located in the basement of the same system. The substation is equipped with a 10kV/0.4kV 400 kVA transformer powering nearby buildings.

Table 7.1 Parameters of the 15 kW PV installation

feature:	characteristic of PV sub-generator		
phase	L1	L2	L3
cell type	mono	cigs	poly
azimuth	135° SE	135° SE	225° SW
transformer	no	no	yes
no. of modules	27	56	21
module type	SUNTECH STP190S-24/Ad+	Q.CELLS Q.SMART 90	SOLAR FUTURE ENERGY PF-6:240
efficiency	14.9%	11.8%	15.5%
max. power	190 W	90 W	240 W
max. voltage	36.5 V	60.8 V	30 V
max. current	5.2	1.48	8 A
dimensions	1580x808x35mm	1196x636x36mm	1680x1040x35mm
elevation	40°	40°	40°

7.2 Research PV installation with 110 kW

A polycrystalline photovoltaic research installation is located at the university campus and arranged on the roof and façade of an existing industrial hall. The arrangement of panels was strongly influenced by the orientation of the building and

areas available for PV panels. There was no possibility to fully optimise toward maximal energy output.

The access to the installation and related measurement data was a courtesy of the BTU university, where the installation is located as a consequence of an extensive research cooperation.

The photovoltaic installation consists of 530 modules with each 220 W_{peak}, therefore 116.6 kW_{peak} for the whole generation facility. The modules of the company *Algatec* have a nominal voltage of 27.22 V, a nominal current of 8.22 A and a modul-efficiency of 14.9 %. The PV panels are distributed over the main roof, the projecting roof and the facade (368 modules with an angle of incidence of 30°, 162 modules with an angle of incidence of 70°; the building is oriented 12° to the south-west). The installation's currents and voltages are registered every second and can be retrieved anytime for evaluation and analysis. The installation consists of 368 panels with an inclination of 30 degrees and 162 panels with an inclination of 70 degrees. All of this panels are tilled by 12 degrees from the South orientation towards the West. This PV system was additionally equipped with spherical irradiation measurement sensor, described in more detail in the next section.

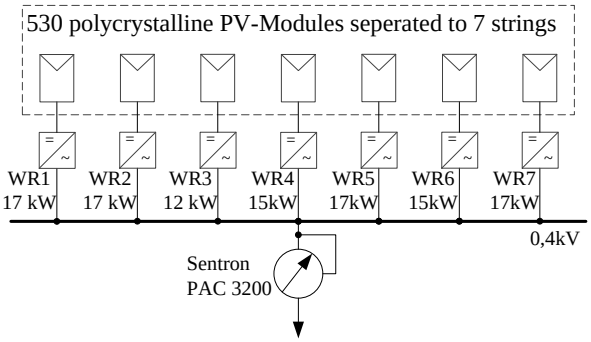

Fig. 7.3 Schematic view of the grid connection of PV panels

The mentioned PV modules rated 116.6 kW_{peak} are grouped in 7 strings. Fig. 7.3 shows the connection of the strings to the *SMA SUNNY TRIPOWER* inverters (WR1 – WR7). The inverters with the max DC power (at cos φ = 1) from 12 250 W to 17 410 W have a max. input voltage of 1 000 V, a mpp voltage range of 360 V (± 20 V) to 800 V, a min input voltage of 150 V and a max. iniput cuttent per string of 33 A.

The rated power at the output is (at voltage 230 V, 50 Hz) 12 000; 15 000; 17000 W. Respectively, the maximum output current is set to 19.2; 24; 24.6 A. Displacement factor can be adjusted in the range between 0.8 (capacitive) and 0.8 (inductive) as well as a maximal efficiency of 98.2 %.

Instantaneous values of voltage and current are captured in the *Sentron PAC 3200* (Fig. 7.3) Averaging is done over a 200ms period. The values can be readout every 300ms over the Ethernet connection port. The timestamp is set at the readout time. Initially a 1 s average values were used to represent a 24-hours curve. However, 10 min. or 1 min. averages were more suitable for the computations presented later on.

7.3 Spherical Irradiation Measurements

The irradiation was measured with 33 reference cells arranged on the surface of a half-sphere. The measuring device is depicted in Fig. 7.4 and Fig. 7.5 showing vertical cross-section and horizontal top view respectively. Fig. 7.6 give further details of the geometrical arrangement, showing indexing of all measuring cells.

In the solar radiation sensor (ISET sensor 01274) [90] the solar radiation is converted into a proportional current by an exact defined solar cell. The output voltage signal is given through a specific shunt resistance with a thermic coupling to the aluminium casing.

Accurate measurement results are possible due to the geometric construction of the reference cell close to PV modules dimensions and specially formed casing enabling a link to outside temperature. The sensor is waterproof and can work in temperatures between -25°C and 80°C.

The calibration of every ISET sensor is achieved with a reference element constructed in identical fashion by an accredited test laboratory in W/m2 and is documented on a quality assurance calibrating certificate. The calibration is conform with [91]. Relative measurement uncertainty is $<\pm 4\%$ for crystalline material.

For the energetic rating and monitoring of a PV system the same cell technology should be applied in sensor and cell production to guarantee same spectral sensitivity. Furthermore, using the same cells results in comparable physical characteristics regarding temperature reflection and degradation.

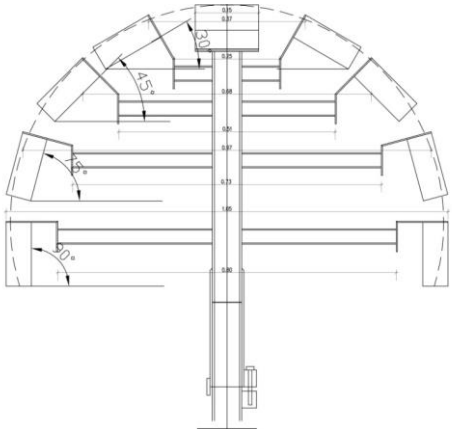

Fig. 7.4 Vertical cross-section of the measurement sensor

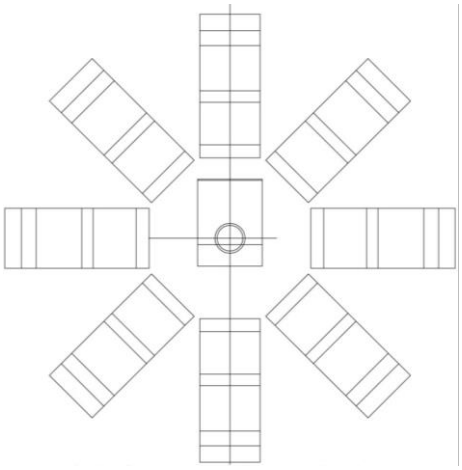

Fig. 7.5 Horizontal view of the measurement sensor (from top)

Fig. 7.7 shows the electrical connection of the 33 sensors with the imc SPARTAN-R-T-16. The measured values are read in a 1-s-intervall and are stored in the same system as the values from the PV Modules.

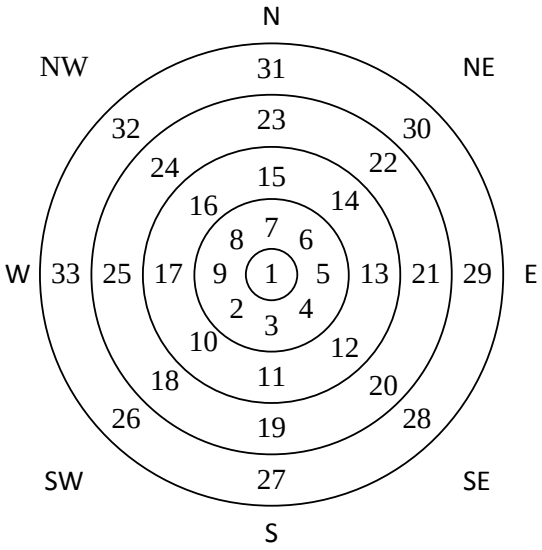

Fig. 7.6 Indexing of irradiation sensors, horizontal view

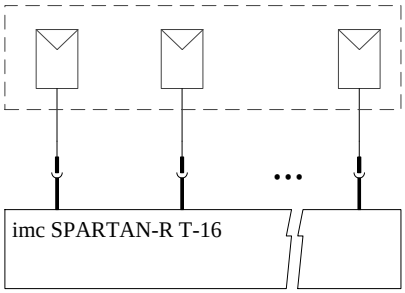

Fig. 7.7 Electrical connection of the measurement equipment

8 Characterisation of the daily power curves in PV system

The daily power output of a PV installation is highly unstable due to seasonal changes and weather conditions variations in cloud coverage or temperature. Transients in solar irradiation are directly determining the shape of the power curve. Fig. 8.1 shows the active power output from the 110 kW installation described in section 7.2, on three subsequent days in July. Not only the days differ significantly from each other but also the variations during a day are noticeable. The changes correlate well with irradiation curves (Fig. 8.2). Both, irradiation and active power values were averaged over the period of one second.

There is an open question for the proper time of averaging. Utilities often propose 15 min. values for power measurement. However, this time may be 10 min. or less if requested and justified [92]. Many power quality indices should be reported every 10 min. [20]. Smart meters [93] enable measurement and data transfer every one minute or even less. Increase in sampling frequency has some disadvantages. Short measurement window reduces the number of smart meters which can be served by one concentrator and increases the amount of data to be stored and evaluated. Continuous measuring of active power values averaged over 200 milliseconds window (as for some power quality analysis) is relatively fare going proposal regarding data amounts and data transfer capabilities in public distribution grids.

Preliminary research results showed that data acquisition every one minute is satisfactory in the approaches presented later on. On the one hand, the data amount to be stored and analysed every day is reasonable and not voluminous. On the other hand, computational results are more precise and accurate than for data averaged over longer periods, 10 min., or 15 min. Therefore, one minute averaging period was selected and used in further analysis.

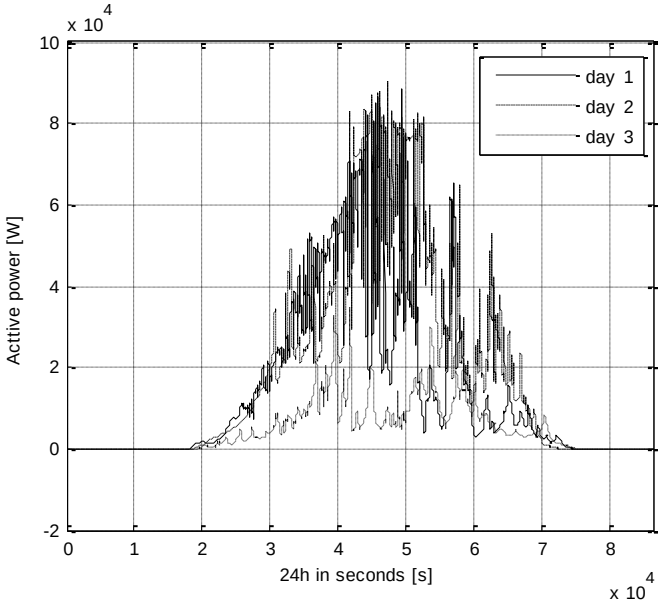

Fig. 8.1 Variations in daily power curves

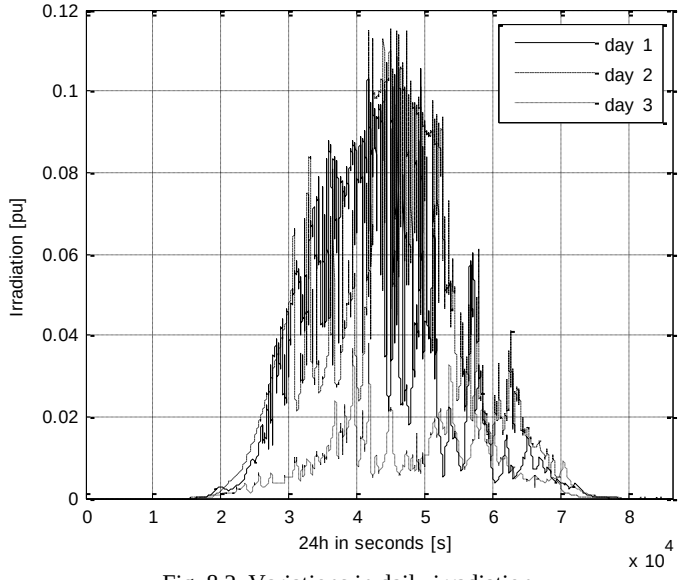

Fig. 8.2 Variations in daily irradiation

Data acquisition intervals used in both PV systems were different. To bring all data to the aforementioned one minute interval a procedure called resampling was applied

[94], [95], [96]. Daily power curve acquired with 1 second averaging period is shown in Fig. 8.3 Its counterpart after down-sampling with 1440 samples per 24 hours (one minute period) is given in Fig. 8.4 Small dots in Fig. 8.4 indicate exact values.

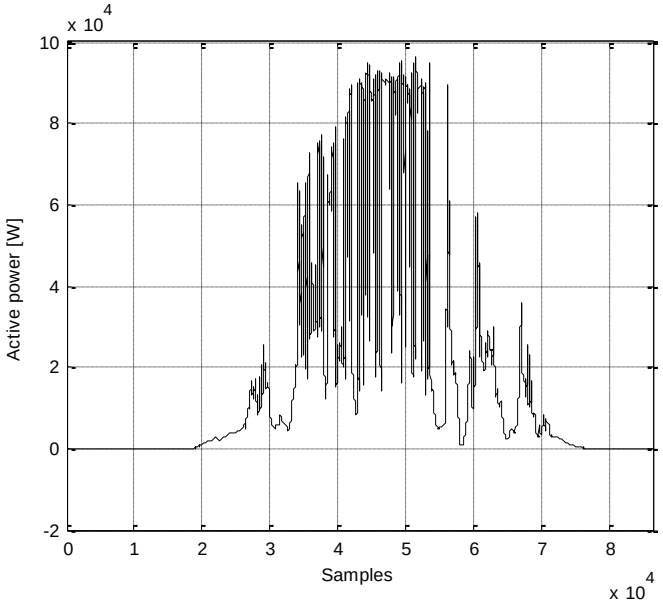

Fig. 8.3 Daily power curve with one second data acquisition

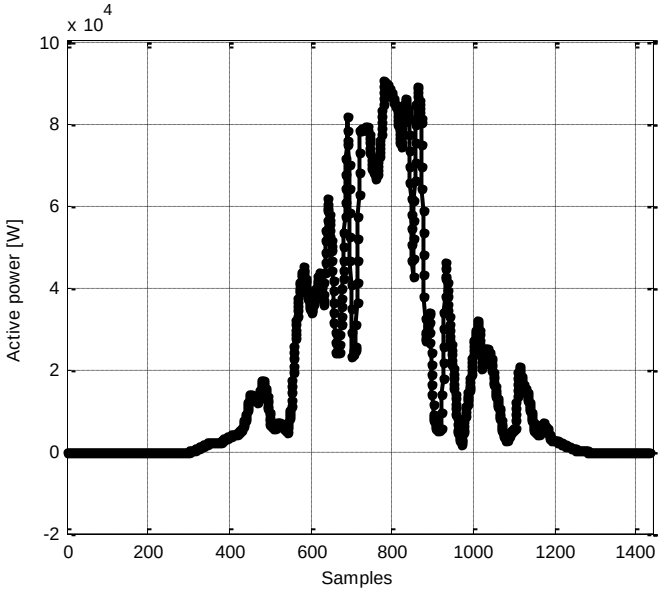

Fig. 8.4 Daily power curve after resampling (down-sampling 1 min. window)

Up-sapling was performed to adjust the daily power curve with 10 minutes interval between samples to the required one minute period between data. Fig. 8.5 shows the original signal form the 15 kW installation described in section 7.2. Fig. 8.6 shows the same signal after up-sampling operation resulting in the required 1440 power values per day. Small dots in Fig. 8.6 indicate exact power values.

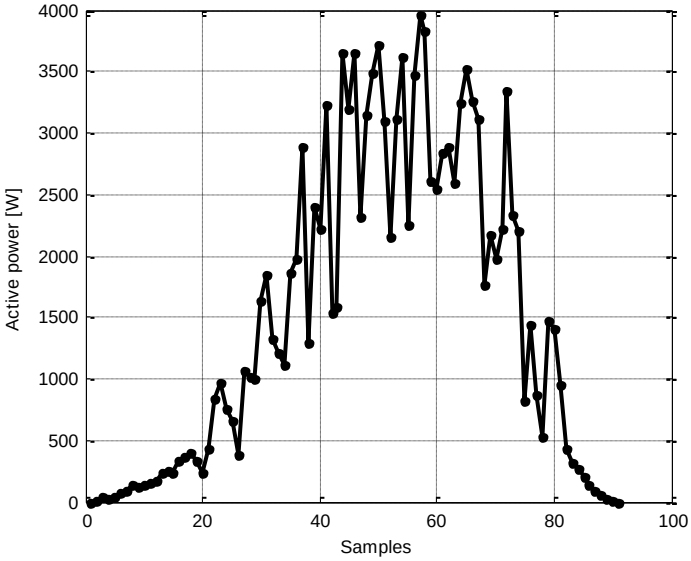

Fig. 8.5 Power curve before resampling (10 min. window)

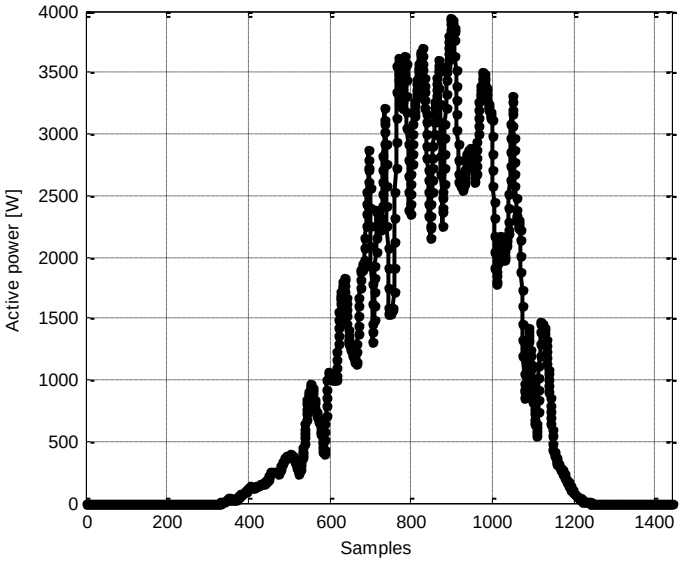

Fig. 8.6 Power curve after resampling (up-sampling, 1 min. window)

8.1 Approximation of a power curve with predefined shape

The daily power curve can hardly be described by a simple equation due to stochastic and seasonal variations depending mostly on irradiation conditions. In terms of a power quality index or a simplified characterisation requiring less memory space than the curve itself it is advisable to use approximated power curve descriptions.

A possible way to reduce data amount is the aforementioned down-sampling. The power curve is then anyway described by a vector of points.

The mean value describes a curve with only one number (Fig. 8.7). Similarly descriptive is a pair of minimum and maximum values during an hour around noon, standard deviation, etc.

One of the simplest methods giving only two descriptive points a day is *a centroid*. It indicates the mass centre of the area below the plot (Fig. 8.7). Generally, the horizontal and vertical coordinates are [97]

$$x_c = \frac{1}{Area}\int_a^b x\big(f(x)-g(x)\big)dx \tag{8.1}$$

$$y_c = \frac{1}{Area}\int_a^b \left(\frac{f(x)-g(x)}{2}\right)\big(f(x)-g(x)\big)dx \tag{8.2}$$

where the area of the region resulting from

$$Area = \int_a^b \left(f(x) - g(x) \right) dx \tag{8.3}$$

In the a equations (8.1) to (8.3) the considered area is bounded by the continuous functions $f(x)$ and $g(x)$ on the interval $[a,b]$, $a \le x \le b$. It is assumed that $f(x) \ge g(x)$.

The horizontal location other than midday indicates a shift of energy production toward morning (left) or afternoon (right). The centroid location in the plot in Fig. 8.7 is shifted to the right due to the westerly orientation of the PV panels (Table 7.1). The vertical location depends on the power values during a day. Fig. 8.7 is an example for the 15 kW PV generator and its subsystem with polycrystalline cells.

This proposed power quality index should have allowed values located in a circle with a predefined radius and origin position. Precise formulation of the radius requires statistical analysis over loner period of data, e.g. one year.

Further description possibilities include a similarity to a predefined curve. It is advantageous, if power production in a PV system is coherent with a predefined function, e.g.:

- a constant line (possible with storage)
- covering a preselected demand curve (possible with storage)
- bell shape (possible with storage)

Without storage it is possible to find the parameters of a curve that best suits a predefined shape type given by a parametric equation, e.g. (8.4).

The aberration from predefined curve can be seen as parameter for the production pattern description and possible fees included in tariff regulations. In a statistical sense it can also be used or the sizing of a storage device allowing strict following of that curve.

The parameters of a predefined curve, fitting optimally the daily production are an index describing the curve in short and therefor predestined to be a quality factor.

For the energy production curve approximation an exponential bell function was used in this work. The general expression for this bell function is

$$y_{comp}(t) = \alpha_1 e^{-\left(\alpha_2 (t-\alpha_3)\right)^2} \tag{8.4}$$

where $\alpha_1, \alpha_2, \alpha_3$ are descriptive parameters. Those parameters are determined in an optimisation process minimising the squared error between real power curve y(t) and the bell shape

$$y_{error} = \left\| y(t) - y_{comp}(t) \right\| \tag{8.5}$$

Optimisation procedure was performed using a method based on evolutionary approach and using a classical gradient based iterative approach.

Other description methods, especially strict statistical analysis including variances, standard deviations, percentiles etc. was purposely left out as they require much more space to be treated accurately and were not in centre of interest in this work. Moreover, longer periods, i.e. one year, have to be taken into the statistical analysis, not a particular daily curve as used therein.

Fig. 8.8 shows the approximating bell shapes resulting from the optimisation procedures trying to fit the bell into the real power curve in sense of least squared error between them. Both bell shapes are very similar and overlap. Detailed parameters of those curves and corresponding approximation errors are given in Table 8.1. The differences of curve parameters are not excessive and correspond with Fig. 8.8.

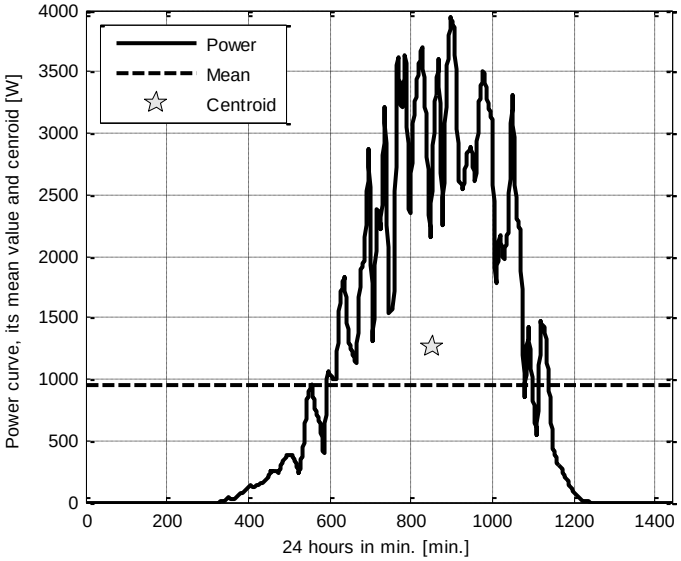

Fig. 8.7 The centroid of a daily power curve

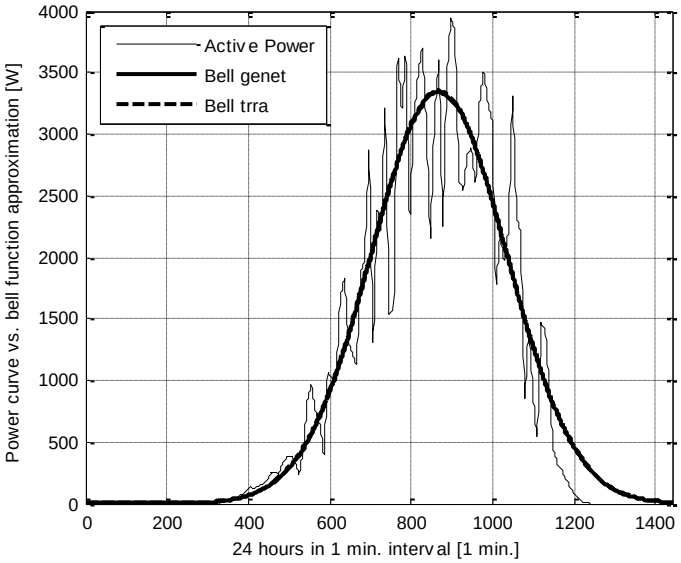

Fig. 8.8 Bell shape function approximating of daily power curve with distortions

Table 8.1 Bell function parameters

parameter	genetic algorithm	trust region refl. algorithm
α_1	3214.388	3350.715
α_2	0000.004	0000.004
α_3	0870.956	0868.058
y_{error}	297780.626	289902.533

Fig. 8.9 shows a power curve on a bright day in May with little distortions. This curve was measured for the polycrystalline subsystem of the 15 kW installation (Table 7.1). Bell functions overlap, so the differences in corresponding values of alpha parameters are negligible. Table 8.2 shows those parameters with corresponding approximation errors. The error values are very similar for both optimisation approaches. The relatively big discrepancy between bell function and real power curve at the end of a day (Fig. 8.8 and Fig. 8.9) can be explained. The main cause for fast decay in power values is shadowing of the panels by a nearby office building. the panels do not get the direct sun bean when the sun is low over the western horizon.

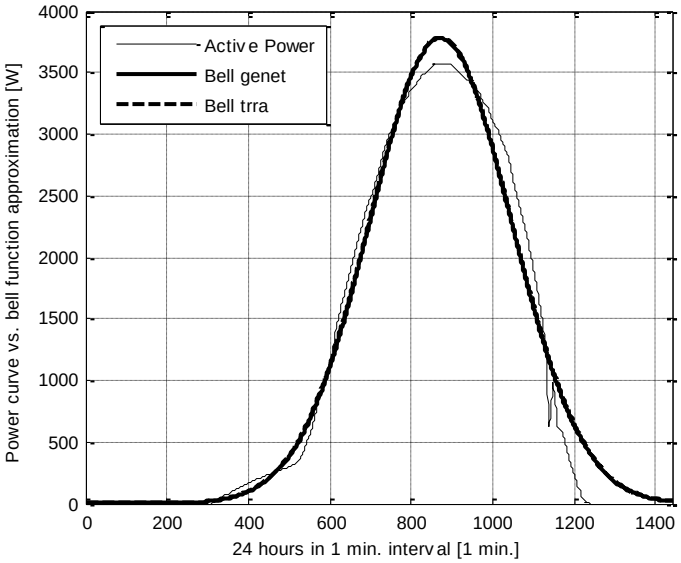

Fig. 8.9 Bell shape function approximating of relatively smooth daily power curve

Table 8.2 Bell function parameters

parameter	genetic algorithm	trust region refl. algorithm
α_1	3744.830	3787.555
α_2	0000.004	0000.004
α_3	0872.041	0871.899
y_{error}	182571.328	182535.944

Similar studies were done for power signals form the 110 kW installation and some examples shown below. Despite the fact, that one min. period is preferred for the analysis, the effects of averaging are indicated again. Fig. 8.10 shows a daily power curve averaged over 10 min., whereas Fig. 8.11 shows the same curve with one minute time interval between power values. Not only the number of variations is higher but also their amplitude is distinctively different. For both variants of averaging the bell shapes obtained by evolutionary algorithm and trust region reflective approach are similar and overlap.

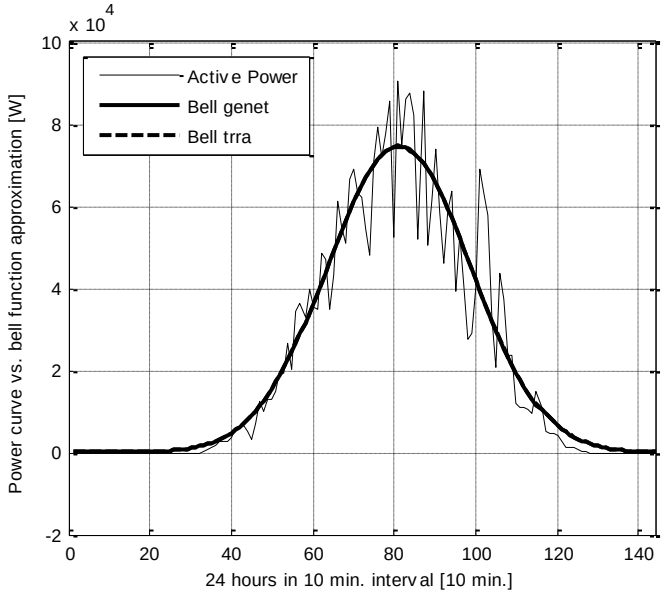

Fig. 8.10 Bell shape function approximating of daily power curve with disturbances, 10 min.

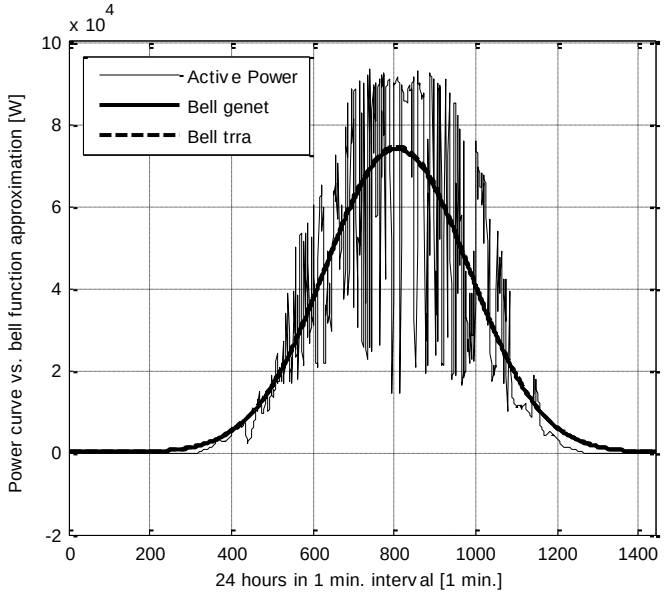

Fig. 8.11 Bell shape function approximating of daily power curve with disturbances, 1 min.

Table 8.3and Table 8.4 show parameters for bell functions depicted in Fig. 8.10 and Fig. 8.11 respectively. The values are similar for both optimisation approaches. It

is noticeable, that α_2 and α_3 in Table 8.3 have to be multiplied by 0.1 and 10 respectively to obtain the values in Table 8.4. It is due to the time interval between samples (1 minute, 10 minutes) differing exactly by factor 10.

Table 8.3 Bell function parameters, 10 min. interval

parameter	genetic algorithm	trust region refl. algorithm
α_1	74609.703	74648.626
α_2	0000.040	0000.040
α_3	0081.146	0081.145
y_{error}	628457.843	629046.063

Table 8.4 Bell function parameters, 1 min. interval

parameter	genetic algorithm	trust region refl. algorithm
α_1	73952.668	74612.969
α_2	0000.004	0000.004
α_3	0807.123	0807.057
y_{error}	10866426.918	10862173.183

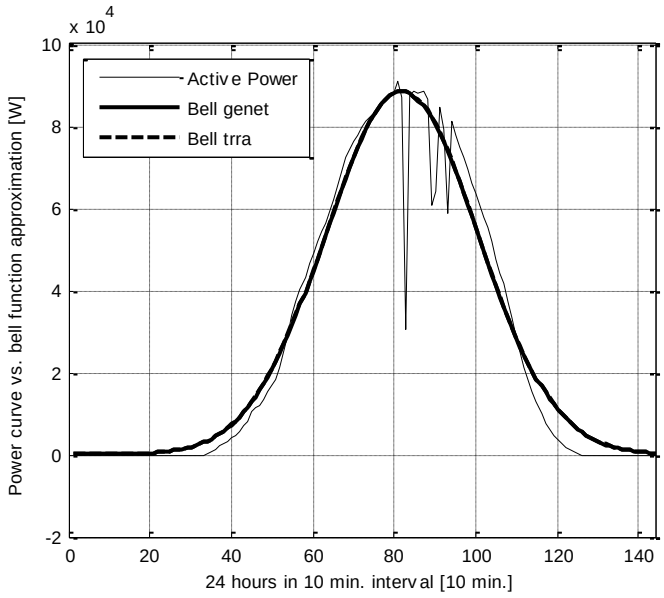

Fig. 8.12 Bell shape function approximating of daily power curve with notches, 10 min.

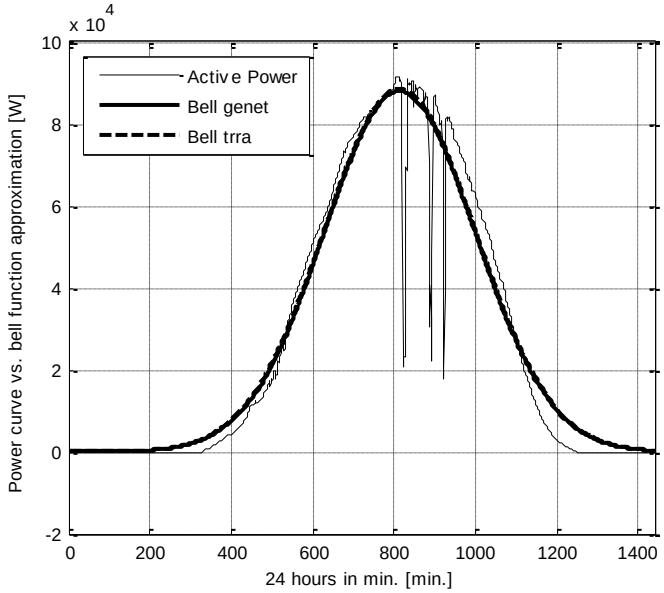

Fig. 8.13 Bell shape function approximating of daily power curve with notches, 1min.

Fig. 8.12 and Fig. 8.13 shows the effect of averaging for a relatively smooth daily power curve with some short duration notches. This notches lost their deepness by more than half after averaging. Once again, bell shapes resulting from both optimisation approaches overlap. Due to the notches the afternoon slope is more flat. Short after peak value the approximation curve is below the actual envelope of power plot, resulting in overestimated values for the late day hours.

Detailed bell shape parameter values along with estimation error are given in Table 8.5 and Table 8.6. Small differences in the values of parameters correspond well with overlapping plots in Fig. 8.12 and Fig. 8.13.

Table 8.5 Bell function parameters, 10 min. interval

parameter	genetic algorithm	trust region refl. algorithm
α_1	88474.797	88566.751
α_2	0000.038	0000.038
α_3	0081.839	0081.839
y_{error}	538274.829	537600.676

Table 8.6 Bell function parameters, 1 min. interval

parameter	genetic algorithm	trust region refl. algorithm
α_1	73952.668	74612.969
α_2	0000.004	0000.004
α_3	0807.123	0807.057
y_{error}	10866426.918	10862173.183

The trust region reflective approach was prone to starting conditions and therefore less stable in comparison to the genetic approach. More often it could get stuck in a local minimum. There is no systematic and robust method for finding the right starting point for the derivative based method. Despite high fidelity of both methods and very similar parameters of the daily power curve approximations it seems advantageous to suggest evolutionary based algorithm for further practical applications.

8.2 Assessment of power variations with wavelets

The power output of a PV power generation unit is highly variable, as indicated in the beginning of Chapter 8. Fig. 8.14 to Fig. 8.16 show the daily power curves (left vertical axes) and corresponding irradiation values (right vertical axes) of all three subsystems in the 15 kW PV research installation on the same day. The daily irradiation and power curves overlap (ignoring different axes scaling) and correspond to each other. Multiplication of the irradiation by an coefficient enables a true match between these two quantities. It is possible, because in this particular installation the irradiation was measured with a reference cell with the same geographical orientation as the panels. This idea of irradiance vs. power relation is further exploited in Chapter 9 where spherical irradiation components are used instead.

The PV subsystem equipped with polycrystalline cells was selected as an example for further analysis as the 110 kW PV system is also fitted with polycrystalline panels.

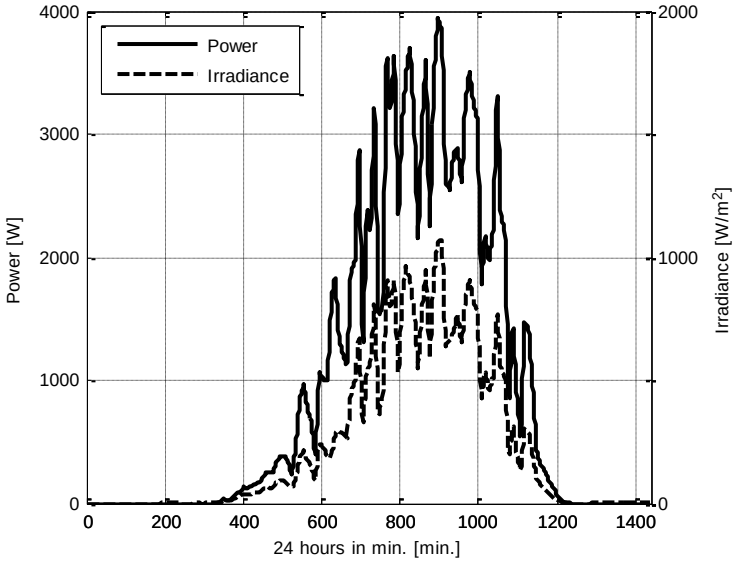

Fig. 8.14 Irradiance and power curve during one day, polycrystalline cells

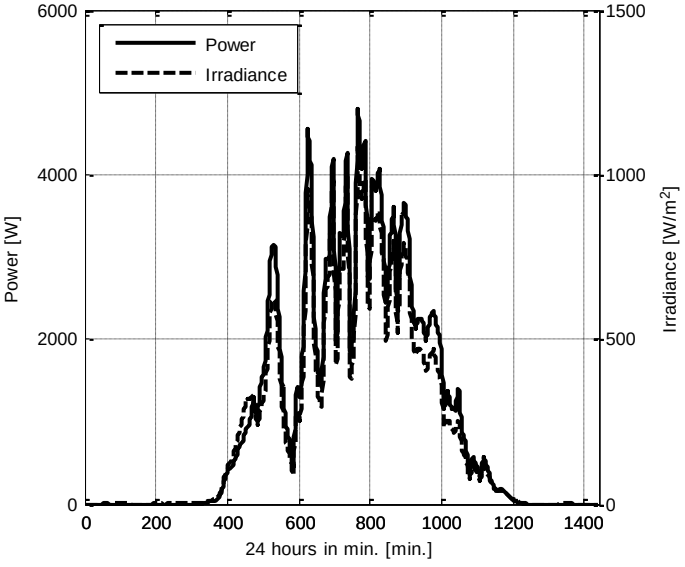

Fig. 8.15 Irradiance and power curve during one day, monocrystalline cells

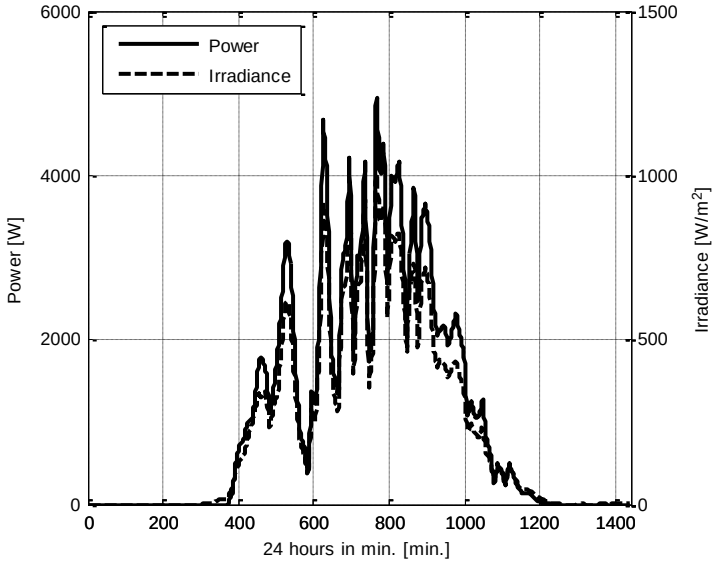

Fig. 8.16 Irradiance and power curve during one day, CIGS cells

During the preliminary research various wavelet functions with varying parameters were used.

Daubechies' waveltets were represented by the *daub* function [98]. This function returns the coefficients of the orthonormal Daubechies filters with maximum number of vanishing moments and minimum phase. The one input of the function, an even number, specifies the number of coefficients in the analysis and synthesis filers.

The function *symlets* [98] generates the least-asmmetric Daubechies' filters. This function returns the coefficients of the orthogonal finite impulse response filters with zeroes of the trigonometrical polynomial selected alternatively inside and outside the unit circle. Such a selection results in nearest design to linear phase and least asymmetric wavelets. As in *daub* the number of filter coefficients must be even.

Another function from the packet [98] used in research was *maxflat*. It returns the coefficients of the orthonormal maximally flat filters. The two input arguments are the degrees of flatness at $\omega = 0$ and $\omega = \pi$.

The quadrature filters proposed by Battle and Lemarie are returned by the function *lemarie* [98]. this function gives coefficients of the orthogonal Battle-Lemarie filters. The only input parameter is the length of filter.

The last considered function was *wspline* computing the spline biorthogonal filters. It returns the analysis and synthesis filters with spline wavelets of compact support. Two input parameters specify the number of zeroes at $z = -1$. The sum of both parameters must be even.

Preliminary considerations and results [99] induced the selection of *symlets* for further use as it guaranties the nearest design to linear phase.

Fig. 8.17 to Fig. 8.21 show the first five details of a daily power curve on the same axes scale to enable a visual comparison between details. In every of those figures the particular detail was plotted with a bold line. The highest number of a detail correspond to the lowest frequency content, the lowest number, i.e. one, indicates highest frequencies. Every higher level imposes the frequency range division of the preceding approximation (original signal in the first step) by two. The division results in a new approximation and a new detail. The sum of all details (Fig. 8.17 to Fig. 8.21) and the approximation (Fig. 8.24) result in the original daily power curve.

Fig. 8.22 and Fig. 8.23 present the second and first detail with highest frequencies on different axes scaling as the values are significantly smaller then higher details (detail with higher value of the index).

The proposed description method for variations in a daily power curve is based on the computation of details. Parameters as min./max. value of the detail, integral of the detail over time, are usefully descriptive and informative. Additionally, the basic ideas of descriptive statistics were used [100]. *Variance* measures how far a set of numbers is spread out. *Standard deviation* measures the amount of variation or dispersion from the average. A low standard deviation indicates that the data points tend to be very close to the mean. A high standard deviation indicates that the data points are spread out over a large range of values.

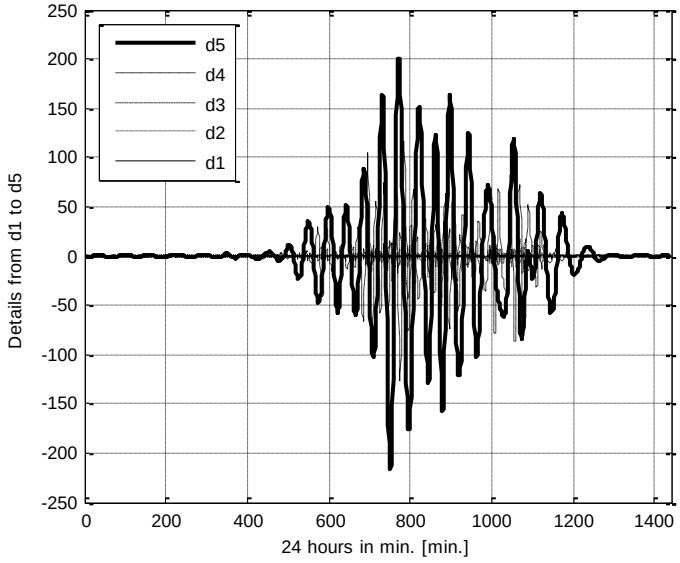

Fig. 8.17 the fifth detail of the daily power curve

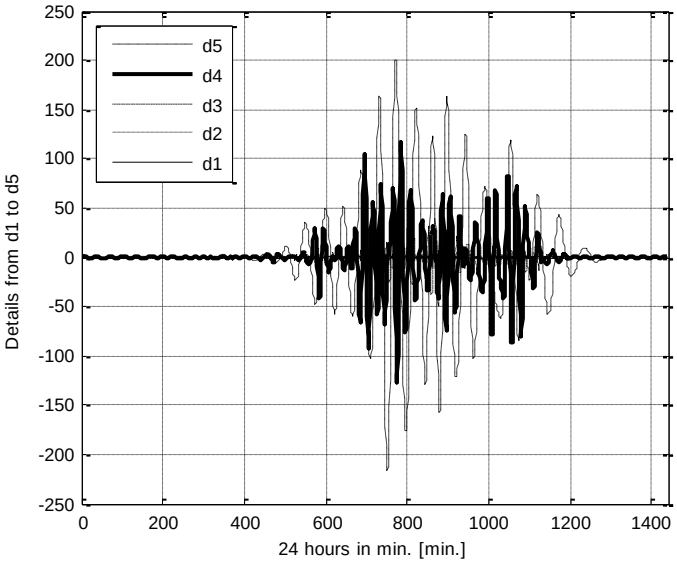

Fig. 8.18 the fourth detail of the daily power curve

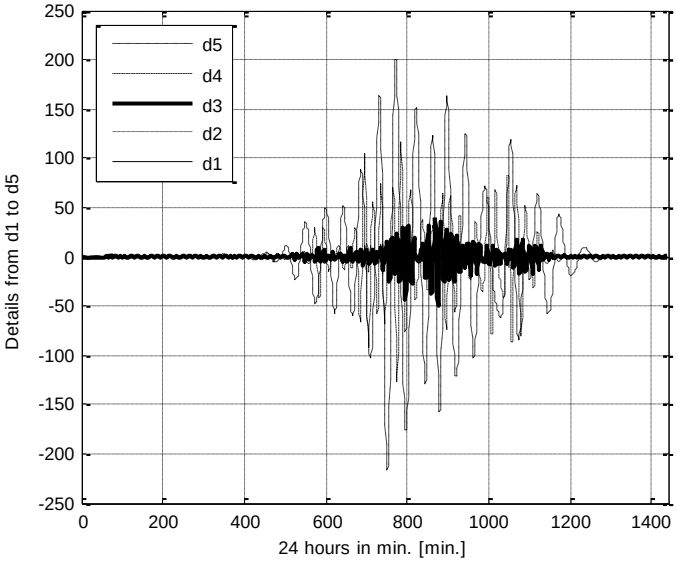

Fig. 8.19 the third detail of the daily power curve

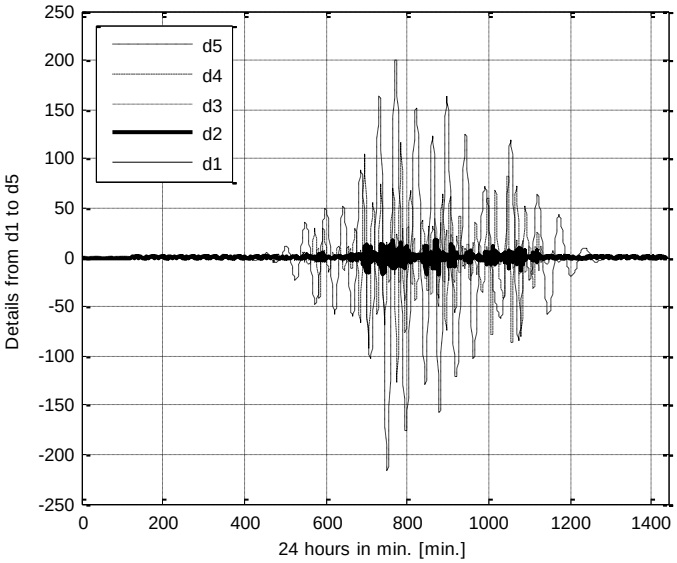

Fig. 8.20 the second detail of the daily power curve

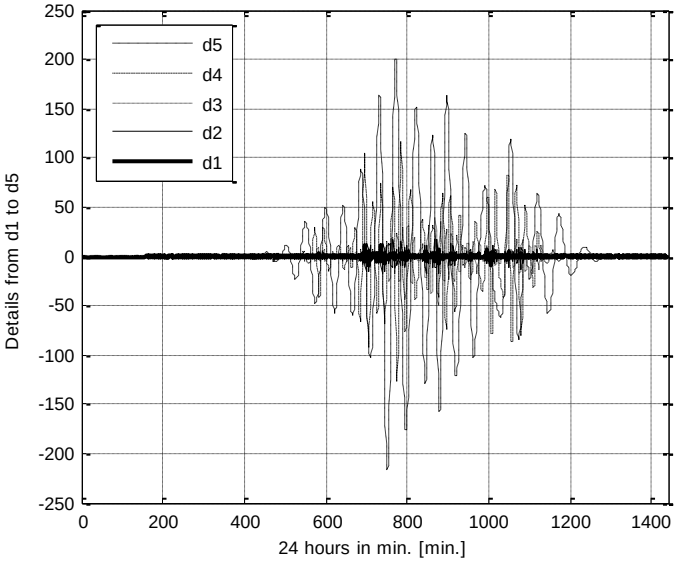

Fig. 8.21 the first detail of the daily power curve

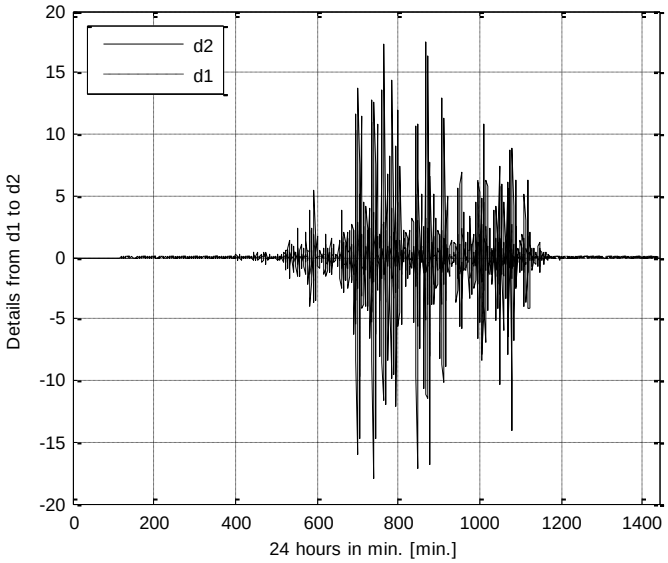

Fig. 8.22 First and second detail of the daily power curve

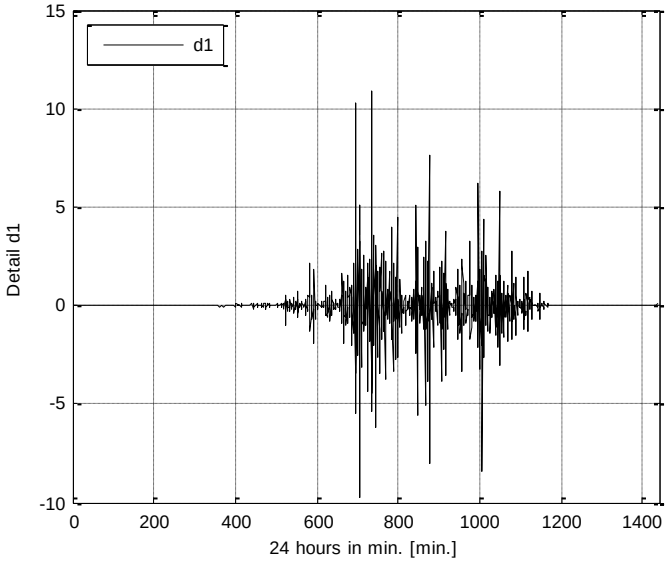

Fig. 8.23 First detail of the daily power curve

The descriptive parameters of details in Fig. 8.17 to Fig. 8.21 are presented in a compact manner in Table 8.7. The integral column indicates the area between the plot

and horizontal time axes, i.e. absolute values were taken for the computation, as integral over original detail curve is approximately zero.

Table 8.7 Descriptive parameters of details

detail no.	min.	max.	integral	variance	std. dev.
d1	-046.311	0049.294	2604.664	0020.579	0004.536
d2	-075.638	0072.750	8627.303	0162.938	0012.765
d3	-185.539	0151.170	21589.907	0874.748	0029.576
d4	-486.890	0528.708	75670.797	10765.547	0103.757
d5	-817.111	0732.435	165429.156	40324.121	0200.809

The approximation of the daily power curve obtained with *symlets* is shown in Fig. 8.24. In wavelet analysis the approximation shows the lowest frequency segment of the original signal. The approximation in Fig. 8.24 is a good indication for the smoothest shape of the daily power curve. The difference between the original curve and the approximation shows the power to be delivered by a storage unit in order to eliminate ripples. However, a statistical analysis of long period data, i.e. one year, is needed to properly size the storage unit and settle its response time to changes. Analysis of longer period data for a preselected storage unit answers a question of probable insufficient elimination of ripple on certain periods during a year. Then, an optimisation procedure may be applied to find a balance between storage unit size and capability and acceptable duration and severity of ripples over a year in statistical sense.

Detailed statistical analysis of long period data was not in the scope of this work.

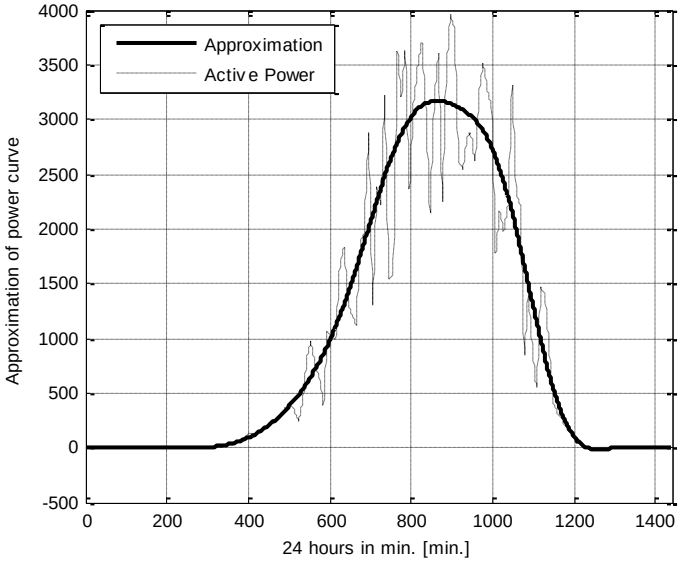

Fig. 8.24 Approximation component of the wavelet analysis of the daily power curve

Fig. 8.25 shows the coefficients of the analysis and synthesis filters (lowpass and highpass) with 32 coefficients obtained with *symlets*. Corresponding wavelet and scaling functions are depicted in Fig. 8.26. The filters in Fig. 8.25 were used for details and approximations computations of all examples in this Chapter.

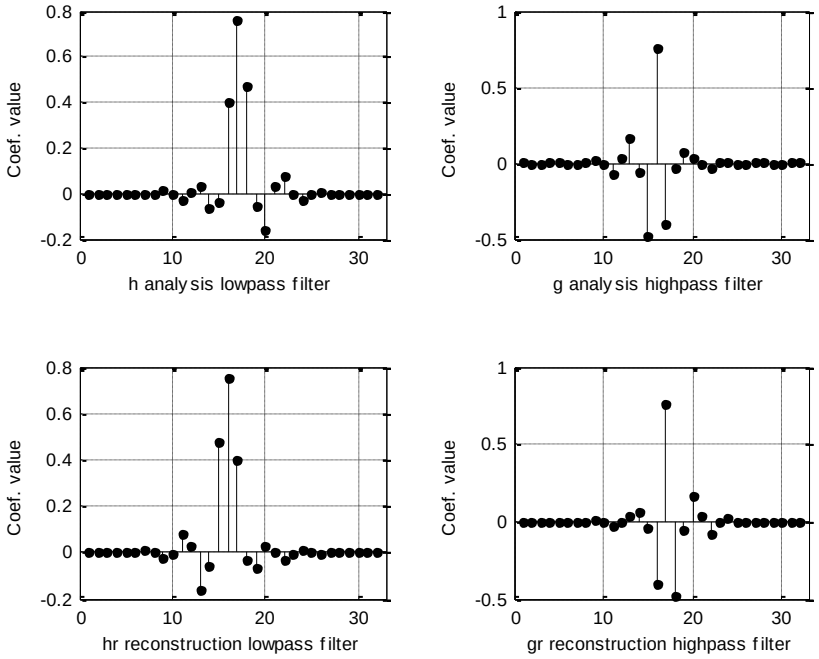

Fig. 8.25 Coefficients of the analysis and reconstruction filters

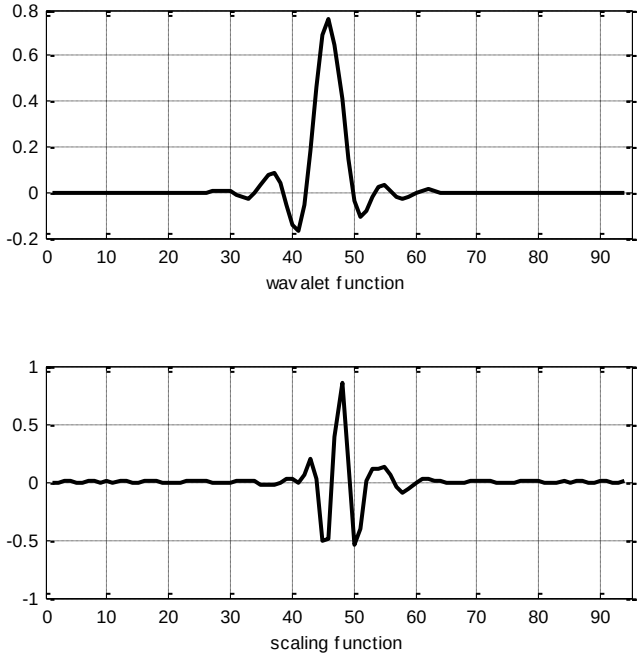

Fig. 8.26 wavelet and scaling function

Similar analysis of daily power curves from the 110 kW installation was made. Two fundamentally different days, i.e. diverse daily power curves, are presented as examples. Fig. 8.27 shows the five details on a very unsteady day. There are numerous very rapid changes during the whole course of a day. Stunning is the number of changes and relatively high amplitude of them. Table 8.8 include descriptive data of curves in Fig. 8.27. The approximation in Fig. 8.28 shows the possible smooth curve of the daily production. Comparison of the smooth curve to measured power values in Fig. 8.28 gives the idea of needed compensating storage in order to smooth out ripples. In real installation the compensation can be done only with a predictive filer and must be entirely based on past power values. For statistical analysis and sizing purposes the whole daily curve can be taken into considerations.

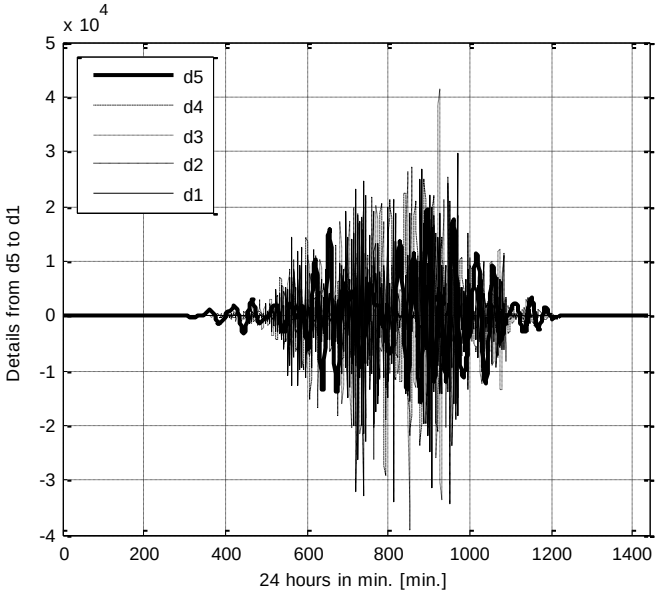

Fig. 8.27 Details for 110 kW installation, day 21

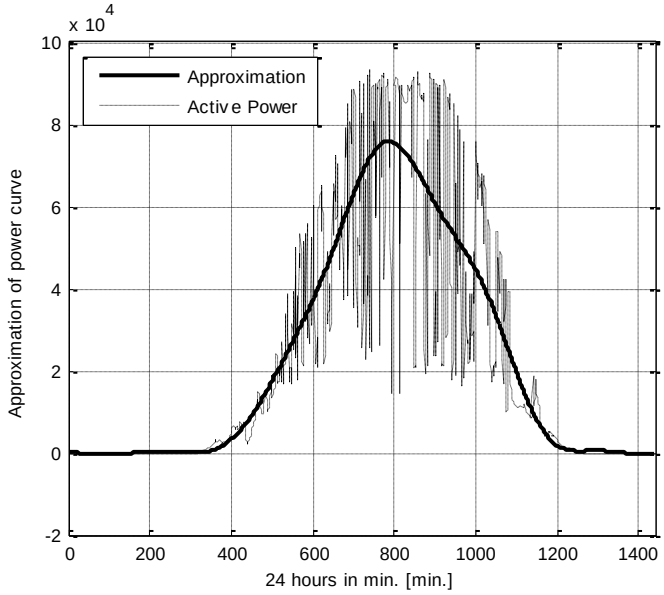

Fig. 8.28 Approximation component of the wavelet analysis of the daily power curve, day 21

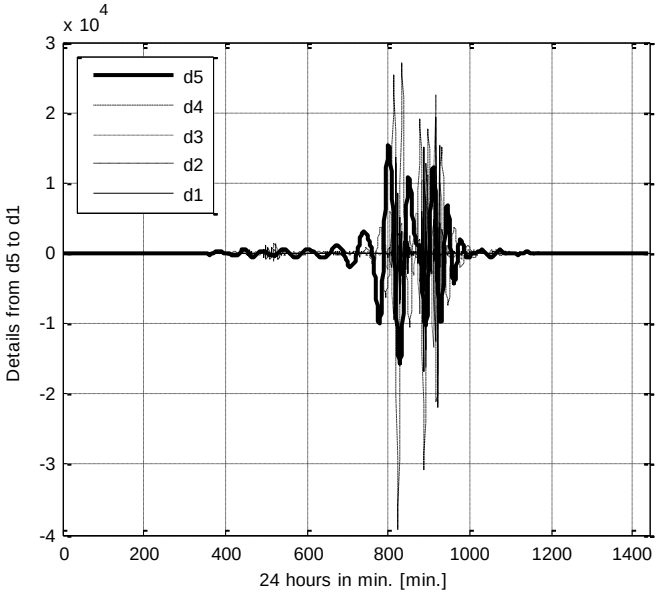

Fig. 8.29 Details for 110 kW installation, d5, day 27

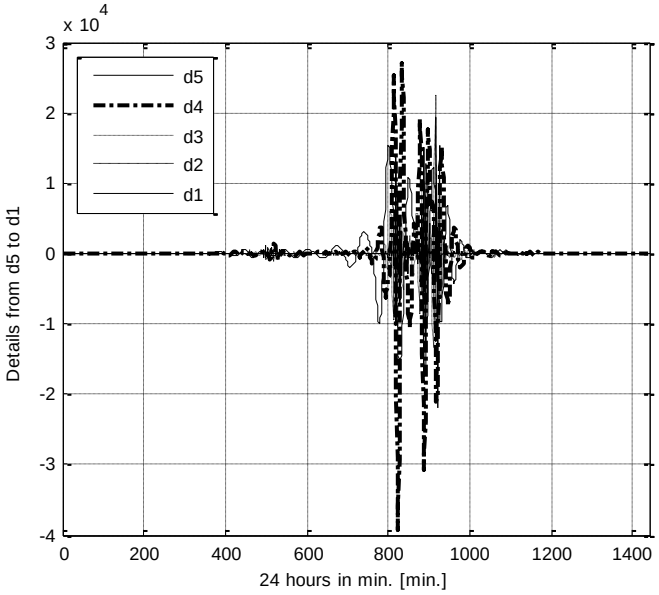

Fig. 8.30 Details for 110 kW installation, d4, day 27

The daily power curve in the 110 kW installation selected as a second example is substantially different form the curve in Fig. 8.28. The day was bright and almost

cloudless so the power plot is relatively smooth. The daily power curve indicates only three major notches (Fig. 8.31). Corresponding details computed using filters in Fig. 8.25 are shown in Fig. 8.29 and Fig. 8.30. Detail d4 in Fig. 8.30 correspond better to the mentioned three notches than the lowest detail d5 in Fig. 8.29. There are three major swings in d4. This comparison shows, that the level of detail at which the changes are the biggest indirectly describes the art of changes taking place in the daily power curve, i.e. how often and for how long is there a notch in the curve. If there were no rapid changes is the curve the approximation would overlap with the power curve, as it does during the most time in Fig. 8.31. Descriptive data of the details fo the power curve in Fig. 8.31 are summarized in Table 8.9.

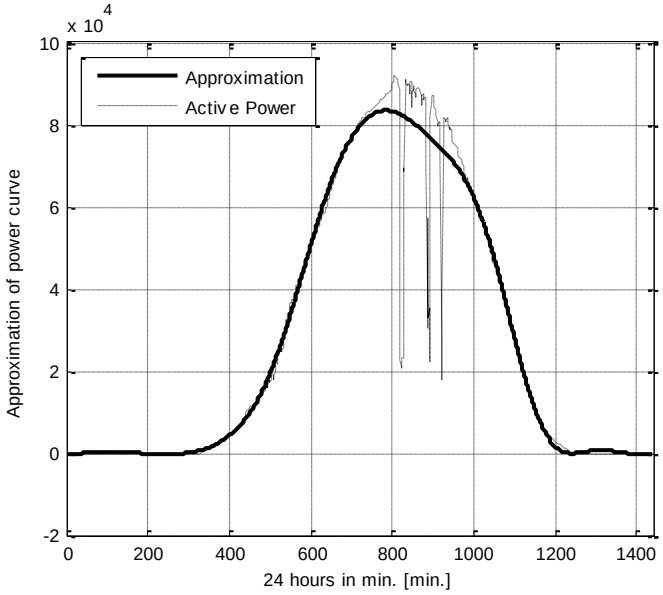

Fig. 8.31 Approximation component of the wavelet analysis of the daily power curve, day 27

Table 8.8 Descriptive parameters of details, 110 kW installation, day 21

detail no.	min.	max.	integral	variance	std. dev.
d1	-31318.431	29860.966	2600274.699	17960333.574	4237.963
d2	-34202.515	24588.936	3414944.446	26003613.762	5099.374
d3	-39053.645	41430.851	4537778.722	41339969.392	6429.617
d4	-29117.598	25057.496	4099598.543	33309175.336	5771.410
d5	-16153.335	19545.179	3802947.038	22710068.665	4765.508

Table 8.9 Descriptive parameters of details, 110 kW installation, day 27

detail no.	min.	max.	integral	variance	std. dev.
d1	-16758.212	14965.064	248139.597	1010334.365	1005.154
d2	-21981.243	19302.920	535960.241	2935331.101	1713.281
d3	-16957.896	22582.856	799661.351	4244896.737	2060.315
d4	-39312.111	26879.074	1973217.888	21655719.845	4653.571
d5	-15620.526	15484.513	1668954.175	9122196.409	3020.297

Generally, wavelet transform is regarded to be an appropriate tool for the analysis of daily power curves in PV installations. The approximation component describes the smooth curve, showing the low frequency block of the signal. It enables considerations about possible compensation with a storage device. The details include information about severity of changes happening in the signal. This information is included in the shape and index of the detail. Descriptive parameters of particular details are regarded as new power quality indicia describing the performance of a PV system. In a statistical sense, they give a possibility to moderate infeed tariffs and justify the ned to refit an PV installation with a storage device compensating rapid power variations. The level of compensation should be correlated to expected statistical improvement of performace.

9 PV system monitoring using spherical irradiation components

Evolutionary algorithm and trust region reflective algorithm perform completely different. The first one is based on a stochastic search whereas the other is an analytical method based on the gradient and Hessian values of the objective function. Both methods were utilized to solve a problem of the type (4.14) given as

$$\sum_{i=1}^{33} Irr_{i,n} \cdot \alpha_{i,n} = P_n \tag{9.1}$$

The weighted sum of all directionally measured irradiations Irr in (9.1) should be equal to the power output of the considered PV power plant. Index i stands for sensor number and n indicates subsequent time instant, i.e. subsequent minutes in a day. In matrix notation the over-determined set of equations is

$$\mathbf{Irr} \cdot \boldsymbol{\alpha} = \mathbf{P} \tag{9.2}$$

Solving (9.2) without constrains using (4.16) may result in vector $\boldsymbol{\alpha}$ with negative entries. A negative coefficient has no physical meaning. A positive coefficient is the weight of a spherical irradiation component contributing to the overall power output. Therefore, a least squares optimisation analysis with *bound type* constrains, guaranteeing values of all coefficients greater or equal zero, must be used. The trust region reflective algorithm and evolutionary algorithms approach are considered to be suitable for the problem and are delivering comparable results.

Daily irradiation and power curves were used and it was assumed that the particular weights in $\boldsymbol{\alpha}$ do not change over the course of a day.

An average over 10 minutes was selected for the presentation, despite the one minute values in the above chapter. 10 min. averaging resulted in a more smooth curve with less points over a 24 hours period and was more suitable for this problem mainly due to the computational burden characterised by long lasting iterative procedures. As the power curve follows the changes in irradiation it was assumed that further averaging of both irradiation and power did not deteriorate general characteristics and features of proposed method. Curves obtained for 24 hours were analysed. Longer peri-

ods (two days, a week or a month) were not used but are possible extension to proposed approach.

Firstly, a simple artificial system was build, consisting of only one cell from the spherical measurement devise. Only one geographical adjustment of the reference cell was used resulting in one spherical irradiance component. Many different sensors were analysed this way. Data from sensor no. 19 was selected as an example for more detailed results presentation. Irradiation curve was multiplied by fictive PV panel area to obtain power output in [W] from the artificial PV power plant.

In this case the optimisation procedure should indicate a correct parameter value for the particular sensor and zeroes for the rest of sensors. Correct value means a coefficient to be multiplied by the irradiation values and resulting in power corresponding to the predefined output.

Fig. 9.2 shows the normalized power curve [pu] of the artificial PV system (virtual PV power plant) and power curves estimated according to (9.1). The curves obtained with trust region reflective algorithm for least-square linear problem (TRRA) and evolutionary algorithm (EVOL) are almost identical and the corresponding plots overlap.

Slightly differences can be seen in the values of estimated daily α parameters in Fig. 9.1. The TRRA algorithm selected a second component (sensor 27) to be multiplied with a small coefficient. It cannot be regarded as failure or wrong plate selection. Sensor 27 has the same azimuth as preselected sensor no. 19 and slightly different elevation (only 15 degrees) resulting in similar irradiation curve (Fig. 7.6).

The mean square error for approximation was 0.083 for TRRA and negligible for EVOL.

Similar results were obtained for artificial PV power plants build upon one measuring sensor selected freely for the set featuring various spherical irradiation components.

Further, a more complicated virtual power plant consisting of three weighed irradiance values from sensors 19, 23, 25 was constructed (Fig. 7.6). The three sensors were oriented to the South, West, and North direction. Fig. 9.4 shows the normalized power curve of the artificial PV system (Virtual PV) and power curves estimated according to (9.1).

The mean square error for approximation was 0.0853 for TRRA and for EVOL was negligible. The sum of absolute values of α coefficients errors of all 33 sensors was 2.1208 for TRRA and also negligible for EVOL.

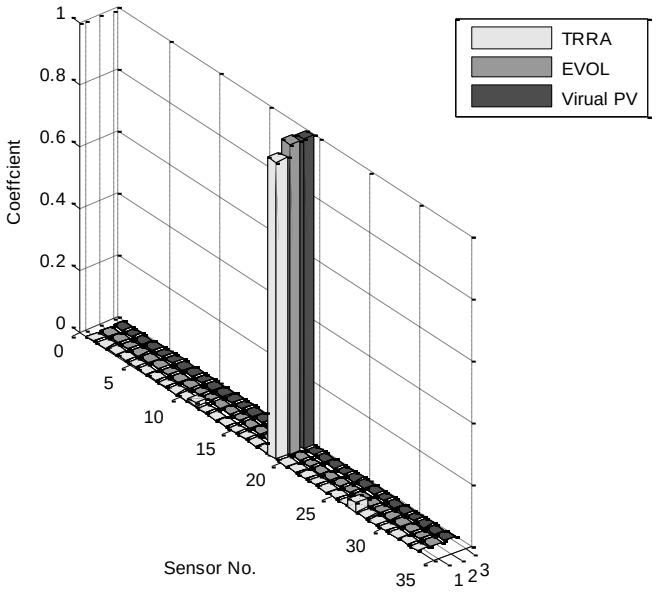

Fig. 9.1 Coefficients for virtual PV with one plate

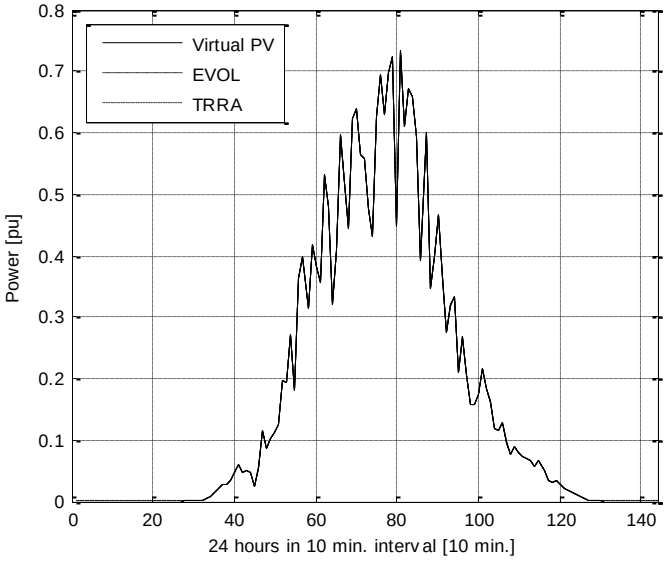

Fig. 9.2 PV system power output, given and estimated

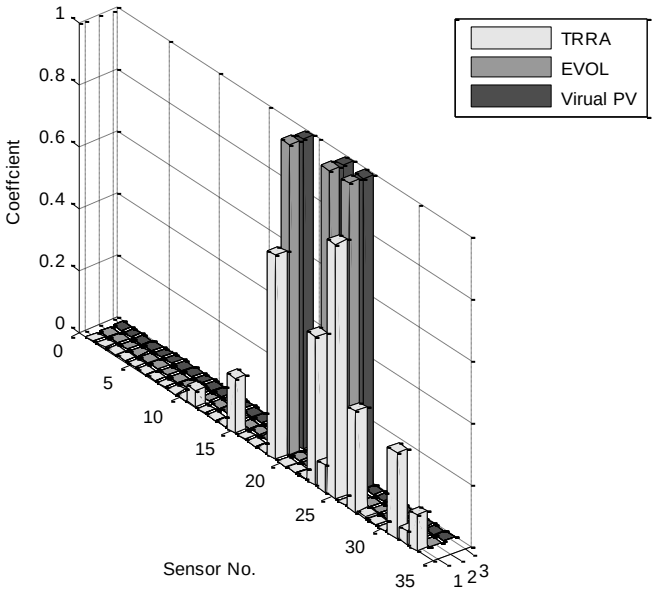

Fig. 9.3 Coefficients for virtual PV with three plates

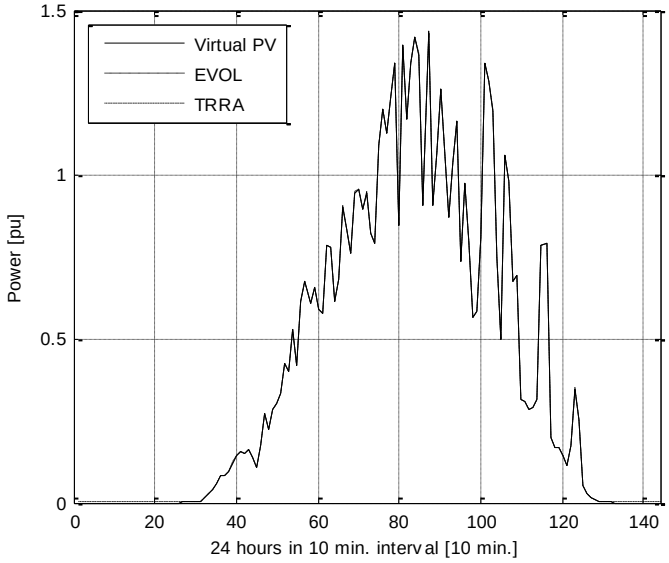

Fig. 9.4 PV system power output, given and estimated

It is noticeable, that the selection of other cells than were used for the construction of the virtual PV power plant by the TRRA algorithm (Fig. 9.3) resulted in an insignificantly different estimation of the daily power curve in Fig. 9.4. The very small estimation error is due to the selection of cells with the same azimuth as were used in the construction of the virtual PV plant but with slightly different elevation (usually 15 degrees difference). The irradiation curve of those cells is very similar, but only different in amplitude. The difference in amplitude can be compensated by higher values of the α coefficients. The TRRA is prone to local minima, so the selection of cells nearby to the original was seen as a good solution in terms of the objective function values.

Assessment of real 110 kW PV power system is shown in Fig. 9.6. The real and estimated power curves overlap. Coefficients values are shown in Fig. 9.5. Sensors no. 19 and 2 were correctly selected by EVOL as the real installation has the same SSW orientation and panels at two elevations. The additional two components indicated by TRRA, cells no. 10 and 11 have SW and S orientation respectively. This orientation correspond with the real installation.

The mean square error for approximation was 0.5293 for TRRA and for 5302 EVOL.

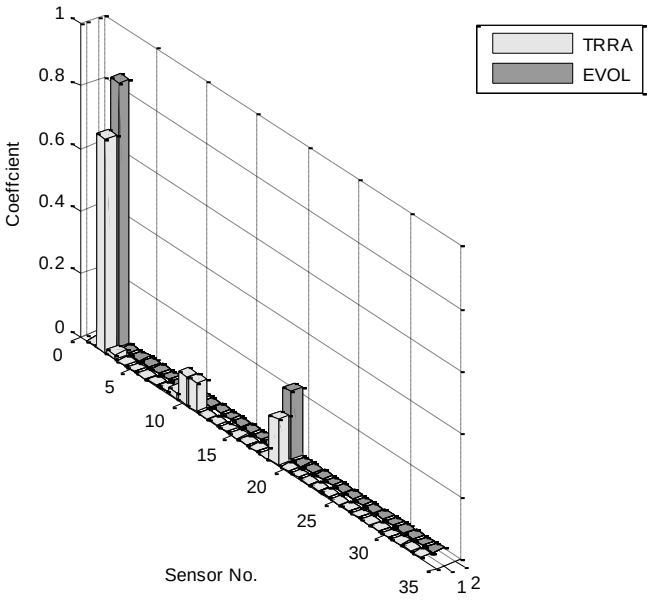

Fig. 9.5 Coefficients for real PV installation

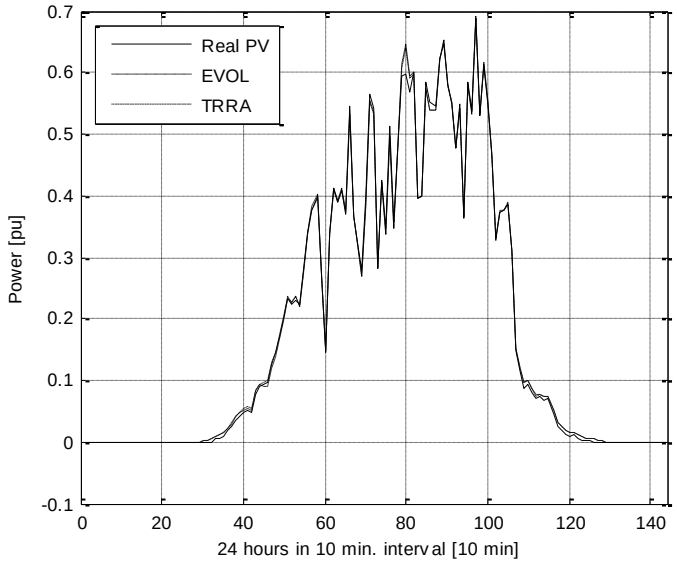

Fig. 9.6 PV system power output, real and estimated

Summarising, both proposed method give quite satisfactory results in terms of power curve estimation. Working with simple virtual power plant as well as with real power output was possible and resulted in successfully overlapping curves. EVOL method is more precise but also more computationally demanding than TRRA.

The proposed approach of finding coefficients matching directional irradiation curve with power output of a real PV power plant as in equation (9.2) has highly practical implications.

An existing power plant with optimised values of α parameters and constant measurement of the power output can be constantly monitored this way. A discrepancy between the estimated and real power output, higher than a predefined threshold indicates a failure in the PV system and a need for inspection. A broken or shaded panels can be the cause. This approach is especially dedicated to building integrated photovoltaic systems whit sophisticated geographical arrangements of cells following the shape of a façade. In such a case a single reference cell is not sufficient. Further, estimated power curve significantly smaller than real one indicates a problem in the spherical measurement device itself.

The collection of spherical irradiation data in a particular urban location justifies the motivation of further expansion of an existing PV system in urban location. The location of PV panels is restricted by existing architecture limiting available areas and geographical orientation of panels. Correlation between existing locations for new PV panels and spherical irradiation components give detailed information about prospective power output of the refitted installation. Knowing the expected power output and

installation costs of new panels and necessary installations a decision in finical terms can be made.

Parameters selection as shown in Fig. 9.4 was deliberately included to show that using cells different from those originally used for the construction of a virtual PV power plant can result in a very accurate power curve. It is possible to construct a correct power curve, i.e. select spherical irradiation components and corresponding coefficients, form data no used for the creation of a virtual PV power plant. A reconstruction of an building or a group of buildings with already existing PV system may results in new locations available for PV but also with the loss of existing spaces, e.g. through construction of additional windows. Further it is assumed that the power curves should remain as they are due to unchanged connection conditions imposed by the local utility. The proposed approach gives a tool to compute the necessary coefficients indicating area needed for new PV panels along with geographical orientation of cells enabling the compensation of the lost panels. Electrical output of old and refitted installation should be approximately unchanged.

10 Conclusion

Research presented in this work was motivated by fast developments of small PV systems connected to the distribution grid by prosumers. The fact, that there is, or will be in the near future, a significant number of distributed PV installations connected to the gird is a substantially new circumstance influencing strongly the operation of distribution grids and safety of energy delivery. PV generation is highly variable and weather depending, so it can hardly be compared to traditional small power sources such as water generators or gas turbine power plants. This traditional means of generation are characterised by constant and predictable power output, which can be regulated by the operator.

The focus of research activities was centred at the analysis methods of output power variations in PV systems – their characterisation in relation to solar irradiation. Adequate assessment of the PV system performance is a prerequisite for safe and reliable operation of distribution networks. Without such an assessment the connection of new PV installations, the decision on implementation of necessary compensating storage devises or power quality enhancement tools cannot be taken.

The complex nature of daily power curve variations requires appropriate assessment tools originating in signal processing and optimization. The aim was to figure out reliable approaches.

Data acquisition is the first step in any signal processing. The sampling of voltage and current is usually done with high frequencies, ca. 10 kHz [101], but computed RMS values, active, reactive power, etc. are averaged, aggregated and saved over longer periods, typically 10 min [20]. Rapid changes in the PV daily power curve require faster rates. It is possible to store power curves with 1 minute or 1 second resolution. Even smaller time windows are thinkable. Practically, a limitation is imposed by the smart meter technology. Large amount of data need longer transmission time, less meters can be served by a concentrator, larger storage capacity is needed. That imposes investments not necessarily welcomed by the utilities. Therefore, *one minute window* was proposed as a compromise for the analysis with wavelets. For irradiation vs. power analysis ten minutes window was considered suitable due to computational burden of optimisation algorithms. Moreover the coefficient settled for longer period should be valid for shorter one, as the power and irradiation curves correlate.

Data transfer in PLC technology was not possible due to high distortion levels in the frequency range up to 150 kHz generated by the operation pf PV converters. It was possible at night when the converters were not operating.

Resampling was successfully applied for the harmonisation of data acquisition frequencies. If the data were stored with shorter window, e.g. one second, and then resampled to longer window, e.g. one minute, then information was lost. The information loss is due to averaging and infects especially short variations with high amplitude as shown in Fig. 8.12 and Fig. 8.13. The up-sampling form ten minutes window to one minute window does not bring new information to the signal, but enables better frequency resolution and better overall performance of wavelet transform analysis. Signal conditioning operation was crucial for the effectiveness of further processing.

Daily active power curves were the basis for any analysis. Therefore, a longer treatment of power component computation was included. The computation of power for sinusoidal circuit was presented as a starting point for the considerations including nonsinusoidal voltage and current waveforms. Active power is usually computed using (6.1) in power quality recorders [101]. Accordingly, the Budeanu and Fryze approaches to power computation were presented. Although new power definitions are currently discussed in the literature, the available data from existing metering systems are not based on those theories. This is definately subject for further research. The computation of power in accordance to (6.1) requires spectral components of current and voltage. They are given in a 5 Hz steps after FFT transform in power quality recorders [101]. The accuracy of component estimation is important for reliable power computation. Therefore *MUSIC method* was proposed as a complementary tool for the identification of spectral components in signals. This method is not restricted to integer multiplies of fundamental frequency, as FFT is, and performs well in noisy conditions.

Full *compensation of reactive power* with a linear capacitor is not possible in case of nonsinusoidal voltage and current waveforms. However, the approach proposed by Shepherd and Zakikhani sizes the capacitor to achieve best possible compensation. This approach, although not guaranteeing full compensation, is suitable for prosumers. It is simple, does not require sophisticated and cost intensive active filters. The level of reactive power is lower than using a capacitor sized with accordance to the fundamental component, as shown in a numerical example. Approach recommended for small prosumers installations with variable generation and demand characteristics.

Real mesurements of active power and irradiance were used during research. The power output to be analysed was not supported by any kind of storage. Two installation with powers in the range representing prosumers installations were studied. However, they were equipped with measurement devices not used in typical commercial PV installations, enabling in-depth analysis. There is no better way of obtaining such research data than real measurements.

Characterisation of daily power curves was done with the idea of a *centroid.* This approach, along with mean value , maximum value, gives only one point per day as a description of the curve. There is huge reduction of data, but also information loss. As a quality factor a circle was proposed, in which the centroid have to be located during all days. The centre and radius of the allowed circle location can be proposed after analysis of data from longer periods, e.g. month or year.

Wavelet transform is a fare more effective tool for the characterisation of daily power curves. *Approximations* characterise the daily curve excluding variations. *Details* inform exactly about variations in the daily curve. Every detail represents different frequency range, so that detail level and its amplitude at a particular time instant- characterise the variations. The overall severity of changes during a day is well described by the integral of the detail curve over the course of a day. The maximum and minimum value characterises daily extremes. Descriptive statistics, variance or standard deviation, further characterise the details. An open question is the level of acceptable variations. Specific threshold values should be the outcome of a compromise between the producers of PV installation components and operators of the distribution grids.

Approximation of the daily power curve by a predefined shape is another way of its characterisation. A bell function (8.4) requires only three parameters to define a daily shape, bringing significant data reduction. The most suitable parameters' values are the result of an optimisation process. Trust region reflective algorithm and evolutionary algorithm delivered satisfactory results, although both methods operate substantially differently. Maintaining the three parameters within a predefined range is a new proposed quality factor for the description of PV installation performance.

Correlation between daily power curves and spherical irradiation components is a new proposal for the characterisation of the PV system performance. The matching between power and irradiance according to (9.2) in useful in various aspects. In building integrated photovoltaic with variously oriented panels it helps to detect a failure in the system, if there is a mismatch between power and irradiation. The mismatch indicates also lost sun energy, when solar generator was turned off due to maintenance or a persisting fault in the grid. The installation of panels with a given orientation in a particular location can be precisely assessed in terms of the power output. Finally, if there is a need for removal of some panels due to reconstruction of a building a new orientations can be proposed in order to compensate for the lost ones. In this case the goal is to keep the power curve unchanged even with differently arranged panels. So that, the infeed into the grid is the same. No need for new connection conditions for the utility. The coefficients in (9.2) matching power and irradiation were successfully figured out with optimisation methods.

Generally, the work presents some new ideas for the assessment of small or medium PV systems along with new power quality factors based on these new approaches. The settlement of specific threshold values is subject to analysis of long term meas-

urement data. Threshold values proposed by the utilities would require a tariff policy forcing necessary investments in the improvement of power generation in PV installations by prosumers in terms of the new power quality factors.

11 Outlook and Future Research

The proliferation of small PV systems into the distribution grid will continue in the future. Reduction of greenhouse gases emission, increasing the share of renewable energy sources, subsidies for local energy production and consumption are the main driving forces for this development. Widespread use of photovoltaic will have the key disruptive influence on the distribution grid in the near future [102]. Further research on methods for PV system assessment and its influence on the distribution grid is therefore justified.

Two PV installations, differently power rated but geographically relatively close, were analysed in this work. Research data from installations connected to various distribution networks (urban areas, rural areas, etc.) should be analysed. The data should come from PV installations at various geographical locations. In this way not only he change in theoretical irradiance value can be captured, but also the influence of local climate (clouds, rainfall, temperature) on the energy production curve.

The varying nature of irradiance and power output from PV installation requires statistical analysis of data measured over longer period of time, e.g. one year. Not only a particular day have to be analysed, but long term data enabling conclusions in a statistical sense. Approaches proposed in his work should be applied to at least one year data. Especially the severity of power fluctuation and optionally the effectiveness of variation compensation by a storage device must be verified statistically.

The concept of spherical irradiation measurement compared to active power was elaborated using artificial PV power plants and one existing PV installation. Research on building integrated photovoltaic, where the panels are a part of the façade or generally the structure of a building should be done. Such an installation on a building is of special importance due to various panels orientation and different panels types used to suit the aesthetic aspects of architecture.

The daily power curves analysis should be extended to cover also the reactive power component. This is an important subject as fare as the reactive power definition for nonsinusoidal waveforms is still a subject for discussion and anyway a base for penalty fees imposed by utilities on consumers. Reactive power is an important power quality factor. Theoretically converter have a predefined power factor [17], but it is not defined at low power output and combines with power factors of other loads of the consumer. Further analysis on this field is urgently needed.

The disturbances in the range up to 150 kHz caused mainly by PV converters are of outmost interest for the data transfer in PLC technology. There is a contradiction between the use of PLC smart meters to capture power curves and other PQ data in PV installations and the use of converters generating disturbances in the voltage at frequencies typical or the communication channel.

12 Bibliography

[1] Y. Hase, Handbook of Power System Engineering, Chichester: John Wiley & Sons, 2008.

[2] L. Philipson, "Distributed and dispersed generation: addressing the spectrum of consumer needs," in *IEEE Power Engineering Society Summer Meeting*, Seattle, 2000.

[3] P. Fox-Penner, Smart Power Climate Change, the Smart Grid, and the Future of Electric Utilities, Washington: Island Press, 2010.

[4] *Directive 2001/80/EC of the European Parliament and of the Council on Large Combustion Plant Directive LCPD,* 2001.

[5] *Directive 2009/31/EC of the European Parliament and the Council on the geological storage of carbon dioxide,* 2009.

[6] *Directive 2009/28/EC of the European Parliament and of the Council on the promotion of use of energy from renewable sources,* 2009.

[7] E. Comission, 2014. [Online]. Available: http://ec.europa.eu/clima/policies/2030/index_en.htm. [Data uzyskania dostępu: 22 06 2014].

[8] E. Comission, 2014. [Online]. Available: http://ec.europa.eu/clima/policies/roadmap/index_en.htm.

[9] *Directive 2001/77/EC of the European Parliament and of the Council on the promotion of electricity produced from renewable energy sources in the internal electricity marked,* 2001.

[10] *Directive 2009/72/EC of the European Parliament and of the Council concerning common rules for the internal market in electricity,* 2009.

[11] N. Hadjsaid and J. C. Sabonnadire, Smart grids, Chichester: John Wiley & Sons, 2012.

[12] A. Keyhani and M. Marwali, Smart Power Grids 2011, Berlin: Springer, 2012.

[13] M. Bollen and F. Hassan, Integration of distributed generation in the power system, Chichester: Jahn Wiley & Sons and IEEE Press, 2011.

[14] J. Paska and et al, Hybrid Power Systems Distance Learning Tool, Warszawa: Hypos DL, 2005.

[15] V. Skendzic, I. Ender i G. Zweigle, „IEC 61850-9-2 Process Bus Is Impact on Power System Protection and Control Reliability," *PAC World,* pp. 20-27, June 2014.

[16] S. Mayer, „Sharing IEC 61850 Sampled Values," *PAC World,* pp. 39-43, June 2014.

[17] *VDE-AR-N 4105:2001-8, Power generation systems connected to the low voltage distribution network - technical minimum requirements for the connection and paralell operation with low*

voltage distribution networks, 2011.

[18] *PN-EN 50438 Standard. Requirements for the connection of micro-generators in parallel with public low-voltage distribution networks,* 2014.

[19] *Ustawa z dnia 10 kwietnia 1997 Prawo energetyczne (Dz. U. z 1997, nr 54, poz. 627) z późniejszymi zmianami Dz.U. 2014 nr 0 poz. 490 2014.04.30, Dz.U. 2014 nr 0 poz. 457 2014.05.09, Dz.U. 2013 nr 0 poz. 1238 2013.11.24, Dz.U. 2013 nr 0 poz. 984 2013.09.*

[20] *PN-EN 50160 Standard. Voltage characteristics of electricity supplied by public electricity networks,* 2010.

[21] P. Büchner, Stromricher Netzrückwirkungen und ihre Beherrschung, Leipzig: VEB Deutcher Verlag für Grundstoffindustrie, 1982.

[22] J. Mindykowski, Assessment of electrical power quality in ship systems fitted with converter subsystems, Gdask: Shipbuilding and Shipping, 2003.

[23] C. Mulcahy, „Plotting and Scheming with wavelets," *Mathematics Magazine,* tom 69, nr 5, pp. 323-343, 1996.

[24] A. Jensen i A. la Cour-Harbo, Ripples in Mathematics. The discrete Wavelet Transform, Berlin: Springer, 2001.

[25] J. Szabatin, Podstawy teorii sygnałów, Warszawa: WKŁ, 2000.

[26] A. Cohen, I. Daubechies i J.-C. Feauveau, „Biorthogonal bases of compactly supported wavelets," *Communications on Pure and Applied Mathematics,* tom 45, nr 5, pp. 485-560, 1992.

[27] G. Uytterhoeven, D. Roose i A. Bultheel, „Wavelet transform using the lifting scheme," Department of Computer Science, K.U. Leuven, Heverlee, Belgium, 1997.

[28] S. Mallat, A wavelet tour of signal processing, San Diego: Academic Press Inc., 1998.

[29] I. Daubechies, Ten lectures on wavelets, Philadelphia: Society for Industrial and Applied Mathematics, 1996.

[30] S. J. J. W. Hoffman W., Reactive Power Compensation. A practical guide., Chichester: John Wiley & Sons, 2012.

[31] E. K. P. Chong and S. H. Zak, An Inroduction to Optimization, Chichester: John Wiley & Sons, 2001.

[32] M. A. Bhatti, Practical Optimization Methods with Mathematica Applications, Heidelberg: Springer Verlag, 2000.

[33] G. B. Dantzig and M. N. Thapa, Linear Programming 1: Introduction, Heilderberg: Springer Verlag, 1997.

[34] G. S. G. Beveridge and S. R.S., Optimization: Theory and Practice, New York: McGraw Hill, 1970.

[35] B. D. Bunday, Basic Optimization Methods, London: Edward Arnold, 1984.

[36] R. Fletcher, Practical Methods of Optimizations, Chichester: John Wiley & Sons, 1987.

[37] D. J. E. i R. B. Schnabel, Numerical Methods for Unconstrained Optimization and Nonlinear Equations, Englewood Cliffs: Prentice-Hall, 1993.

[38] R. W. Pike, Optimization for Engineering Systems, New York: Van Nostrand Reinhold, 1986.

[39] M. S. Bazaraa i H. D. Sherali, Nonlinear Programming. Theory and Algorithms, Chichester: John Wiley & Sons, 1993.

[40] D. G. Luenberg, Linear and Nonlinear Programming, Reading: Addison-Wsley, 1984.

[41] A. L. Peressini i F. E. Sullivan, The Mathematics of Nonlinear Programming, Heidelberg: Springer Verlag, 1988.

[42] G. V. Reklaitis, R. A. i R. K. M., Engineering Optimization: Methods and Applications, Chichester: John Wiley & Sons, 1983.

[43] D. J. Wilde, Optimum Seeking Methods, Englewood Cliffs: Prentice-Hall, 1964.

[44] A. Cichocki i U. R., Neural Networks for Optimization and Signal Processing, Chichester: John Wiley & Sons and B. G. Teubner, 1994.

[45] R. R., Theorie der neuronalen Netze, Heidelberg: Springer, 1996.

[46] H. S., Nerual Networks. A Comprehensive Foundation, New York: Macmillan College Publishing Company, 1994.

[47] D. Nauk, F. Klawonn i R. Kruse, Neuronale Netze und Fuzzy Systeme, Braunschweig: Vieweg, 1996.

[48] Schrijver, Theory of Linear and Integer Programming, Chichester: John Wiley & Sons, 1986.

[49] D. M. Himmelblau, Applied Nonlinear Programming, New York: McGraw-Hill, 1972.

[50] D. P. Bertsekas, Nonlinear Programming, Belmont: Athena Scientific, 1995.

[51] D. P. Bertsekas, „Necessary and suffcient conditions for a penalty method to be exact," *Mathematical Programming*, tom 5, nr 9, pp. 87-99, 1975.

[52] S. G. Nash and A. Softer, Linear and Nonlinear Programming, New York: McGraw-Hill, 1996.

[53] J. H. Holland, Adaptation in Natural and Artificial Systems: An Introductory Analysis with Applications to Biology, Control, and Artificial Intelligence, Cambridge MA: MIT Press, 1992.

[54] L. e. Davis, "Genetic Algorithms and Simulated Annealing," in *Research Notes in Artificial Intelligence*, London, Pitman, 1987.

[55] M. Gen and R. Cheng, Genetic Algorithms and Engineering Design, Chichester: John Wiley & Sons, 1997.

[56] M. Wael, A. Hasawi i K. M. El-Naggar, „A Genetic Based Algorithm for Digitally Recorded Impuls Parameters Estimation," w *IEEE PowerTech Conference*, Bologna, 2003.

[57] D. Goldberg, Genetic Algorithms in Search, Optimisation and Machine Learning, Addison-Wesley Pub. Co., 1989.

[58] M. Mitchell, An Introduction to Genetic Algorithms, Cambridge: MIT Press, 1996.

[59] C. Houck, J. Joines and M. Kay, "A genetic algorithm for function optimization: a Matlab

implementation Technical Report: NCSU-IE-TR-95-09," North Carolina State University, Releigh, NC, 1995.

[60] D. E. Goldberg, Genetic Algorithms in Search, Optimization and Machine Learning, Boston: Addison-Wesley, 1989.

[61] R. J. Patton i G. P. Liu, „Robust control design via eigenstructure assign, genetic algorithms and gradient-based optimisation," *IEE Proceedings on Control Theory Applications,* tom 141, nr 3, pp. 202-208, 1994.

[62] M. Wael, A. Hasawi, M. Khaled i M. El-Naggar, „A genetic based algorithm for digitally recorded impulse parameter estimation," w *IEEE Power Tech Conference*, Bolognia, Italy, June 2003.

[63] G. P. L. R. J. Patton, „Robust control design via eigenstructure assignment, genetic algorithms and gradient-based optimisation," *IEE Proceedings on Control Theory Applications,* tom 141, nr 3, pp. 202-208, 1994.

[64] L. Kolev, „Iterative algorithm for the minimum fuel and minimum amplitude problems for linear discrete problems," *International Journal on Control,* tom 21, nr 5, pp. 779-784, 1975.

[65] T. F. Coleman and Y. Li, "A Reflective Newton Method for Minimizing a Quadratic Function Subject to Bounds on Some of the Variables," *SIAM Journal on Optimization,* vol. 6, no. 4, pp. 1040-1058, 1996.

[66] P. E. Gill, W. Murray i M. H. Wright, Practical Optimization, London: Academic Press, 1981.

[67] K. G. Binmore, Calculus, Cambridge: Cambridge University Press, 1986.

[68] W. Z. W. F. Su Shi, „Estimation of solar irradiation based on multiple stepwise regression," w *IEEE PES Innovative Smart Grid Technologies Asia ISGT*, 2011.

[69] C. P. Steinmetz, „Findet eine Phasenverschiebung im Wechselstromlichtbogen statt," *Elektrotechnische Zeitschrift,* tom 42, pp. 567-568, 1892.

[70] L. S. Czarnecki, Moce w obwodach elektrycznych z niesinusoidalnymi przebiegami prądów i napięć, Warszawa: Oficyna Wydawnicza Politechniki Wrocławskiej, 2005.

[71] Z. P. Shepherd W., „Power-factor compensation of thyristor-controlled single-phase load," *Proceedings of the Institution of Electrical Engineers,* tom 120, nr 2, pp. 245-246, 1973.

[72] Z. P. Shepherd W., "Reactive-power definitions and power-factor improvement in nonlinear systems," *Proccedings of IEE,* vol. 121, no. 5, pp. 390-392, 1974.

[73] L. S. Czarnecki, "Budeanu and Fryze: Two frameworks for interpreting power properties of circuits with nonsinusoidal voltages and currents," *Electrical Engineering,* vol. 80, pp. 359-367, 1997.

[74] C. I. Budeanu, Puissances reactives et fictives, Bucharest: I.E.R, 1927.

[75] R. H., Mercury arc converters, Pitman, 1963.

[76] N. Z., „Generalised theory of electic power," *Archive fuer Elektrotechnik,* tom 63, pp. 177-182, 1981.

[77] „Rapports et discussions sur la puissance reactive," CIGRE, Paris, 1929.

[78] B. .. O., FFT Schnelle Fourier-Transformation, München: R. Oldenbourg Verlag, 1995.

[79] L. R. G., Understanding Digital Signal Processing, Reading: Addison Wesley Longman, 1997.

[80] Z. T. P., Cyfrowe przetwarzanie sygnałów, Warszawa: WKŁ, 2005.

[81] Orfanidis S. J., Englewood Cliffs: Prentice Hall, 1996.

[82] I. M.A., "Definition et mesurede la puissance et de l'energie reactives," Bull. Soc. Franc. Electriciens, 1925.

[83] Shepherd W., Zakikhani P. , "Suggested definition of reactive power for nonsinusoidal systems," *Proceedings of the Institution of Electrical Engineers,* vol. vol. 119, no. 9, pp. 1361-1362, 1972.

[84] F. S., „Moc rzeczywista, urojona i pozorna w obwodach elektrycznych o przebiegach odkształconych prądu i napięcia," *Przegląd Elektrotechniczny,* nr 7, pp. 193-203, 1931.

[85] S. D., „Discussion of Suggested Definition of reactive power for nonsinusoidal systems," *Proceedings of the Institution of Electrical Engineers,* tom 120, nr 1, p. 108, 1973.

[86] S. D., „Reactive-power definitions and power-factor improvement in nonlinear systems," *Proceedings of the Institution of Electrical Engineers,* tom 120, nr 6, pp. 704-706, 1973.

[87] S. W. Z. P. Micu E., „Suggested definition of reactive power for non-sinusoidal systems (discussion)," *Proceedings of the Institution of Electrical Engineers,* tom 120, nr 7, pp. 796-798, 1973.

[88] V. N. Nedelcu, "Suggested Definition of Reactive Power for nonsinusoidal Systems (Correspondence)," *Proccedings of IEE,* vol. 121, no. 5, pp. 389-392, 1974.

[89] Emanuel A. E., „Suggested Definiion of Reactive Power in Nonsinusoidal Sstems and Reactive power Definitions and Power-Factor Inprovement in Nonlinear Systems (Correspondence)," *Procesing of* , tom 121, nr 7, pp. 705-706, 1974.

[90] *ISET Sensor – solar irradiation sensor, User Guide, IKS Photovoltaic GmbH,* 2013.

[91] *PN-EN ISO/IEC 17025:2005/AC Standard, General requirements for the competence of testing and calibration laboratories,* 2005.

[92] *Transmission Code 2007: Network and System Rules of the German Transmission System Operators. VDN,* 2007.

[93] Q. Wells, Smart Grid Home, Clifton Park: Delmar, Cengage Learning, 2013.

[94] R. G. Lyons, Understanding Digital Signal Processing, Reading: Addison Wesley, 2007.

[95] A. V. Oppenheim, A. S. Willsky and S. H. Nawab, Signals and Systems, Englewood Cliffs: Prentice Hall, 1997.

[96] S. J. Orfenidis, Introduction to Signal Processing, Englewood Cliffs: Prentice Hall, 1996.

[97] R. E. Larson, R. P. Hostetler i B. H. Edwards, Calculus of a Single Variable, Boston: Houghton Mifflin Company, 1998.

[98] S. G. Sanchez, N. G. Prelcic i S. J. G. Galan, „Uvi Wave. Wavelt Toolbox for the use with Matlab," Universidad de Vigo, Vigo, 1996.

[99] P. Janik, P. Kostyla, J. Rezmer, J. Szymanda, T. Sikorski, Z. Waclawek i L. D., „Performance characterization of a PV system using wavelet transform and genetic algorithm," *Renevable Energy and Power Quality Journal*, March 2013.

[100] S. M. Ross, Introductory Statistics, Kidlington: Elsevier Inc., 2010.

[101] "1760 Power Quality Recorder; User Manual," Fluke corporation, 2006.

[102] J. S. John, "From Smart Meters to Smart Inverters: How DVI is Optimising the Distribution Grid," [Online]. Available: http://www.greentechmedia.com/articles/read/DVIs-grid-edge-vision-from-smart-meters-to-smart-inverters. [Accessed 15 July 2104].

[103] T. Cholewicki, Elektrotechnika Teoretyczna, Warszawa: WNT, 1973.

[104] Greer M., Electricity cost modelling calculations, Amsterdam: Elsevier, 2011.

[105] M. W. Kusters N. L., „On the definition of reactive power under nonsinusoidal conditions," *IEEE Transactions on Power Apparatus and Systems* .

13 List of Figures

14 List of Tables